Dissertation

submitted to the

Combined Faculties for the Natural Sciences and for Mathematics
of the Ruperto-Carola University of Heidelberg, Germany

for the degree of

Doctor of Natural Sciences

presented by

Nathalie Knappe, nee Schöler; **Master of Science in Molecular Medicine**
Born in Ostercappeln
Oral examination date: March 24th, 2015

Partial reprogramming of melanoma cells mimics the phenotype switch and reveals SNAI3 as a novel invasion-associated marker

Referees

Prof. Dr. Viktor Umansky

Prof. Dr. Jochen Utikal

This thesis is dedicated to my Mom,
who inspires me with her passion, her love and her laugh.

Declarations according to § 8 (3) b) and c) of the doctoral degree regulations:

b) I hereby declare that I have written the submitted dissertation myself and in this process have used no other sources or materials than those expressly indicated;

c) I hereby declare that I have not applied to be examined at any other institution, nor have I used the dissertation in this or any other form at any other institution as an examination paper, nor submitted it to any other faculty as a dissertation.

Heidelberg, 23.01.2015

_____

Nathalie Knappe, nee Schöler

Table of content

Abstract

The major challenge in anti-melanoma therapy is the tremendous plasticity of melanoma cells that leads to acquisition of resistance mechanisms and ultimately, to treatment failure and death. An emerging concept of melanoma cell plasticity is the so-called phenotype switch that describes the conversion of highly proliferative and little invasive into less proliferative and highly invasive melanoma cells. *In vitro* models of this phenotype switch are needed to understand the molecular mechanisms that drive cellular plasticity. Here, I demonstrate that abortion of reprogramming towards pluripotency converts HCmel17 melanoma cells into slowly proliferating cells with substantially elevated invasive potential. In detail, I show that reprogramming of murine melanoma cells is a stable process that induces gene expression changes in a time-dependent manner. Partially reprogrammed cells exhibit elevated invasive potential *in vitro* and increased lung colonization *in vivo* at day 12 after transgene induction. By global gene expression analysis in partially reprogrammed cells, I identified SNAI3 as a novel invasion-related marker in human melanoma. Protein expression of SNAI3 correlates with tumor thickness in primary melanomas and thus, might be of prognostic value for patient stratification.

Partial reprogramming of murine melanoma cells is an innovative *in vitro* model to study phenotype switch-associated gene expression and identified SNAI3 as a novel invasion-related marker with potential for clinical application.

Zusammenfassung

Die größte Herausforderung bei der Therapie des Malignen Melanoms ist die hohe Plastizität der Melanomzellen. Diese führt dazu, dass Melanomzellen schnell Resistenzen gegen Therapieansätze bilden, was letztendlich zu Therapieversagen und der hohen Todesrate beim Malignen Melanom führt. Ein immer wichtiger werdendes Konzept, das die Umwandlung von stark proliferierenden und wenig invasiven zu langsam proliferierenden, aber dafür hoch invasiven Melanomzellen beschreibt, ist der sogenannte Phänotyp-Wechsel. Trotz ihrer Notwendigkeit, um die molekularen Mechanismen zu untersuchen, die die zelluläre Plastizität induzieren, sind *in vitro* Modelle zur Untersuchung dieses Phänotyp-Wechsels bisher kaum etabliert. In dieser Arbeit zeige ich, dass der Abbruch der Reprogrammierung muriner HCmel17 Melanomzellen diese in langsame wachsende Zellen mit stark erhöhter Invasionskapazität umwandelt. Ich zeige, dass Reprogrammierung muriner Melanomzellen ein stabiler und zeitabhängiger Prozess ist, der die globale Genexpression schrittweise verändert. Im Detail zeichnen sich Zellen an Tag 12 der Reprogrammierung durch erhöhtes Invasionspotential *in vitro* und erhöhte Lungeninfiltration *in vivo* aus. Des Weiteren habe ich anhand globaler Genexpressions-Analyse der partiell reprogrammierten Zellen den Transkriptionsfaktor SNAI3 als neuen invasionsassoziierten Marker für humane Melanome identifiziert. Proteinexpression von SNAI3 korreliert mit der Tumordicke in primären Melanomen und besitzt dadurch Potential für die klinische Anwendung, beispielsweise als prognostischer Marker für die Einteilung in Patientenkohorten. Zusammenfassend ist die partielle Reprogrammierung muriner Melanomzellen ein innovatives *in vitro* Modell, um die Genexpression zu untersuchen, die mit dem Phänotyp-Wechsel in Melanomzellen einhergeht. Dieses System habe ich genutzt um den neuen, invasionsassoziierten Marker SNAI3 zu identifizieren.

List of figures and tables

Figures

Tables

Supplemental figures

Supplemental tables

List of abbreviations

°C	Degree Celsius
AEC	3-amino-9-ethylcarbazole
ATP	Adenosine triphosphate
BCA	Bichinonic Acid Protein Assay
BME	Basal Membrane Equivalent
bp	Base Pairs
BRAF	v-Raf Murine Sarcoma Viral Oncogene Homolog B
Brn2	POU domain, class 3, transcription factor 2
BSA	Bovine Serum Albumin
CCLE	Cancer Cell Line Encyclopedia
CD	Cluster of Differentiation
CDK	Cyclin-dependent Kinase
cDNA	Complementary Desoxyribonucleic Acid
CI	Confidence Interval
c-KIT	c-Tyrosine Kinase KIT
CSCs	Cancer Stem Cells
CT	Cholera Toxin
ctrl	Control
DAPI	4′,6-Diamidin-2-phenylindol
DCT	Dopachrome Tautomerase (TRP2)
dH2O	Distilled Water
DKFZ	Deutsches Krebsforschungszentrum/German Cancer Research Center
DMEM	Dulbecco's Modified Eagle's medium
DMSO	Dimethylsulfoxide
DNA	Deoxyribonucleic Acid
Dox	Doxycycline
dpi	Days post coitus
ECM	Extracellular Matrix
EGF	Epidermal Growth Factor
EMT	Epithelial-to-Mesenchymal Transition
ERK	Extracellular-Signal Regulated Kinase
ESCs	Embryonic Stem Cells
ES-FCS	Embryonic Stem Cells-grade Fetal Calf Serum
et. al.	*et alteri*
etc.	*et cetera*
EtOH	Ethanol
FACS	Fluorescence Activated Cell Sorting
FCS	Fetal Calf Serum
FDA	Food and Drug Administration
Fst	Follistatin
Gapdh	Glyceraldehyde 3-phosphate Dehydrogenase
GDP	Guanosine Diphosphate
GFP	Green Fluorescence Protein
GPCR	G-protein Coupled Receptor

GTP	Guanosine Triphosphate
h	Hour
H&E	Hematoxylin and Eosin
HEPES	2-(4-(2-Hydroxyethyl)-1-piperazinyl)-ethansulfonsäure
HRP	Horseradish Peroxidase
ICM	Inner Cell Mass
IF	Immunofluorescence
IHC	Immunohistochemistry
IHC	Immunohistochemistry
iPCCs	Induced Pluripotent Cancer Cells
iPSCs	Induced Pluripotent Stem Cells
IRES	Internal Ribosome Entry Site
KD	Knockdown
kDa	Kilo Dalton
LIF	Leukemia Inhibiting Factor
M2	M2-reverse tetracycline-responsible transactivator
MAPK	Mitogen Activated Protein Kinase
MEF	Murine Embryonic Fibroblast
MEK	Mitogen-activated Protein Kinase Kinase
mESC	Murine Embryonic Stem Cells
MET	Mesenchymal-to-Epithelial Transition
min	Minute
miRNA	Micro RNA
MITF	Microphthalmia-associated Transcription Factor
MMP	Matrix Metalloprotease
mRNA	Messenger Ribonucleic Acid
mRNA	Messenger Ribonucleic Acid
mTOR	Mammalian Target of Rapamycin
MTX	Methotrexate
NC	Neural Crest
NCC	Neural Crest Cell
NCT	National Center of Tumor Diseases, Heidelberg, Germany
NGF	Nerve Growth Factor
NHM	Normal Human Melanocytes
NHM	Normal Human Melanocytes
NOD/SCID	Nonobese Diabetic/Severe Combined Immunodeficient
NRAS	Neuroblastoma RAS Viral Oncogene Homolog
NSG	Nonobese Diabetic/Severe Combined Immunodeficient interleukin-2 Receptor-γ chain$^{-/-}$
OE	Overexpression
OKSM	Oct4+ Klf4+Sox2+c-Myc
p.a.	Post Administration (of Doxycycline)
p.i.	Post Injection
PBS	Phosphate Buffered Saline
PCR	Polymerase Chain Reaction
PDGF	Platelet Derived Growth Factor
PFA	Paraformaldehyde
PI	Propidium Iodide

PTEN	Phosphatase and tensin homolog
PVDF	Polyvinylidenfluorid
qPCR	Quantitative Polymerase Chain Reaction
RAF	Rapidly Accelerated Fibrosarcoma
RANK	Receptor Activator of NF-κB
RAS	Rat Sarcoma
RB	Retinoblastom Protein
Rho	Ras homolog gene family
RIPA	Radioimmuno Precipitation Assay
ROCK	Rho-Kinase
rpm	Rotations per Minute
RT	Room Temperature
S2	Safety Level 2
SD	Standard Deviation
SDS-PAGE	Sodium Dodecyl Sulfate Polyacrylamide Gel Electrophoresis
siRNA	Small interfering RNA
Smuc	Snail-related in Muscle Cells
SNAI3	Snail Family Zinc Finger 3
Sox10	SRY (sex determining region Y)-Box 10
Sox2	SRY (sex determining region Y)-Box 2
STAT3	Signal Transducer and Activator of Transcription 3
TAD	Transactivation Domain
TBST	Tris-Buffered Saline supplemented with 0.05 % Tween
TGF-β	Transforming Growth Factor β
TIC	Tumor Initiating Cell
TMA	Tissue Microarray
TPA	12-0-tetradecanoyl-phorbol-13-acetate
Trp1	Tyrosinase Related Protein 1
Trp2	Tyrosinase Related Protein 2
Tyr	Tyrosinase
UMM	Universitätsmedizin Mannheim (University Medical Center Mannheim)
UV	Ultraviolett
V	Volt
wt	Wildtype

1. Introduction

This thesis covers two main areas of research: melanoma, as the cancer of interest, and reprogramming, as a technical tool used to gain novel insights into melanomagenesis. The first part of the introduction gives an overview of melanoma and its current therapeutic challenges. This section focuses on molecular resistance mechanisms against targeted therapy and the role of melanoma cells' tremendous plasticity for therapy resistance. In the second part stem cells, pluripotency, reprogramming and its connection to cancer will be discussed. The third part introduces SNAI3, which I identified, using partial reprogramming, as a promising invasion-associated marker with prognostic value for melanoma patients.

1.1. Melanoma

Malignant melanoma is a tumor with high morbidity rates and increasing incidence. Since the 1930's, the risk for an American to develop melanoma in the United States has risen more than 18-fold, as stated in 1996 [1]. With 20 diagnoses per 100,000 in 2012, Germany is the 17th country on the list of incidence [2]. Incidence and mortality hot spots are located in Australia and New Zealand, where there is high ozone depletion [2]. This can in part be explained by the close connection between ultraviolet (UV)-radiation and melanomagenesis [3].

With around 232,000 new cases diagnosed in 2012 malignant melanoma is the 19th most common cancer worldwide [2]. Although malignant melanoma only accounts for less than two percent of all skin cancers it is responsible for the vast majority of skin cancer related deaths highlighting the aggressiveness of this cancer type and the need for improvement of therapies [4].

1.1.1. Melanoma Origin

Melanomas arise upon malignant transformation of melanocytes, the pigment-producing cells within the skin that generally protect skin cells from UV-radiation induced DNA-damage. Melanocytes represent the second largest cell population within the skin after keratinocytes and are located and consistently distributed in the basal layer of epidermis [5]. In order to fulfill their protective role, upon UV-radiation melanocytes produce the pigment melanin in specialized organelles called melanosomes, which is transferred to adjacent keratinocytes [6]. Once relocated into the keratinocyte, the pigment accumulates around the nucleus building a photo-protective barrier against UV-radiation [7]. On a molecular level, melanocytes are characterized by the expression of a set of genes linked to melanin

production including tyrosinase (Tyr), tyrosinase-related protein 1 and 2 (Tryp1, Tryp2/Dct), melanosomal matrix proteins (Pmel17, Mart-1) and microphthalmia transcription factor (Mitf), which is one of the most important key players in melanogenesis [8].

During embryonic development, melanocytes are generated from the neural crest population, which also gives rise to mesenchymal and neural derivatives including neurons, glia, and endocrine cells [9]. After the differentiation of the embryonic disc into the neuroectoderm during early embryogenesis, neurolation occurs. This process describes the folding of the neural plate into the neural tube that will give rise to future central nervous system elements including the brain and spinal cord. During this neurolation process, a group of cells derived from the edges of the neural plate undergoes a phenotypic change from the epithelial to the mesenchymal type, which are called neural crest cells (NCCs). Directly after formation of these multipotent cells, they acquire migratory properties, separate from the neuroepithelium and progressively become lineage-restricted [8,10,11]. Dependent on their anatomical localization, NCCs form different functional groups, one of which is the trunk neural crest that further undergoes one of two major pathways [12]. One population migrates ventrolaterally forming the dorsal root ganglia that contain, among others, sympathetic ganglia and sensory neurons. In contrast, those neural crest cells that migrate dorsolaterally into the ectoderm towards the ventral midline become melanocytes.

The precursor cells of melanocytes – melanoblasts – arise on the neural crest cells' journey through the dermis and already comprise melanocyte-associated features but do not produce melanin yet [13]. The most commonly listed molecular markers include the tyrosine kinase receptor KIT (c-KIT); melanocyte-associated transcription factors such as Mitf, Sox10, Pax3 and the melanogenic enzyme Tyrp2 but in contrast to fully differentiated melanocytes, the precursors lack Tyr expression [14–16]. Tyr is only expressed when melanoablasts reach their final destination within the basal lamina and become terminally differentiated melanocytes [14].

In addition to this classical understanding of melanocyte development recent studies revealed that there is another origin for this cell type (reviewed in [14]). Studies in mice using lineage-tracing experiments suggest a major contribution of melanocytes from Schwann cell progenitors in the postnatal skin. In this scenario, NCCs, which fail to acquire a neuronal fate, associate with nerves and gain a Schwann cell precursor fate. Dorsal and ventral branches of the spinal nerve guide these precursors to cutaneous locations. When reaching the ends of nerves, some Schwann cell precursors acquire a melanocyte-fate and migrate to the skin where they vastly proliferate and populate the skin [14].

1.1.2. Important mutations in melanoma

Cellular differentiation is induced by activation of particular signaling cascades in order to translate extracellular signals to gene expression and ultimately induce cellular development. In melanocytes, the mitogen-activated protein kinase (MAPK) pathway is one of the essential signaling cascades that drives melanogenesis but is also involved in malignant transformation of melanocytes. MAPK signaling involves a set of particular players and a phosphorylation cascade (schematically displayed in **Figure 1**). In melanoma cells, the MAPK pathway includes rat *s*arcoma (RAS) protein, rapidly accelerated fibrosarcoma (RAF) protein and further downstream the mitogen-activated protein kinase kinase (MEK) and the extracellular signal-regulated kinase (ERK)1/2 [17]. Activated RAS-RAF-MEK-ERK signaling conducts growth and survival signals upon ligand binding and a subsequent phosphorylation chain. Activating ligands include a variety of growth factors, i.e. epidermal growth factor (EGF), platelet-derived growth factor (PDGF), and nerve growth factor (NGF) as well as ligands for G-protein-coupled receptors (GPCRs) and cytokines [18]. Ligand binding to tyrosine-receptor-kinases results in exchange of guanosine diphosphate (GDP) to guanosine triphosphate (GTP) in the G-protein RAS that initiates phosphorylation of membrane-recruited RAF [19]. Phosphorylation-activated RAF can induce downstream signaling by triggering phosphorylation of MEK that in turn phosphorylates ERK. ERK phosphorylation leads to stimulated gene expression of survival-, differentiation- and cell cycle progression-associated genes [17].

MAPK signaling and especially RAF molecules have gained more importance and clinical value after studies have demonstrated the high occurrence of activating RAF mutations in several different human cancers [20]. RAF-hyperactivation eventually results in uncontrolled MAPK signaling, driving cellular proliferation and survival and thus malignant transformation. Melanoma heavily relies on RAS/RAF/MEK/ERK signaling [20]. A mutation study showed that in general 48 % of metastatic melanoma patients harbor some kind of an activating BRAF (v-raf murine sarcoma viral oncogene homolog B) mutation, one of the family members of RAF proteins [21]. Interestingly, of all melanoma patients with BRAF-mutations, about 74 % demonstrate a substitution of valine by glutamic acid at codon 600 (V600E), which makes this mutation as the most common in melanoma. In addition, the replacement of the exact same valine by lysine (V600K) is observed in 20 % of melanoma patients while 6 % show other genotypes [21]. Next to RAF mutations, the upstream regulator RAS is also affected in melanoma with approximately 18 % of melanoma patients exhibiting a NRAS mutation [22]. Together, this supports the hypothesis that the RAS/RAF axis constitutes a major signaling checkpoint in the MAPK pathway that will promote malignant transformation upon uncontrolled hyperactivation [17].

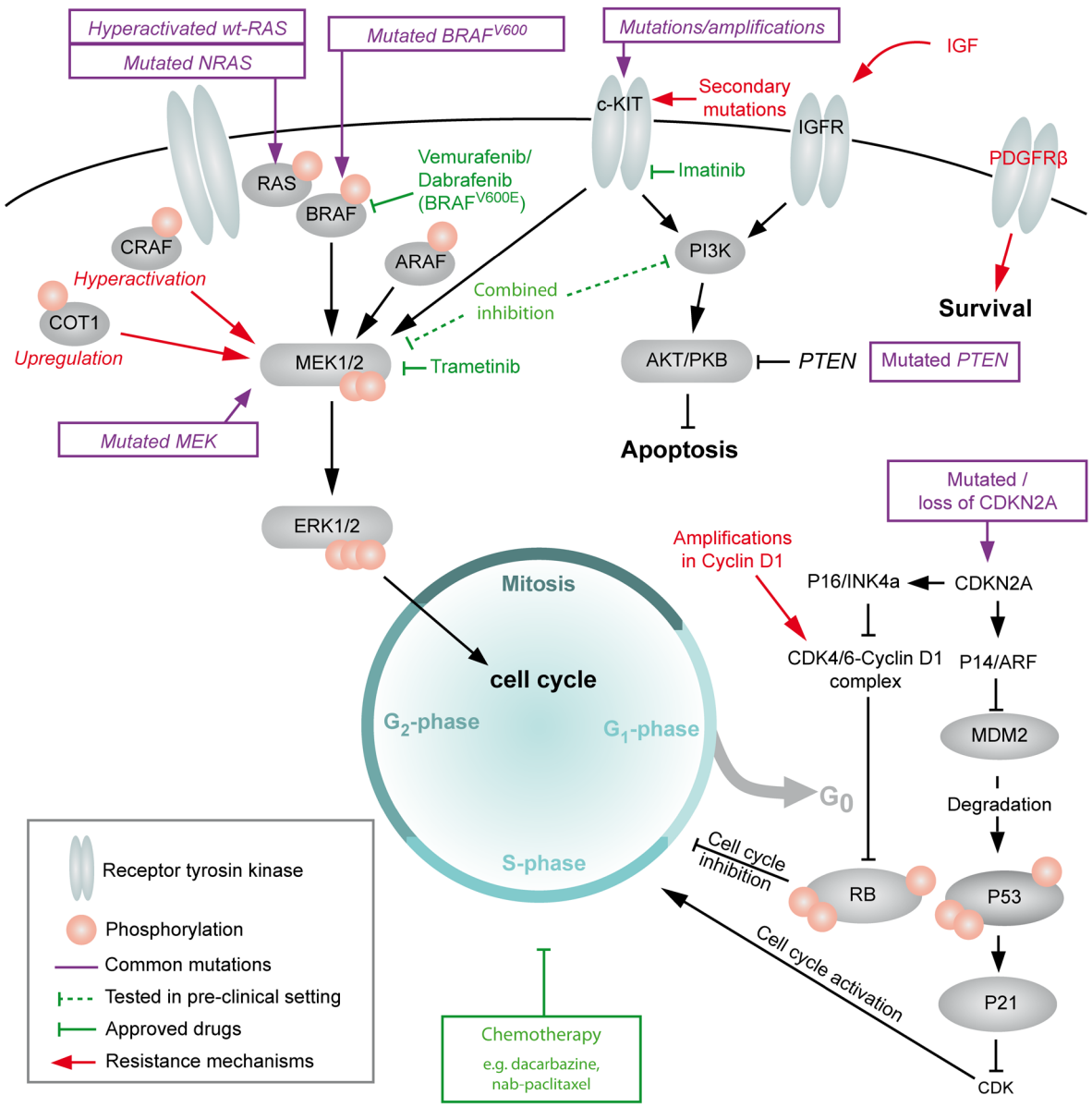

Figure 1 | Common mutations, targeted therapy and resistance mechanisms in melanoma

Anti-melanoma therapy has several different targeting strategies. The most common treatment for BRAF^{V600E}-mutated patients is the inhibition of autoactive BRAF using direct inhibitors such as vemurafenib and dabrafenib. MEK1/2 can also be inhibited with therapeutic inhibitors (e.g. trametinib). C-Kit amplifications and mutations are observed in melanoma patients and imatinib, as a receptor-tyrosine-kinase inhibitor, has been tested for anti-melanoma therapy. C-Kit inhibition is accompanied by secondary mutations in this gene leading to resistance. Although targeted therapy is established for anti-melanoma therapy also chemotherapeutic agents inhibiting proliferation *via* DNA damage and inhibition of DNA synthesis are available (e.g. dacarbazine, nab-paclitaxel). In addition, *in vitro* experiments demonstrated that combined inhibition of IGF-R and AKT/PKB leads to inhibition of proliferation in melanoma cells. Red boxes and lines indicate resistance mechanisms that in part explain the fast evolving therapy failure in melanoma patients. Enhanced IGF-signaling, elevated PDGFRß signaling, secondary c-Kit mutations as well as genetic amplifications in Cyclin D1 and upregulation of COT1 or CRAF have been observed upon resistance towards braf inhibitors.

AKT/PKB=protein kinase b; Arf=alternate reading frame protein product of the CDKN2A locus; CDK=cyclin-dependent kinase; CKIT=type III receptor tyrosine kinase (KIT); COT1=MAP3K8/mitogen-activated protein kinase kinase kinase 8; ERK=extracellular regulated kinase; IGF(R)=insulin-like growth factor (receptor); INK4a=cyclin-dependent kinase inhibitor 2A; MDM2=mouse double minute 2 homolog; MEK=MAPK-kinase/ERK-kinase; P53=tumor suppressor protein 53; PDGF(Rβ)=platelet-derived growth factor (receptor β); PTEN=Phosphatase and tensin homolog; RB=retinoblastom

In addition to mutations occurring directly within the MAPK signaling pathways, other genes are mutated in melanomas including *PTEN* (phosphatase and tensin homologue) and CDKN2A (Cyclin-dependent Kinase Inhibitor 2A). Loss or inactivating mutations in PTEN are present in melanoma cells lines and melanoma patients [23] **(Figure 1)**. The loss of PTEN results in hyperactivation of Protein-Kinase-B(PKB)/AKT-signaling whereby induction of apoptosis is downregulated. The CDKN2A gene encodes for several different transcripts including those for two major tumor suppressor proteins, $P16^{INK4a}$ and $P14^{ARF}$, which both act as cyclin dependent kinase (CDK) inhibitors, although different in their structure and mechanism of action [24]. $P14^{ARF}$ stabilizes the tumor suppressor protein P53 by inhibiting the E3 ubiquitin-protein ligase MDM2, a protein that triggers degradation of P53 and with intact cellular P53 cell cycle arrest is induced *via* P21-mediated CDK inhibition [24]. In contrast, $P16^{INK4a}$ regulates cell cycle control by targeting the retinoblastoma (RB) pathway. It inhibits CDK4/6-cyclineD1 complexes and thus prevents the phosphorylation of RB proteins leading to stable RB-E2F complexes. In the presents of these complexes elongation is inhibited and cells do not enter the S-phase of the cell cycle, thus they are primed for senescence and differentiation [25]. Dysfunction of these two important cell cycle control regulators due to loss of the CDKN2A locus can lead to malignant transformation. Hemizygous or homozygous loss of the CDKN2A gene occurs in about 56 % of melanoma patients [26].

1.1.3. Targeted therapy – BRAF inhibition

Vemurafinib was the first targeted therapy compound approved by the U.S. Food and Drug Administration (FDA) in 2011 for BRAF-mutated malignant melanoma patients. It reversibly competes with adenosine-triphosphate (ATP) to bind to the kinase domain of BRAF ultimately inhibiting BRAF-induced MEK-activation [27]. Results from a randomized study comparing the common chemotherapeutic agent dacarbazine with vemurafinib in previously untreated melanoma harboring V600E-mutations demonstrated improvement in progression-free survival (6.9 versus 1.6 months) and in median overall survival (13.2 versus 9.6 months) [28]. In contrast to its improvement in progression-free survival as the most important parameter for the patient, vermurafinib can lead to adverse events including development of cutaneous squamous cell carcinoma, kerato-acanthoma, and skin papilloma [28].

Upon successful introduction of the first targeted therapy compound, researchers and clinicians introduced another BRAF inhibitor to the market. In 2013, the FDA and the European Union approved dabrafenib on the basis of a randomized trial of patients with previously untreated $BRAF^{V600}$-mutated melanomas comparing the BRAF inhibitor with the standard chemotherapy, dacarbazine [29]. Similar to vemurafinib, dabrafenib increased

median progression-free survival from 2.7 months for dacarbazine treated patients to 5.1 months.

Despite the success of targeted therapy, melanoma patients acquire resistance to these RAF-inhibitors approximately six months after initial administration. The underlying mechanisms of resistance drive disease progression and understanding these mechanisms is required for successful melanoma therapy. Interestingly, no secondary mutations in the drug target BRAF upon treatment have been identified neither in samples from patients nor in cell lines [30]. Melanoma cells rather re-activate the RAS-RAF-MEK-ERK cascade through different molecules up- and downstream of BRAF. Signal transducers upstream of BRAF include RAS, which recruits RAF to the membranous receptor tyrosine kinase complex to be activated. Cells with mutated NRAS (ca. 15 % of melanomas) or hyperactivated wildtype RAS show enhanced MEK/ERK signaling upon BRAF inhibitor treatment leading to therapy failure (reviewed in [31]). In addition to this upstream modulation, it is known that BRAF activity can be substituted by activation of CRAF and ARAF, paralogs of BRAF. These RAF molecules are activated in vemurafenib-resistant cell lines and knockdown of CRAF re-sensitizes vemurafenib-resistant clones to BRAF inhibition [32]. In addition to BRAF paralogs, other kinases are involved in MEK/ERK activation. The non-RAF MAP3-Kinase COT1 was identified in a complementary DNA screen for kinases that prevent BRAF inhibitor (PLX4720)-mediated cell growth arrest [33]. This study demonstrated that BRAF inhibition in cell lines leads to increased COT1 expression. In addition, biopsy studies revealed that COT1 upregulation is an adaptive response to vemurafenib (PLX4032) treatment ultimately causing resistance. These results are of clinical interest since two out of three tumors from melanoma patients, who are resistant to BRAF inhibition, show elevated *COT1* mRNA [33]. Also, therapy resistance is in part caused by paradoxical activation of RAF *via* RAF dimerization in BRAF wildtype cells [34]. The pan-RAF inhibitor TAK-632 inhibits the kinase activity of these RAF dimers resulting in reduced wildtype-RAF signaling and thus indicates a more effective treatment without resistance caused by vemurafenib- or dabrafenib-induced paradox wildtype RAF activation [35].

Besides these mechanisms, cells can possess endogenous or acquired resistance to BRAF inhibition due to the modulation of signal transducers downstream of RAF. In this context, mutated MEK is one of the clinically relevant mechanisms [36]. Alterations in ERK1/2-regulated cell cycle events can also contribute to insensitivity against BRAF inhibition. Cyclin D1 in part mediates cell cycle control in a manner that increased cyclin D1 leads to hyper-phosphorylation of RB and ultimately to cell cycle progression from G1 to S-Phase. This check point is part of a melanoma resistance mechanism and approximately 25 % of mutant BRAF melanoma cell lines and tumor samples harbor genomic amplifications in Cyclin D1 [37].

1.1.4. Targeted therapy – MEK inhibition

Targeting the MEK/ERK signaling downstream of BRAF is proven successful with trametinib, a small-molecule inhibitor of MEK1/2. The FDA approved its use in May 2013 for treatment of BRAF V600E- or V600K- mutated melanomas [38]. Its efficacy was tested in randomized phase III trial involving patients with the required mutations, in which trametinib was compared to standard chemotherapy with dacarbazine similar to the first trials for vemurafenib [39]. Overall survival at six months was increased from 67 % to 81 % comparing trametinib with dacarbazine. Although patients suffered from adverse side effects including heart toxicity, other side effects like cutaneous neoplasms as reported for vemurafenib treatment were absent [39].

1.1.5. Targeted therapy – combined BRAF and MEK inhibition

The observation that trametinib-treated patients do not suffer from cutaneous neoplasms and the resistance development under monotherapy with vemurafenib or dabrafenib led to the design of a combinational trial with dabrafenib and trametinib. Due to promising results of the combinational therapy in a phase I and II study in 2012 the FDA approved the combination regimen in January 2014 [40]. In a phase III trial the combination of dabrafenib and trametinib was compared with dabrafenib monotherapy and revealed improved progression-free survival from 5.8 months (monotherapy) to 9.4 months (combination) [41]. The median duration of therapy response was prolonged from 5.6 to 10.5 months with stronger tumor regression in the combinational setting (76 % versus 54 % with complete or partial response) [41]. In addition, a recent study confirmed the advantage of combined inhibition of mutated BRAF and MEK using vemurafenib in combination with the MEK inhibitor cobimetinib. Progression-free survival was prolonged from 6.2 months to 9.9 months [42].

In conclusion, the combinational therapy regimen reveals two main advantages, i.e. (i) the delay of acquired monotherapy resistance, and (ii) the reduced incidence of squamous cell carcinoma [41]. However, despite these great advantages, this treatment results in increased adverse events and total required hospitalization raises from 2 % to 25 % [41].

Although targeted therapy improves anti-melanoma therapy, the high plasticity of melanoma cells allows a variety of resistance mechanisms that impede therapy success **(Figure 1)**. Next to the mechanisms described above, melanoma cells also activate signaling pathways independent from MEK/ERK signaling that ultimately results in accelerated cell cycle progression and therapy resistance despite inhibited MEK/ERK signaling. It was shown that cancer cells can bypass MEK/ERK inhibition by activating PDGF-signaling [30] or by activation of the AKT/PIP3 pathway [43]. For example, one study showed that MEK inhibition in combination with a phosphatidylinositol-3 kinase inhibitor induced cell death in RAF-

inhibitor resistant cell populations [43]. These data reveal novel options for targeting melanoma progression and therapy resistance besides RAF and MEK inhibition.

1.1.6. Targeted therapy – tyrosine kinase inhibitors

Imatinib is a small molecule inhibitor mainly used in patients with chronic myeloid leukemia. It competes with adenosine triphosphate and thus, inhibits several tyrosine kinases, including bcr-abl, c-KIT, and PDGF-R. Due to c-KIT amplifications or activating mutations in melanoma patients [44], clinical trials were designed to test the effect of this drug in anti-melanoma treatment. C-KIT is a transmembrane tyrosine kinase mediating cell cycle progression *via* activation of MAPK- and PI3K-cascades and thus, its activation leads to tumor progression if not properly controlled. The phase II trial of imatinib in melanoma patients harboring c-KIT mutations or amplifications revealed durable responses in 16 % of patients with a median time to progression of 12 weeks [45]. In contrast to the resistance mechanisms seen in BRAF-inhibitor treated patients, c-KIT-inhibited cells circumvent treatment by the acquisition of secondary c-KIT mutations (**Figure 1**, [46]).

In summary, targeted therapy provides a great advantage over conventional chemotherapy for anti-melanoma treatment. However, extensive prolongation of progression-free and overall survival is hampered by melanoma cells' resistance mechanisms. Also, patients suffering from malignant melanoma without carrying particular mutations described above are in need of different therapy options. In fact, some therapy alternatives are available including immunotherapy and oncolytic viruses. Immunotherapy involves antibody-directed inhibition of immunosuppression that is mediated by impeding the crosstalk between T cells and their environment [47–50]. In addition, the first-ever phase III clinical trial for an oncolytic virus was conducted for melanoma patients with promising results after interim analysis [51]. Conversely, after closing the trial in 2013, preliminary analysis revealed that despite significant elevation of dose response rates, the overall survival of patients receiving the oncolytic treatment was not significantly improved compared to patients with control treatment [52]. Next to targeted and immune-effecting therapies, also novel chemotherapeutic compounds are under investigation. Nab-paclitaxel is a novel chemotherapeutic agent, which is delivered as an albumin-bound compound [53]. This facilitates binding to the tumor due to albumin's water-soluble properties, ultimately resulting in inhibition of mitosis and increased tumor cell apoptosis with an advantageous pharmacokinetic profile [53]. A phase III clinical trial revealed an increase in both progression-free survival and interim overall survival when melanoma patients were treated with nab-paclitaxel compared to dacarbazine regardless of the BRAF-mutation status [54].

1.1.7. Therapeutic challenges

The high risk for metastasis is a major issue once melanoma has been diagnosed. Thus early diagnosis is crucial for the chance to cure melanoma patients. Great success has been made by finding novel targets for anti-melanoma therapy that result in good clinical responses (see sections *1.1.3-1.1.6 targeted therapy*) but rapidly emerging resistance to every therapeutic intervention results in the barely improved treatment of this cancer once it has metastasized. The high plasticity of melanoma cells leads to evasion of therapy and thus, is the major challenge for anti-melanoma therapy. Despite responsive treatment at the beginning of therapy, cells alter their tolerance to drugs, which ultimately leads to reoccurrence of tumors and metastatic burden causing the high mortality rate in melanoma [1,2]. Therefore, understanding the dynamic phenotypes of melanoma cells will help identifying different strategies of anti-melanoma therapy, which are independent of the tumor's mutational status. This approach will open novel therapeutic options especially for patients without common mutations.

1.1.8. Cancer stem cells in melanoma

In order to identify the mechanisms behind the high plasticity, different attempts have been made including the investigation of cancer stem cells in melanoma. Cancer has been thought of as a homogenous tumor mass before research revealed the opposite: Tumors generally consist of different cells that show different morphology, gene expression and functional properties. Huge effort is being made to analyze tumor subpopulations and the concept of cancer stem cells (CSCs) since John E. Dicks provided first evidence for their existence in 1994 [55]. CSCs are described to (i) exist as a small subpopulation within the tumor bulk, (ii) be rather slowly proliferative making them immune against proliferation-dependent chemotherapeutics, and (iii) having the power to repopulate the whole tumor with its original heterogeneity. The CSC-theory describes a tumor to be hierarchically organized and to consist of different subpopulations with different capabilities regarding clonogenic and tumorigenic potential. CSCs initiate and support tumor progression, metastasis and chemoresistance [56]. These attributes make CSCs the perfect target for anti-cancer therapy leading to complete cure without relapse.

In acute myeloid leukemia, this CSC model has been conclusively established and specific CSCs or tumor initiating cells (TICs) are well described [55,57,58]. In addition, CSC were found in pancreatic cancer [59], in head and neck squamous cell carcinoma (reviewed in [60]), in mesenchymal neoplasms [61] and in colorectal cancer [62]. Despite the research progress in other cancer types regarding the identification and isolation of CSCs, different studies about the presence of CSCs in melanoma have shown conflicting results. Expression of a variety of molecules has been described as melanoma stem cell markers but succeeding

research has often contradicted published data. Initially, enhanced tumorigenic potential in melanoma cells expressing the ATP-binding cassette (ABC) transporter ABCG2 and the surface marker cluster of differentiation (CD) 133 were reported [63] and these markers have already been associated with CSCs in other solid malignancies including brain tumors [64]. In addition, another study demonstrated that ABCB5-positive melanoma cells are capable of tumorigenesis, self-renewal and differentiation into a heterogeneous population when primary patient-derived tumor cells are serially transplanted into NOD/SCID mice. In contrast, their ABCB5-negative counterparts lack these tumor initiating properties indicating ABCB5 as a marker for melanoma stem cells [65].

The surface marker CD271 (p75/ Nerve Growth Factor-Receptor/ NGFR) is argued to be a genuine stem cell marker [66]. CD271-positive cells from fetal nerves of rats represent a subpopulation that is enriched in cells that are phenotypically and functionally comparable to neural crest stem cells, indicating that CD271 is a potential marker of stemness in neuroectoderm-derived cells [67]. Distribution of CD271 within human malignant tissue resembles that of normal tissue suggesting that also in tumors a subpopulation of CD271-positive cells is present [68]. Today, the potential of CD271 to label melanoma stem cells is discussed controversially. Although some groups cannot find indications of a stable CD271-positive CSC-subpopulation in melanoma [69], recently published data provide evidence that CD271-positive cells have significantly increased tumorigenic potential [66,70]. The huge variation between results regarding CD271-positive melanoma stem cells can in part be explained by differences in methodologies. Next to the method for single cell extraction from primary melanomas and surface marker stability, also the immune competence level of mice used for injections can have great impact on tumorigenic potential of melanoma cells [56,66].

Another report stated that human melanoma cells with high aldehyde dehydrogenase (ALDH) activity are enriched in tumorigenic cells over unfractionated cells in NOD/SCID as well as in NSG mice. Next to enhanced tumorigenicity of ALDH-positive cells, they also possess superior self-renewal ability making ALDH a potential melanoma stem cell marker [71]. In addition, receptor activator of nuclear factor κ B (RANK) expression is co-expressed with ABCB5 and CD133 connecting this receptor to melanoma stem cells [72]. Its expression is significantly increased in peripherally circulating melanoma cells and metastases from stage IV melanoma patients compared with tumor cells from stage I melanoma patients. The authors suggest that RANK is involved in the development and maintenance of melanoma-initiating cells and possibly in metastatic spreading [72].

Despite all evidences showing that these markers label melanoma stem cells as a stable subpopulation within melanomas other studies revise this concept and show that melanoma cells feature a highly dynamic expression of genes. Investigations on the lysine demethylase 5b (KDM5b/Jarid1b) reveal a more dynamic and transient presence of CSCs, thus

contradicting the classical CSC model [73]. The study suggests a dynamic expression of KDM5b that is required for long-term melanoma maintenance [73]. In the end, the classical CSC model becomes questioned not only due to dynamic expression of all potential melanoma stem cells markers but also because of studies showing that melanoma initiating cells are not rare at all and one in four to one in nine melanoma cells can establish melanoma growth in mice models [69,74].

In summary, genes associated with melanoma stem cells are dynamically regulated and fail to distinguish between tumorigenic and non-tumorigenic cells. Recent studies display that not specific individual genes are responsible for the particularly aggressive growth in melanoma but that these cancer cells rather hijack portions of the embryonic neural crest invasion program [75]. This observation links melanomagenesis tighter to its developmental path by focusing on the migratory capabilities of NCCs that might in part explain the extreme metastatic power of melanomas compared to cancers derived from other lineages.

1.1.9. De-differentiation, EMT and invasion in melanoma

The origin of melanocytes from NCCs is of great importance for melanoma research since the neural crest population has unique features connecting it to aggressive cancer. The natural gene expression profile of NCCs correlates with that of transformed melanocytes [76]. Since the conversion from an epithelial to mesenchymal cell type is essential during normal embryogenesis and particularly attained by the neural crest, melanocytes are epithelial cells that have already been subjected to epithelial-to-mesenchymal-transition (EMT) during their normal development. Thus, melanocytes are thought to possess an inherent predisposition to gain EMT-induced invasive potential but the true impact of genes associated with the neural crest remains to be fully evaluated [75–77]. Some studies suggest that de-differentiation of melanoma cells towards a neural crest-like type is a major step in order to gain invasive potential and enhance disease progression [78]. Following this assumption it is of interest whether forced differentiation can revert invasiveness in these cells. One study provided experimental evidence for this kind of anti-melanoma tactic. The prodrug 3-O-(3,4,5-trimethoxybenzoyl)-(-)-epicatechin (TMECG) is a dihydrofolate reductase inhibitor and requires activation by melanocyte-specific tyrosinase. Thus, tyrosinase expressing melanoma cells can be pushed into apoptosis by TMECG-induced depletion of the thymidine pool and ultimately inhibition of DNA synthesis [79]. Since de-differentiated melanoma cells lose expression of melanocyte-specific genes, i.e. Mitf and Tyr, re-activation of these genes is required for this approach. Interestingly, the differentiation-agent methotrexate (MTX) induces expression of tyrosinase in de-differentiated melanoma cells by elevated Mitf expression and thus, MTX/TMECG combination therapy results in apoptosis under experimental conditions *in vitro* and *in vivo* [79].

In contrast, other experiments propose that invasive expression patterns are independent from neural crest signaling and that expression of neural crest-related genes labels melanoma cell populations with low invasive potential [80]. Despite the controversial data regarding neural crest-related mechanisms that are taken over by melanoma cells, initiating metastasis is a crucial step in disease progression and understanding its molecular mechanisms will help improve therapy. Obviously, motility is a defined requirement for any cancer cells to become invasive and induce metastasis. Since melanoma is a malignancy derived from non-motile cells, migration and ultimately invasion and metastatic potential need to be acquired throughout disease progression. This section discusses some key signaling pathways involved in common and melanoma-specific invasion programs.

Generally, there are two main modes that are used by cancer cells to acquire motility and that ultimately lead to tumor dissemination and metastatic spread. The most common way is through increased proteolytic activity *via* the upregulation of matrix-degrading enzymes including matrix-metalloproteases (MMPs). MMPs are well-established markers for invasive properties and allow poor prognosis for a variety of cancer types including colorectal cancer [81], breast cancer [82], head and neck squamous cell carcinoma [83] and lung cancer [84]. In melanoma, expression of several MMPs correlates with tumor progression and invasive capacity *in vitro* and *in vivo*. Membrane type-I matrix metalloproteinase (MT-MMP1, MMP14), for example, is generally involved in melanoma growth and progression since its expression correlates with invasive potential through matrigel *in vitro* and facilitates growth upon intra-dermal injections of melanoma cells lines *in vivo* [85]. Also, upon de-differentiation of melanoma cells MMP14 expression was elevated and invasive potential increased [86]. In addition, *in vitro* experiments revealed that MMP2 activity modifies adhesion features as well as the interaction with, and extension on components of the extracellular matrix (ECM) [87]. Since loss of adhesion and the capability of anchor independent growth are essential elements of invasive cancer cells, MMP2 became an interesting regulator of cancer spreading [87]. *In vivo* analysis of melanoma cells expressing latent or functionally active MMP2 demonstrated that increased endogenous MMP2 correlates with elevated invasive potential [88]. Next to MMP14 and MMP2, also MMP3 and MMP9 are expressed at invasive tumor borders *in vivo* or enhance invasive properties in melanoma cell lines upon exogenous overexpression *in vitro* [89,90].

The second central pathway to gain cellular motility involves upregulated RHO-signaling through RHO-Kinase (ROCK). This mechanism is independent of ECM-proteolysis since cellular motility is acquired through adjustment to 3D-environment by contraction of the cortical actin network. This is accompanied by transient membrane blebbing and subsequent

retraction of cells. Thus, cells can invade through 3D-structures by changing their morphology to a small, round shape and enable movement by membrane re-organization representing a amoeboid-like movement pattern [91]. RHO enzymes comprise one subgroup of RAS-related small guanosin-triphosphatases (GTPases) and they are dominantly involved in cytoskeleton remodeling since they control actin polymerization and bundling of actin filaments [92]. This modification of the cytoskeletal arrangement is crucial to induce amoeboid-like motility and introduces RHO signaling as a major pathway in control of cellular motility. Importance of RHO signaling in melanoma progression is demonstrated by its requirement to maintain metastatic potential in human melanoma cells [93]. This study demonstrated that overexpression of RHO-C is required for metastatic potential of human melanoma cells in xenograft transplantation assays. Strikingly, overexpression of this single gene is sufficient to enhance experimental metastasis formation *in vivo* and thus, cytoskeleton remodeling induced by RHO-C signaling might be a key element in metastasis formation [93].

In cancer cells these different modes of motility and metastatic invasion are reversible. This might in part explain the discouraging results from clinical trials using MMP inhibitors as metastasis blockers (reviewed in [94]) since tumor cells escape MMP-dependency by switching to other migratory strategies. In experimental settings it is proven that tumor cells can shift their migratory behavior from the proteolytic manner towards the proteolysis-independent, amoeboid-like form without any impairment of their invasive capacity [95].

1.1.10. Cellular phenotype switch during melanoma progression

Melanoma cells seem to de-differentiate in order to enhance their migratory and invasive capacity. Therefore, not all factors that are essential for the initial malignant transformation of melanocytes are also crucial for the acquisition of invasive properties. Regarding their gene expression, melanoma cells can be separated *in vitro* into cohorts that show distinct proliferative and invasive behavior [80]. One set of cells shows high proliferation and low motility whereas the other group comprises strong invasion potential but little proliferation [80]. Of note, these phenotypes correlate with metastatic potential but are independent from any BRAF mutations indicating a tumor progression program that is detached from genetic aberrations involved in melanoma initiation [80]. In addition, the phenotype switch of melanoma cells occurs in a dynamic manner so that melanoma cells, independent of their original proliferative or invasive phenotype, induce growth of tumors that comprise of cells exhibiting both phenotypes [96].

It is further shown that highly proliferative melanoma cells that are subjected to a hypoxic environment convert into highly invasive cells whereas originally invasive cells do not respond to hypoxic stimuli. Researchers suggest that proliferative melanoma cells are

subjected to hypoxic microenvironments *in vivo* and that this condition is sufficient to induce de-differentiation and results in increased invasion [97].

After the emergence of the melanoma phenotype switch as a concept of melanoma plasticity, an increasing number of markers have been identified that correlate with and induce the switch from a proliferative to an invasive phenotype. The inversely expressed receptors ROR1 and ROR2, which negatively regulate each other, serve as potential indicators for this conversion. After hypoxic conditions were applied *in vitro* the expression of ROR1 in highly proliferative melanoma cells shifted towards a ROR2-dominated pattern and correlated with elevated invasion [98]. This indicates that microenvironmental stimuli, such as hypoxia, are sensed by these receptors to induce an invasive signaling cascade. This progression from a proliferative to an invasive cell type is also connected to therapy resistance. Invasive expression patterns including hypoxia-induced ROR2 upregulation were shown to correlate with clinical responses to BRAF inhibition [98]. Another study showed that melanoma cells grown as spheroids in a neural cell crest display the phenotype switch with concomitant increase in stem cell marker expression including Nanog and Oct4 [78] (discussed in section 1.1.9). Interestingly, the occurrence of this invasive phenotype was connected to PHF19 expression [78]. PHF19 is a protein that is involved in polycomb group repressive complex (PRC) 2-mediated inhibition of stem cell-associated genes during embryonic differentiation [99]. Thus, melanoma cells undergoing phenotype switching suppress stem cell marker-inhibition through decreased PHF19 expression and subsequent de-differentiation is associated with increased invasiveness [100].

BRN2 is another gene that is expressed in a subpopulation of melanoma cells that are negative for MITF [101]. Functionally, BRN2 directly represses MITF expression and correlates with enhanced invasion capacity of melanoma cells [101]. Further investigations revealed that these BRN2 expressing cells within the primary tumor are the cells with extravasation capacity indicating enhanced invasion *in vivo* [102]. Thus, non-pigmented cells highly expressing BRN2 are found in the circulation indicating that they possess extravasation capability. However, after entering second sites cells re-adjust their expression and switch to increased MITF expression so that metastatic tumors mainly comprise of pigmented, MITF-positive and BRN2-negative cells [102]. Therefore, hypoxic conditions within primary tumors can convert proliferative cells into highly motile ones that enter the circulation. After homing to distant organs, cells increase their proliferative capacity in order to establish a novel metastasis.

In summary, melanoma cells possess the ability to alter their proliferation and invasion capacity in response to environmental signals. This reversible phenotype switch enables melanoma cells to disseminate from the primary tumor and establish metastasis at

secondary sites, which exhibit the heterogeneity of the primary tumor. Interestingly, the differentiation status of melanoma cells has a huge impact on this phenotype switch: Expression of melanocyte-specific genes labels highly proliferative cells whereas increased invasion is accompanied by de-differentiation. Deeper understanding of the molecular mechanisms inducing the phenotype switch is required to fully discover the metastatic drive of melanoma cells and identify new targets for anti-melanoma therapy.

1.2. Stem cells and reprogramming

This study uses reprogramming as a technical tool, so in the next section stem cells and cellular reprogramming will be discussed in order to give an outline of known techniques and important regulators. In addition, similarities between reprogramming and malignant transformation of cells will be summarized.

1.2.1. Stem cells

By definition, stem cells are cells, which possess unlimited self-renewal capacity in combination with the ability to generate progenies of a more differentiated state. The potency of specific stem cells depends on their range of differentiation potential and thus, stem cells can be divided into different stages: totipotent, pluripotent and monopotent stem cells. Mammalian totipotent stem cells are the only stem cells giving rise to all cells of the organism including extra-embryonic tissue required for implantation of the embryo and its proper development. This totipotency has only been determined for the zygote state of a mammalian embryo. After cleavage divisions of the zygote the so-called morula is generated. This cell cluster further separates into a blastocyst that consists of the extra-embryonic trophoectoderm and the inner cell mass (ICM) [103]. Shortly after the formation of this mixed ICM, cells segregate into the extra-embryonic primodal endoderm expressing Gata6 and the Nanog-expressing epiblast containing pluripotent cells that give rise to all embryonic tissues from every germ layer including germ cells (discussed in [104]). Cells within the epiblast of an embryo gradually lose their differentiation capacity and give rise to different types of multipotent cells, that form cells from different tissues within one germ layer, i.e. hematopoietic stem cells [105]. Monopotent stem cells are cells that fulfill the criteria of stemness but they only give rise to a single type of differentiated cells, such as epidermal stem cells generating keratinocytes throughout the life of humans [106].

For research and for clinical applications, especially pluripotent cells are of great interest since they contain the capability to generate any cell in the human body and thus, their potential for regenerative medicine is vast. Studying embryonic development in mice helps to understand the sources of this pluripotent cells, i.e. the inner cell mass of the blastocyst or the epiblast, respectively. These cells can successfully be cultured *in vitro* and by now, a large variety of murine embryonic stem cells (ESCs) are available [107,108]. Due to developmental processes described above, ethical issues are the limiting factor for investigating human pluripotent stem cells. Working with any kind of human embryonic stem cell is prohibited by law in most European countries including Germany [109]. It has already been shown that somatic cells can be converted into pluripotent stem cells using transplantation of somatic nuclei into enucleated oocytes [110] or cellular fusion with an oocyte [111,112]. However, these techniques still require embryonic stem cells and due to

coherent restriction in using human embryonic cells, stem cell research has been limited. The discovery of Yamanaka and colleagues opened up an entire new field of stem cell research with the induced pluripotent stem cells (iPSCs) they generated [113].

1.2.2. Reprogramming somatic cells into induced pluripotent stem cells

In 2006, Yamanaka *et al.* demonstrated for the first time that somatic cells can be reprogrammed into a pluripotent state by forced expression of defined factors, the so-called Yamanaka-factors [113]. The authors use exogenous expression of Oct4, Klf4, Sox2 and c-Myc (OKSM) by retroviral gene transfer in order to reprogram embryonic and adult murine fibroblasts into pluripotent stem cells [113]. This study initiated intense research on a variety of methodologies to induce pluripotency in somatic cells and to dissect the molecular steps of the reprogramming process. Following this new discovery in cellular plasticity, several assays became highly important in order to define the developmental potential of iPSCs. In this context, the least stringent functional assay is *in vitro* differentiation since no conclusion can be made regarding their *in vivo* potential. Therefore, a widely established *in vivo* assay to confirm the stem-like state of reprogrammed cells is the generation of teratomas upon subcutaneous injections into mice [114]. These tumors comprise of differentiated cells from all three germ layers and thus provide evidence for true pluripotency of iPSCs. In addition, chimera formation and germ line contribution after injection into the ICM of the blastocyst demonstrates pluripotency with higher stringency followed by the most exact test - the injection of cells into tetraploid-host blastocysts [115]. Since tetraploid cells cannot contribute to embryogenesis, embryos derived from these injections are so-called “all iPSC” embryos or animals.

There are many possibilities to generate iPSCs. In addition to lenti- or retroviral gene transfer, there are several different non-integrating methods that are established to keep the cellular genome intact. Researchers successfully reprogrammed murine as well as human fibroblasts using continual transfection with plasmid vectors and subsequent transient expression of required transcription factors [116,117]. Also, adenoviral transfer [118,119] or sendai virus-mediated gene expression have been used as viral vectors of choice due to their non-integrating feature [120,121]. In addition to these DNA-based methodologies, other groups demonstrated successful reprogramming towards pluripotency by DNA-free technique such as messenger RNA transfection [122] or direct protein delivery [123]. Since reprogramming requires expression of certain genes and gene expression can be mediated by microRNA (miRNA)-controlled pathways, different miRNA clusters have been used to enhance iPSC generation or create iPSCs from human or murine origin without additional expression of exogenous transcription factors [124–126]. In 2013, researchers used a single, synthetic self-replicating RNA replicon derived from the Venezuelan equine encephalitis virus

to induce pluripotency in human fibroblasts [127]. This RNA expresses four reprogramming factors, Oct4, Klf4, Sox2 with c-Myc or Glis1 at consistently high levels with the advantage of directed degradation so that no exogenous RNA remains within the reprogrammed cell [127]. Another technique that possesses high potential to ultimately meet the needs for regenerative medicine is reprogramming somatic cells by administration of small molecule compounds. After the discovery that a specific combination of chemical compounds is sufficient to permit reprogramming from mouse fibroblasts in the presence of only Oct4 [128], all reprogramming factors could successfully be replaced by seven small molecule compounds that bind to nuclear receptors, histone-modifying enzymes and DNA-modifying enzymes as well as to protein kinases and signaling molecules [129]. This approach demonstrates that somatic cells harbor an endogenous pluripotency program that can be reactivated by the modulation of molecular pathways *via* small molecules in the absence of ectopic “master regulators” [129].

In summary, reprogramming is defined by accompanying processes that can be induced by several different methodologies including exogenous miRNA expression or transient treatment with small molecule compounds. However, the induction of a stable pluripotency-associated gene expression network is essential for maintaining the high developmental potential of pluripotent cells.

1.2.3. The circuit of pluripotency

It is widely accepted that the most important players in pluripotency are Oct4, Sox2 and Nanog. These transcription factors are not only used to induce pluripotency [130] but their endogenous expression is key criterion in order to maintain pluripotency in cultured ESCs. Their unique expression pattern during early development suggests a major role of these transcription factors for the specification of embryonic stem cell identity [131–133]. The precise control of the master regulators’ expression is, for example, demonstrated by the restriction of Oct4 expression to ESCs, cells of the inner cell mass and to cells of the germ line [134]. Repression of Oct4 upon differentiation and lineage commitment and subsequent activation of Oct4-repressed developmental genes is crucial for normal development in mammalian organisms. Thus, massive expansion of poorly differentiated cells occurs upon systemic, ectopic Oct4-expression in adult mice underlining the importance of complete silencing of this pluripotency-associated factor during differentiation [135]. Regarding reprogramming, the importance of Nanog is demonstrated by proving that selecting for Nanog-expressing cells leads to superior reprogramming results [136] compared to initially established selection for Fbx15-positive cells [113]. Enhanced iPSC formation of Nanog-positive cells is observed and established Nanog-iPSCs mimic DNA methylation patterns of

ESCs and can give rise to chimera formation indicating complete reprogramming into the ESC-state [136,137]. Nanog-selected iPSCs are also indistinguishable from ESCs regarding their global gene expression and their chromatin configuration in contrast to Fbx15-selected iPSCs [136]. In addition, reactivation of the inactivated X-chromosome in female cells is confirmed in Oct4- or Nanog-positive iPSCs [137]. These *in vitro* analyses of pluripotency are verified using the most stringent assays in order to define the stem-like state of these reprogrammed cells: Oct4- or Nanog-positive iPSCs generate postnatal chimeras upon blastocyst injection, contribute to the germ line [136–138] and generate "all iPSC-embryos" through tetraploid complementation [138].

Other studies showed that Sox2 is also required, not only for normal embryonic development and lineage specification but also for successful reprogramming. Embryos that carry a homozygous deletion of the Sox2 gene die soon after implantation of the embryo revealing the essential role of the regulator [139]. Interestingly, Sox2 requirement is phenotypically not manifested until after implantation due to sufficient maternal Sox2 protein in these early days of embryonic development [139]. Deeper insight was given by a study that used small interfering (si) RNA-mediated depletion of both, maternal and embryonic, Sox2 mRNA at the two-cell stage [140]. *In vitro* observation of embryonic development revealed that these embryos arrest at the morula stage and fail to form trophectoderm revealing a major role for Sox2 in establishment of the trophectoderm lineage. Interestingly, expression of the pluripotency-associated markers Oct4 and Nanog remained unaffected when Sox2 was depleted indicating that these three transcription factors exhibit independent functions despite of their high connectivity in regards to pluripotency [140]. The role of Sox2 in the process of reprogramming has also been investigated and studies showed that endogenous expression of Sox2 facilitates the conversion of melanocytes into iPSCs indicating that particular cell type are more susceptible to reprogramming than others, dependent on their endogenous gene expression signature [141].

Knowing that Oct4, Sox2 and Nanog are of individual importance in regards to pluripotency, also their direct or indirect interaction is of great interest. Transcription factors generally work in a complex interaction system including several different proteins rather than playing an isolated role during development and homeostasis. This holds true for the pluripotency-associated factors Oct4, Sox2 and Nanog, which demonstrate a high degree of complex interactions with promoter regions and other proteins. For instance, Sox2 supports maintenance of pluripotency in part by regulating Oct4 levels whereas Oct4 can heterodimerize with Sox2 showing the interconnected regulatory network [142]. On transcriptional level it is known that Oct4, Sox2 and Nanog bind together on their own promoters to form an auto-regulatory loop, which stabilizes the pluripotent state (summarized in **Figure 2**). This auto-regulatory circuitry in combination with para-regulatory effects on

each of the factors suggests that the three factors function collaboratively to maintain their own and each other's expression. Aside from direct binding to each other's promoters, these three factors often co-occupy their target genes indicating a synergistic role in regulation of gene expression. One study using chromatin immunoprecipitation and a hybridization-based screening of promoter sequences established a model that includes a subset of active and a subset of repressed target genes, which promoters are co-occupied by Oct4, Sox2, and Nanog [143]. The active set includes genes encoding factors of chromatin-remodeling and histone-modifying complexes as well as genes that directly encode for transcription factors such as signal transducer and activator of transcription 3 (STAT3), which themselves are known to regulate specific genes [143]. These data indicate that the three key players of pluripotency guide a complex gene expression signature and work as a regulatory unit aside of their independent functions.

On protein level, direct interactions are shown for Oct4, Sox2 and Nanog. In ESCs a multi-protein complex containing Oct4 and Nanog has been identified by iterative immunoprecipitation [144]. In addition, Sox2, Oct4 and Nanog do not only associate with one another in pluripotent cells, they also cluster together with common transcription factors

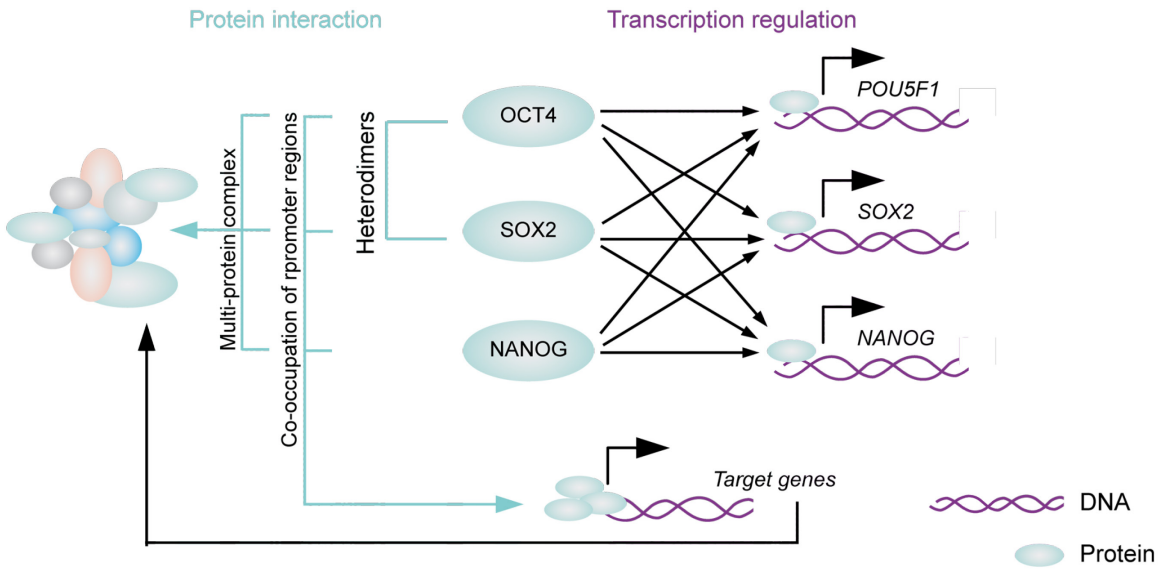

Figure 2 | Regulatory interactions between members of the pluripotency-circuit
OCT4, SOX2 and NANOG are the key players in initiation and maintenance of pluripotency in embryonic stem cells and induced pluripotent stem cells. These three transcription factors interact with each other and regulate each other's expression and that of common target genes in a complex manner. This scheme summarizes the proteomic-based analyses of interactions between OCT4, SOX2 and NANOG. OCT4 and SOX2 can build heterodimers and all three transcription factors are found in huge multi-protein complexes. In addition, each of them was found to bind the others and its own regulatory regions. They also co-occupy a variety of different promoters of common target genes. Strikingly, subsets of these genes encode for proteins that are found in the multi-protein-complexes, e.g. Sall4, further underlining the complexity of these interactions.

providing further evidence that multiple interacting proteins synergistically control pluripotency. For instance, using embryonic stem cells engineered for inducible expression of the four reprogramming factors (OKSM), more than 70 proteins that associate with Sox2 in ESC were identified [145]. Strikingly, 25 % of these proteins have been shown to be part of the Oct4-interactome studied previously [145]. In an Oct4-centered analysis a larger dense interaction network was detected, which contains 166 proteins and includes Sall4, Tcfcp2l1, Dax1, and Esrrb. The network is not only comprised of transcription factors and chromatin-modifying complexes that are known to possess roles in self-renewal, but many factors have not been previously associated with the pluripotency network [146]. In addition, a comprehensive study in murine embryonic stem cells revealed a complex DNA-protein interactome of Oct4, Nanog and Sox2. The three transcription factors co-occupy promoters of genes, whose translated proteins in turn are present in protein-complexes containing Oct4 ([147], simplified in **Figure 2**). Sall4, for instance, is a downstream target of all three master regulators and was found in the Oct4-centered protein-network purified from mouse embryonic stem cells [147]. This further underlines the interconnectivity of regulatory loops used by Oct4, Sox2 and Nanog in order to maintain pluripotency.
Considering the tight interplay between these three master regulators of pluripotency, it is plausible that overexpression of one or two transcription factors, for instance in OSKM-directed reprogramming, re-activates expression of endogenous Oct4, Sox2 and Nanog, the products of which in turn contribute to maintenance of their own gene expression guiding the cellular state towards pluripotency (reviewed in [148]).

1.2.4. Dissecting the reprogramming process

After disproving the dogma of irreversible differentiation, several research groups focused on dissecting the molecular and cellular events associated with nuclear reprogramming. Since the generation of iPSCs from murine embryonic fibroblasts (MEFs) occurs at a frequency of less than 0.1 % and is delayed by omission of c-Myc, it was of interest to reveal molecular mechanisms and roadblocks during reprogramming in order to elucidate how cellular identity can be reset [137,138,149]. It was demonstrated that reprogramming MEFs is a gradual process that requires 15 to 20 days upon transduction of somatic cells with retroviruses expressing Oct4, Sox2, Klf4, and c-Myc and results in fully reprogrammed MEF-iPSCs re-expressing endogenous pluripotency-associated genes including Oct4 and Nanog [137,138,150]. When reprogramming is induced by forced expression of Oct4, klf4, Sox2 and c-Myc, cells become independent of exogenous factors after ten to 12 days [150,151]. Regarding the controversial discussion whether reprogramming is a deterministic/hierarchic or a more probabilistic/stoichiometric process, evidence for both theories were found [152]. In one study, high-resolution live time–lapse imaging was used to trace the reprogramming

process from single donor cells to iPSC-colonies and an early specifying event during reprogramming was found to support the idea of a deterministic reprogramming process [153]. In contrast, profiling of 48 genes in single cells at various stages during the reprogramming process revealed heterogeneous gene expression at early stage of reprogramming that is followed by a Sox2-guided deterministic phase [154]. Data from both studies suggest a more complex theory of reprogramming by investigating not only alterations of mRNA and miRNA expression but also DNA-methylation, chromatin status and histone modifications [151]. Hochedlinger *et al.* revealed that reprogramming is accompanied by two deterministic phases at early and late stages of reprogramming, separated by a phase of stoichiometric events [151].

Focusing on the gradual process of changes in gene expression, it is shown that during the reprogramming process, MEFs undergo a process called mesenchymal-to-epithelial-transition (MET) encompassing downregulation of Snai1, a mesenchymal marker, and upregulation of E-cadherin [151]. This is confirmed by other studies showing that reprogramming is accompanied by transient expression of epithelial markers indicating that this conversion of cell fate is not the simple reversion of differentiation [155]. In addition, studies reveal that this MET observed during reprogramming is an essential process for successful iPSC generation [156,157]. In order to further characterize the transiently occurring MET, proteomic analysis of OKSM-induced reprogramming in MEFs was performed. An early stage of reprogramming (day 0-3) was identified as the time point of changes in protein expression pattern that represent this MET [158]. Further studies revealed that expression of epithelial markers and not the MET-conversion itself is the limiting factor to successfully induce pluripotency [159,160]. Detailed investigations showed that the requirement of E-cadherin expression can be bypassed by N-cadherin expression in order to induce MET in mesenchymal cells and restore the ability to acquire induced pluripotency. Taken together, these results showed that neither the process of MET nor the expression of E-cadherin is required for successful reprogramming. Instead, the adhesion capacity is mediated by more than one cadherin which enables reprogramming [161].

In addition to the MET process, another study demonstrated that cytoskeletal remodeling is essential for reprogramming. The authors identified expression of two kinases, which stabilize actin stress fibers in fibroblasts, as barriers for iPSC-generation from murine or human fibroblasts [162]. Using a kinome-wide RNAi-based screen, 734 kinase genes were targeted by lentivirus-mediated knockdown. Individual knockdowns were investigated regarding their effects on iPSC generation using Oct4-driven green fluorescence protein (GFP) expression in MEFs. Seven out of 59 kinases, which showed an effect on reprogramming, were further characterized and knockdown of the serine/threonine kinases

Tesk1 and Limk2 was found to promote EMT and disrupt actin filament structures during reprogramming [162].
In summary, reprogramming is comprised of a variety of different developmental processes including MET and cytoskeleton remodeling, and despite intense research many roadblocks and involved pathways are still to be elucidated.

1.2.5. Similarities between malignant transformation and reprogramming

Both, malignant transformation and reprogramming, lead to acquisition of unlimited self-renewal. Initial indications of connections between these two processes, which convert the functional fate of a cell, were found by identifying regulatory pathways common for both. One well-studied pathway involved in tumorigenesis that also plays a crucial role in reprogramming is p53-mediated signaling. Functional analyses of several p53-regulated genes identified by DNA microarray analyses demonstrated that the p53–p21 pathway serves as a barrier not only in tumorigenesis, but also in iPSC-generation [163]. This was confirmed by Utikal *et al.* who disclosed that the acquisition of immortality is a crucial and rate-limiting step towards the establishment of a pluripotent state in somatic cells [164].
Another pathway that is common between reprogramming and tumorigenesis is the metabolic switch in favor of glycolysis. The conversion from oxidative phosphorylation to glycolysis despite sufficient oxygen supply, which is observed after malignant transformation of cells, is well known as the Warburg-effect ([165], discussed in [166]). Interestingly, stimulation of glycolysis promotes, while blockade of glycolytic enzyme activity blunts reprogramming efficiency indicating that the metabolic conversion is also essential for the reprogramming process [167]. These data indicate that reprogramming and malignant transformation use identical mechanisms in order to change the cellular function either towards pluripotent characteristics or towards malignant properties. This is further supported by several other studies proving a connection between stem cell-associated gene expression and tumor initiation or progression, respectively. Oct4, a major pluripotency-associated marker, is detected not only in adult human stem cells but also in cultured tumor cell lines [168]. In addition, Oct4 is found to be expressed in different breast cancer cell lines in contrast to untransformed cell lines indicating a *de novo* acquisition of Oct4 expression in somatic cells after transformation [169,170]. In 2005, Hochedlinger and colleagues demonstrate that the activation of Oct4 using a doxycycline-inducible system is sufficient to induce dysplastic growths in epithelial tissues in a reversible manner. This suggests that aberrant expression of Oct4 is connected to uncontrolled proliferation and malignant transformation [135].
Oct4 is not the only member of the pluripotency-circuit known to be involved in carcinogenesis. In breast cancer cells, different studies showed a correlation between

Oct4/Nanog expression and clinical outcome or metastatic potential of cancer cells, respectively. Oct4 and Nanog also promote EMT in breast cancer stem cells and are associated with poor prognosis for breast cancer patients [171]. Another study showed that Nanog is involved in self-renewal and EMT in breast cancer cells supporting the hypothesis that these stem cell-associated factors are key players in the EMT and thus involved in cancer progression and metastasis [172]. Although overexpression of Nanog in the mammary gland of mice is not sufficient to induce breast cancer, it promotes migration and invasion of breast cancer cells indicating a major role in metastasis, not in tumor initiation [173]. In contrast, when Nanog is ectopically expressed together with Oct4, these transcription factors trigger Slug expression and enhance the tumor-initiating capability of lung adenocarcinoma cells. This work suggests an important interplay between these stem cell factors regarding tumorigenesis and tumor progression [174]. Moreover, Slug promotes tumor progression by stimulating Sox2 and Nanog expression in hepatocellular carcinoma, further underling the complexity and variety of stem cell maker-pathways that are affected during tumorigenesis [175].

A study comparing expression of pluripotency-associated genes in samples from cancer patients revealed that Sox2 is overexpressed at later stages in several cancers compared to early stages. Among others, this was shown for bladder carcinoma, glioma, head and neck cancers and breast tumors [176]. In addition, some studies discuss Sox2 and its expression as a marker for cell invasion in melanoma. Experimental knockdown of Sox2 in human melanoma cell lines possessing high levels of endogenous Sox2 resulted in decreased invasion potential *in vitro* with diminished expression of Mmp3. In addition, analysis of patient samples and xenograft melanomas disclosed that Sox2 is co-expressed with Mmp3 in regions of stromal infiltration [90]. This indicates a role of Sox2 in invading melanoma cells with Mmp3 being a potential mediator of proteolytic invasion during disease progression. Using tissue microarray analysis of nevi and melanomas, it was further demonstrated that co-expression of Sox2 and another neural progenitor cell biomarker, nestin, correlated with tumor progression. Moreover, co-expression of Sox2 and nestin labels cells exhibiting a rather spindle shape-like cell morphology compared to the epithelioid cell shape of Sox2 negative cells [177].

Another study manifests the link between ESC-like gene expression patterns and tumor progression since generally, more aggressive cancer subtypes with a rather de-differentiated phenotype demonstrate upregulation of ESC-like genes leading to worse clinical outcome. Genes that are activated by Nanog, Oct4 or Sox2, and encode transcription regulators were most consistently overexpressed in high-grade breast tumors [178]. These studies support the hypothesis that stem cell–like expression signatures observed in several tumors, is connected to disease progression.

All three members of the circuit of pluripotency are linked to tumor initiation and progression (reviewed in [179]) indicating that pluripotency-associated features can be at least in part affect different stages of carcinogenesis including malignant transformation, tumor maintenance and metastatic spreading. Thus, cancer research can significantly benefit from the detailed investigation of reprogramming.

1.2.6. Reprogramming of cancer cells

Since studies in reprogramming have revealed strong connections between the modulation of pluripotency and cancer, it is of interest to investigate whether reprogramming itself influences cancer and its characteristics. A historical study in frogs in 1969 showed that triploid tumor cells can be transplanted into activated and enucleated eggs leading to formation of swimming triploid tad-poles demonstrating pluripotency [180]. These data demonstrated that epigenetic alterations induced by factors present in the oocyte are sufficient for turning a tumor genome into that of a normal pluripotent cell that is capable of differentiating into different normal tissues. In 2003, a group re-assessed this hypothesis in mice and showed that blastocysts derived from medulloblastoma nuclei form post-implantation embryos with typical cell layers [181]. Another study supporting this hypothesis by Hochedlinger and colleagues revealed that a cancer cell can be reprogrammed into ESC-like cells by nuclear transfer of a malignant melanoma nucleus into an oocyte [182]. In 2011, researchers discovered that a tumor cell can be converted into a pluripotent status using just the oocyte extract without nuclear transfer further proofing the tremendous effect of pluripotency induction on tumor cell-characteristics [183].

After the discovery of iPSCs and reprogramming with defined factors, it is of great interest whether transcription factor-mediated reprogramming also applies for cancer cells. By now several studies have shown successful reprogramming of murine and human cancer cells towards a pluripotent stem cell-like cell type using overexpression of the classical Yamanaka factors, Yamanaka factors in combination with Nanog and Lin28 [184,185], with three factors only (Oct4, Klf4 and c-Myc) [141] or with two factors only [186] depending on the cancer cell-source. For example, a technical approach by Utikal *et al*. demonstrated that melanoma cells still remain susceptible to transcription factor-mediated reprogramming and that endogenously expressed pluripotency-associated factors, i.e. Sox2, facilitate reprogramming of these cells [141].

After revealing the possibility of cancer cell reprogramming, different studies were performed to identify the effects of pluripotency induction on tumor cells. It was shown, that reprogramming towards pluripotency reversed the aberrantly deregulated genes in non-small cell lung cancer cells *via* methylation changes and subsequent alteration of transcriptional activity. This leads to upregulation of silenced tumor suppressor genes and suppression of

oncogene expression indicating that epigenetic modifications can convert cancer-associated gene expression into expression patterns of normal cells [184]. In addition, it was shown that generation of so-called induced pluripotent cancer cells (iPCCs) from gastrointestinal cancer cell lines results in higher sensitivity to chemotherapeutic agents and differentiation-inducing treatment [185]. This work is of high interest especially regarding therapeutic challenges and drug resistance.

Investigations on human sarcoma cells showed that they can be reprogrammed and subsequently terminally differentiated with abrogation of tumorigenicity [187]. This revealed that reprogrammed cancer cells re-assemble all required *in vitro* criteria for full reprogramming towards pluripotency, although promoter methylation analysis discloses that cells remain in a de-differentiated state slightly before the mesenchymal stem cell differentiation stage. Thus, cancer cells can lose their tumorigenicity without the need to completely revert to an embryonic state [187]. Strikingly, they demonstrated that reprogrammed cells can be terminally differentiated into mature connective tissue and red blood cells and that this differentiation is accompanied with loss of both proliferation and tumorigenicity [187].

In addition, it was discovered that reprogramming of glioma-derived tumor cells and subsequent loss of tumorigenicity in differentiated cells is lineage-dependent. This indicates that only an epigenome associated with an alternative developmental lineage can suppress malignant behavior. In this study, glioma-derived iPCCs were directed to neuronal cell types, which were highly malignant upon xeno-transplantation. In contrast, when differentiated into non-neural cell types, sustained expression of reactivated tumor suppressors and reduced infiltrative behavior was observed [186].

Due to the loss of tumorigenicity in cancer cells upon reprogramming towards pluripotency, some researchers claim reprogramming to be a potential clinical application for anti-cancer treatment [187]. However, reprogramming *in vivo* as a therapeutic treatment does not meet the needs of clinical applications for obvious reasons, including unlimited self-renewal of iPSCs, spontaneous differentiation *in vivo* and tumor formation. Thus, reprogramming of cancer cells so far is not a clinical solution but rather an innovative tool to investigate particular cellular functions in order to understand underlying mechanisms in tumorigenesis. A recent study disclosed that overexpression of defined transcription factors in cells from a glioblastoma tumor resulted in the reprogramming of these cells into the tumor-propagating CSC-like cell [188]. This result indicates that tumor cells show divers responses to nuclear reprogramming and that this process can be used to establish *in vitro* systems for more detailed analyses of tumor progression including investigation of CSCs.

1.3. SNAI3 and the Snail transcription factor family

In this final section of the introduction the Snail transcription factor family will be discussed with the major focus on SNAI3, the most recent member.

SNAI3 belongs to the Snail gene family that is firstly identified in drosophila melanogaster and consists of three genes: Snai1/Snail, Snai2/Slug and Snai3/Smuc [189]. Today, human SNAI1 and SNAI2 are widely accepted to play important roles throughout development and disease such as cancer, whereas little is known about the recently discovered third family member, SNAI3 [190].

1.3.1. Identification and expression of SNAI3

In mouse, Snail1/Sna, Snail2/Slug, and Snai3/Smuc encode for transcriptional repressors that represent a subfamily of Snag zinc finger proteins (reviewed in [191]). All Snai family genes are evolutionarily conserved and despite identification of human SNAI1/SNAIL gene on chromosome 20ql3 and human SNAI2/SLUG gene on chromosome 8qll decades ago [192,193], human SNAI3/SMUC was detected *in silico* on chromosome 16q24.3 in 2002 for the first time [194]. The coding region of the human SNAI3 gene spans nucleotide position 320214-328221 of human reference genomic contig NT_010404.8 in the reverse orientation [194].

Using *in silico* differential expression analyses by listing sources of expressed sequence tags, human SNAI3 mRNA was shown to be only present in B cells [195]. However, using *in vitro* and *in vivo* assays, SNAI3 was further characterized and its function was evaluated in mice. Since SNAI3 can be isolated from murine adult muscle, it was named Smuc (Snail-related in muscle cells) [196]. Functional assays support a potential role for SNAI3 in muscle differentiation processes, since overexpression of SNAI3 in myoblasts repressed transactivation of muscle differentiation marker Troponin T [196].

In situ hybridization analysis at various stages of mouse development disclosed that SNAI3

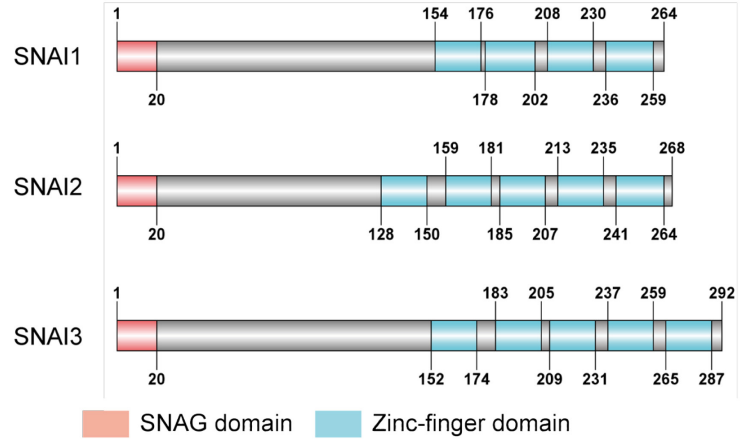

Figure 3 | SNAI-zinc finger protein structure
Displayed are protein domain structures of all SNAI-family members (SNAI1, SNAI2, SNAI3) that are confirmed to exist in human. Blue indicates zinc-finger domains and red indicates SNAG domain predicted by similarity.

expression cannot be detected until 12.5 days post-coitus (dpc). Its expression was exclusively observed in skeletal muscles and thymus at 13.5 and 15.5 dpc and these organs remained the major sites of SNAI3 expression until postnatal day two [197]. Thus, analysis of SNAI3's function during embryonic development revealed that it might play a role in morphogenesis of skeletal muscles and thymus at a relatively late stage of mouse development [197]. However, SNAI3 is not required for normal development in mouse since mice lacking SNAI3 show no obvious malformations [198].

1.3.2. Structure and molecular function of SNAI3

Figure 3 shows a schematic overview of all human SNAI transcription factors and their protein structure derived from UniProt data using Dog1.0 software [199]. All three transcription factors enclose a highly conserved carboxy (C)-terminal region containing four to six C2H2-type zinc fingers. This C-terminal region conducts sequence-specific interactions with DNA promoters, which comprise the so-called E-box sequence (CAGGTG) [200]. This specificity of target sequences is also shown for SNAI3 using electrophoretic mobility shift assays [196]. More specific, the 292 amino-acid-long polypeptide SNAI3 competes with basic helix loop helix transcription factors for binding DNA at the E-box sequence in a dose-dependent manner [194–196]. In addition, its non-zinc finger repressor domain is required for repressing transcription activity and each SNAI protein possesses an amino terminal SNAG (Snail and Gfi-1) domain, that is, at least for SNAI1 and SNAI2, known to interact with various histone deacetylases resulting in silencing of target gene expression [196,201,202].

1.3.3. Snail/Snai1 and Slug/Snai2 and their role in EMT

The first member of the snail gene family, Snai1/Snail, was shown to play an important role in mesodermal formation during embryogenesis by repressing expression of target genes [195,203]. Snai1 is required for successful gastrulation, since Snai1-mutant mice die at this stage of development due to defects in EMT and subsequent mesoderm formation [204]. Strikingly, it is not the absence of mesoderm formation that leads to ineffective development of the organism but rather the inability to downregulate E-cadherin. This repression of E-cadherin is required for migratory properties of cells and despite mesodermal marker expression, i.e. branchury, defective migration leads to abortion of development during gastrulation in the absence of Snai1 [204]. These data suggest a major role for Snai1 regarding cellular movement and adhesion rather than determining mesodermal cell fate.
Motility and migratory capacities are essential for the EMT process and both Snai1 and Snai2 were shown to play a major role in inducing this phenotypic transition in different contexts. Using EMT, cells can contribute to formation of many tissues during embryonic development but EMT also enables acquisition of invasive properties in epithelial tumors

(reviewed in [205]) and thus, genes involved in EMT are potential tumor-promoting targets for therapeutic interventions. Therefore, understanding the pathway of inducing SNAI-family transcription factors during EMT gives insights into tumorigenesis and especially into metastasis formation. Although the most popular function Snai1 and Snai2 are associated with is EMT induction, some developmental and pathological characteristics prove EMT-independent functions including survival *via* attenuation of cell cycle and resistance to pro-apoptotic stimuli upon growth factor deprivation or DNA-damage [206–208].

1.3.4. SNAI3 in cancer

The role of SNAI3 in pathological conditions has not been investigated in detail. The location of SNAI3 on chromosome 16q24.3 comprises a region that is affected in different types of cancer including hepatocellular carcinoma and ovarian cancer [194]. Also, preliminary expression screening *in silico* demonstrated its messenger expression in lung epidermoid carcinoma, germ cell tumors and skin cutaneous melanoma [194]. These data indicate a potential role for SNAI3 in tumor formation, maintenance or metastasis and in this study its role in melanoma progression is evaluated.

2. Objectives

Despite vast investigations of the reprogramming process, its impact and use for cancer research is far less elucidated. Some studies have shown that cancer cells can be converted into a pluripotent state and that this is accompanied by altered cellular function, including proliferation and tumor formation capacity. However, cellular alterations have only been assessed after complete conversion of tumor cells into the pluripotent state, which leaves the de-differentiation stages during reprogramming aside.

This project aims to dissect the process of reprogramming murine melanoma cells towards a pluripotent state in order to investigate the impact of directed de-differentiation on melanoma cells' function. In order to establish a platform that can be used for this approach, I first aim to convert murine melanoma cells into a pluripotent state. The main part of this project comprises the stepwise analysis of reprogramming melanoma cells at defined time points. Cellular function including migration and invasion will be investigated since especially in melanoma, de-differentiation is linked to higher metastatic potential. Thus, I aim to clarify

- whether or not partial reprogramming of melanoma cells is a stable and reproducible process
- if proliferation and/or invasion capacities changes during the process of reprogramming
- whether this *in vitro* model of partial reprogramming can be used to identify novel target genes with clinical relevance for melanoma progression

In summary, I aim to establish a novel *in vitro* system with potential to mimic metastasis-promoting events in melanoma cells in order to identify novel genes that are connected to invasive properties and might serve as biomarkers for melanoma progression.

3. Materials and methods

3.1. Materials

3.1.1. Reagents

Product description	Company	Branch
Agarose NEEO Ultra Qualität	Carl Roth	Karlsruhe, Germany
Amersham™ ECL™ Prime Western Blotting Detection Reagent	GE Healthcare	UK Limited Little Chalfont
cOmplete Mini - Protease Inhibitor Cocktail Tablets in EASYpacks	Roche Diagnostics Corporation Roche Applied Science	Mannheim, Germany
DAKO mounting medium	DAKO Agilent Technology	Hamburg, Germany
Dimethylsulfoxide (DMSO)	Dimethylsulfoxide (DMSO)	Dimethylsulfoxide (DMSO)
NuPAGE® LDS Sample Buffer	Invitrogen. ® Life Technologies	Darmstadt, Germany
NuPAGE® MES SDS Running Buffer	Invitrogen. ® Life Technologies	Darmstadt, Germany
Phusion® High-Fidelity DNA Polymerase	New England Biolabs GmbH	Ipswich, MA, USA
Propidium Iodide	Sigma Aldrich	Steinheim, Germany
RIPA Buffer	Sigma Aldrich	Steinheim, Germany
Rotiphorese® gel 30	Carl Roth	Karlsruhe, Germany
Skim milk powder	Fluka analytical	Steinheim, Germany
TMED (C6H16N2)	Carl Roth	Karlsruhe, Germany
Tween20	Applichem	Darmstadt, Germany

3.1.2. Materials

Product description	Company	Branch
Whatman chromatography paper	GE Healthcare	Buckinghamshire, UK
Immobilon-P Transfer Membrane Pore size 0.45 µM	Millipore	Schwalbach, Germany
NuPAGE® Novex® 4-12 % Bis-Tris Mini Gels	Invitrogen. ® Life Technologies	Darmstadt, Germany

3.1.3. Antibodies

Product description	Working dilution	Company	Branch
anti-Ki67 antibody (ab15580)	1:400	Abcam	Cambridge, UK
anti-mouse HRP labeled	1:10,000 (IB)	Jackson ImmunoResearch Inc.	Suffolk, UK
anti-Nanog ab80892	1:500 (IF)	Abcam	Cambridge, UK
anti-rabbit HRP labeled	1:10,000 (IB)	New England Biolabs GmbH	Ipswich, MA, USA
α-actinin Antibody sc-17829	1:10,000 (IB)	Santa Cruz Biotechnology	Heidelberg, Germany
Anti-SOX2	1:100	Novus Biologicals	Cambridge, UK
Anti-OCT4	1:500	Abcam	Cambridge, UK
Anti-S100B	1:400	Abcam	Cambridge, UK
Anti-SNAI3 (IHC)	1:400	Sigma-Aldrich	Steinheim, Germany
Anti-SNAI3 (western)	1:1000	Abgent	Maidenhead, UK

3.1.4. Cell culture materials

Product description	Company	Branch
2-Mercaptoethanol	Gibco® Life Technologies	Darmstadt, Germany
Alamar Blue®	AbD Serotec	Puchheim, Germany
Cholera Toxin	Sigma-Aldrich	Steinheim, Germany
DMEM AQmedia	Sigma-Aldrich	Steinheim, Germany
Doxycyline	Sigma-Aldrich	Steinheim, Germany
Dulbecco‘s Phosphate Buffered Saline	Sigma-Aldrich	Steinheim, Germany
ES-Cult™ Fetal Bovine Serum for Maintenance	STEMCELL Technologies SARL	Cologne, Germany
Fetal Calf Serum (FCS)	Biochrom	Berlin, Germany
X-tremeGENE Transfection Reagent	Roche	Mannheim, Germany
Glutamax DMEM	Sigma-Aldrich	Steinheim, Germany
Non-essential amino acids	Sigma-Aldrich	Steinheim, Germany
Penicillin Streptomycin	Sigma-Aldrich	Steinheim, Germany
Recombinant human TGFβ-1	PeproTech	Rocky Hill, NJ USA
Sodium Pyruvate	Sigma-Aldrich	Steinheim, Germany

Trypan Blue solution	Sigma-Aldrich	Steinheim, Germany
Trypsin	Sigma-Aldrich	Steinheim, Germany
12-0-tetradecanoyl phorbol acetate (TPA)	Sigma-Aldrich	Steinheim, Germany

3.1.5. Cell lines

	Cell line	Source	Authentification	Origin	Mutation
Human	SK Mel 28	ATCC	100 % (Multiplexion, Heidelberg Germany)	Malignant Melanoma	BRAF V600E
	SK Mel 30		100 % (Multiplexion, Heidelberg Germany)	Melanoma	NRAS Q61R
	MeWo	Ballotti lab, Nice	100 % (Multiplexion, Heidelberg Germany)	Malignant Melanoma	WT/WT
	A375	ATCC	100 % (Multiplexion, Heidelberg Germany)	Malignant Melanoma	BRAF V600E
	Fibroblasts	Lab intern	NA	Human skin biopsy	NA
Murine	Ret2	Prof. Umansky	NA	Ret mouse	NA
	HCmel12	Prof. Tüting	Yes (individual library at IDEXX BioResearch)	HC/mel mouse	HGF/ $CDK4^{R24C}$
	HCmel12-iPCCs	-	100 % identity of HCmel12 (individual library at IDEXX BioResearch)	HC/mel mouse	HGF/ $CDK4^{R24C}$
	HCmel17	Prof. Tüting	Yes (individual library at IDEXX BioResearch)	HC/mel mouse	HGF/ $CDK4^{R24C}$
	HCmel17-iPCCs	-	100 % identity of HCmel17 (individual library at IDEXX BioResearch)	HC/mel mouse	HGF/ $CDK4^{R24C}$
	MEF	Lab intern	NA	C57B/6J mouse	none

3.1.6. Plasmids

Plasmids	Used for	Source
pLU-EF1aL-rtTA3-iCherry	Partial reprogramming	The Wistar Institute
pLX304-human SNAI3	SNAI3 overexpression	Genecopoeia
pLX304-control	SNAI3 overexpression control	Genecopoeia

3.1.7. Kits

Product description	Company	Branch
Alkaline Phosphatase Staining Kit #II00-0055	Stemgent	Cambridge, USA
ARCTURUS PicoPure RNA Isolation Kit #KIT0204	Life Technologies	Darmstadt, Germany
BD Mouse Pluripotent Stem Cell Transcription Factor mAnalysis Kit	BD (Becton, Dickinson and Company)	Heidelberg, Germany
CytoSelect™ 24-Well Cell Migration and Invasion Assay	Cell Biolabs, Inc.	
First Strand cDNA Synthesis Kit #K1612	Fisher Scientific Germany GmbH	Schwerte , Germany
Pierce BCA protein assay kit	ThermoScientific	Karlsruhe, Germany
RevertAid RT Kit	ThermoScientific	Karlsruhe, Germany
RNase-free DNase set	Qiagen	Hilden, Germany
RNeasy Mini Kit	Qiagen	Hilden, Germany
Sybr®Green PCR mastermix	Applied Biosciences	Warrington, UK

3.1.8. Devices

Product description	Company	Branch
AB 7500 Real Time PCR machine	Applied Biosciences ® Life Technologies	Darmstadt, Germany
BD LSRFortessa™ cell analyzer	BD Biosciences™	Heidelberg, Germany
ImageQuant LAS 4000	GE Healthcare Life Sciences "	UK Limited Little Chalfont
Nanodrop Spectophotometer ND-1000	Peqlab Biotechnologie GmbH	Erlangen, Germany
Nikon Eclipse Ti Fluorescence microscope	Nikon	Düsseldorf, Germany
Nikon Eclipse TS100	Nikon	Düsseldorf, Germany
Tecan infinite F200 PRO	Tecan	Crailsheim, Germany

3.1.9. Solutions

	Description	Components
Immunoblotting	Blocking buffer	5 % Skim milk powder in Washing Buffer
	Washing Buffer	0,02 % Tween 20 1x TBS
	Transfer buffer	39 mM Glycin 48 mM Tris SDS (20 %) dH2O
	RIPA buffer	1x cOmplete Mini (Roche)

3.1.10. Software

Product description	Source
7500 Software v.2.0.6	Life Technologies, Darmstadt, Germany
ApE	University of Utah
Chipster	Chipster Open source
FlowJo 7.6.5	FlowJo Enterprise
ImageJ	NIH, USA
Mendeley	Mendeley Ltd., UK
NIS-Elements	Nikon
Prism 5.0	GraphPad Software, Inc. USA

3.1.11. Online database

Product description	Source
Human Protein Atlas	http://www.proteinatlas.org/

3.2. Methods

3.2.1. Cell culture

HCmel12 and HCmel17 cell lines were cultured in dulbecco's modified eagle's medium (DMEM) supplemented with 20 % FCS, 1 % penicillin (100 units/ ml) and streptomycin (100 µg/ ml), 1 % natriumpyruvat (100 mM), 1 % non-essential amino acids solution (10 mM), 0.01 % HEPES (1 M), 0.75 % β-mercaptoethanol, hereafter referred to as Mel medium.

Ret2 cells were cultured in RPMI supplemented with 10 % FCS, 1 % penicillin (100 units/ ml) and 1 % streptomycin (100 µg/ ml).

MEFs and all human cell lines were cultured in DMEM supplemented with 10 % FCS, 1 % penicillin (100 units/ ml) and streptomycin (100 µg/ ml), 1 % non-essential amino acids solution (10 mM) and 0.75 % β-mercaptoethanol, hereafter referred to as MEF medium.

Human fibroblasts were immortalized using transduction with SV40 and cultured for more than 5 passages before they were used for experiments.

All pluripotent cells were cultured in KnockOut™ DMEM supplemented with 10 % ES-FCS, 1 % glutamine, 1 % penicillin (100 units/ ml) and streptomycin (100 µg/ ml), 1 % non-essential amino acid solution and 100 U/ ml murine leukemia inhibiting factor (LIF), hereafter referred to as mESC medium. Established pluripotent cells were cultured on a layer of post-mitotic feeder cells (see section 3.2.5 for preparation) and splitted every other day using trypsin to generate single cell suspension.

MEF-conditioned mESC medium was generated by culturing MEFs (culture passage < 5) in mESC medium and medium was harvested every 12 hours.

All cell lines were cultured in a humidified incubator with 5 % CO2 and 95 % air.

3.2.2. Production of lentiviral particles

For production of infectious lentiviral particles, HEK293T cells were transfected with the target vector in combination with the packaging plasmids VSVG and Δ8.9 using Fugene (Roche) according to the manufacturer's protocol and supernatant was discarded 12 h after transduction. Viral supernatant was harvested 24 h, 36 h and 48 h after transfection and was directly used for transduction of target cells, or centrifuged at 13.500 rpm 5 h (4°C) and stored as concentrated virus, respectively.

3.2.3. Transduction with lentiviral particles

Cells were seeded with 40-50 % confluence and incubated for 12-24 h to fully attach. Medium was changed and virus added (500 µl – 1 ml supernatant or 5 µl concentrated virus, respectively) in the presence of 10 µg/ ml polybrene under S2 conditions. After 24 h cells were transduced again as described above before transduction was stopped after 48 h total

by washing cells three to five times with PBS. Cells were cultured in regular medium for at least 12 h to let them recover before performing further experiments.

3.2.4. Blasticidin selection

Cell line	Concentration (µg/ ml)
HCmel17-M2	17
Ret2	10
MEFs	10
Hepa 1.6	5
A375	5
Mewo	5
SKmel28	10
SKmel30	10

Table 1 | Blasticidin selection
Table summarizes blasticidin concentrations, which were used for selecting indicated cells lines.

Cells transduced with a plasmid containing a blasticidin cassette were selected with defined blasticidin concentrations optimized for each cell line. For optimization, non- transduced cells were seeded in 12-well plates at 50 % confluence and blasticidin was added in six different concentrations including a negative control without blasticidin (50, 17, 10, 5, 2.5 and 0 ng/ ml). Optimized selection concentration was defined as the concentration killing all cells after three days of selection **(Table 1)**.

3.2.5. Extraction of murine embryonic fibroblasts and feeder preparation

Mouse embryos from Bl/6 mice were dissected between 12.5 to 13.5 days postcoitum into 10 to 20 ml sterile PBS in a 100-mm tissue culture dish. Under sterile conditions, heads of embryos were removed using sterile scalpels. After transfer of the embryos to a clean 100-mm tissue culture dish containing sterile PBS, embryos were dissected manually into little pieces using scalpels. Embryos were dissociated by aspirating into a 10-ml syringe through a 16-G needle and incubated in trypsin/EDTA solution to 10 to 20 min in a 37°C incubator. After neutralization of EDTA/Trypsin solution with MEF medium, large tissue pieces were removed and cell suspension was centrifuged for 5 min at 1000 × g. Cells were plated on 150 mm^2 tissue culture plates and grown until confluent (2 to 5 days). For expansion, fibroblasts were plated on five to ten 75 cm^2 flasks and when confluent (3 to 5 days) cells were frozen with $1x10^6$ cells per aliquot in freezing medium. For direct use as feeder cells, MEFs were treated with mitomycinC for 4-5 h with a concentration of 8 µg/ ml. For storage, feeder cells were frozen in regular freezing medium.

3.2.6. Reprogramming (Stemcca and Stemcca-blasticidin)

In order to reprogram cells, a doxycycline-inducible polycictronic lentiviral vector encoding for Oct4, Sox2, Klf4 and c-Myc (Stemcca) was used in combination with a lentiviral vector encoding for the constitutively active M2 reverse tetracycline controlled transactivator (M2) as described previously by Sommer *et al.* (**Suppl. Figure 1a**, [209]). One day after the transduction, mESC medium containing doxycycline with a concentration of 1 µg/ ml was added to induce transgene expression. Fresh mESC medium supplemented with doxycycline was added every other day until iPSC colonies developed.

To establish fully reprogrammed induced pluripotent stem cells (iPSCs) or induced pluripotent cancer cells (iPCCs), colonies were picked, single cell suspensions were generated and transferred into dishes coated with dense feeder cells. Picked iPSCs/iPCCs were cultured on feeder cells in mESC medium without doxycycline and were replated until stable colonies could be passaged by trypsinization and single cell suspension. Stable iPSCs/iPCCs were used for further experiments.

For partial reprogramming, cells were transduced with a doxycycline-inducible polycictronic lentiviral vector encoding for Oct4, Sox2, Klf4 and a blasticidin resistance gene (Stemcca-blasti) in combination with a lentiviral vector encoding for the constitutively active M2 coupled to mCherry (obtained from the Wistar Institute, [210]). For producing the Stemcca-blasti vector, two DNA fragments were generated by overlapping PCRs. One fragment consisting of the complementary DNA (cDNA) of murine Sox2 coupled to the N-terminal part of the E2F protein was amplified form the Stemcca vector [210]:

PrimerA: GGTATCGTACATATGATGTATAACATGATGGAGACGGAGCTGAAG,

primerB:TTTCAACATCGCCAGCGAGTTTCAACAAAGCGTAGTTAGTACATTGCCCACTAC CCATGTGCGACAGGGGCAGTGTGCCGTTAATGGCCG.

The second fragment containing the cDNA of the blasticidin-S-deaminase (blasticidin) coupled to the C-terminal region of the E2A protein was amplified from a blasticidin selectable, modified Tet-O-cMyc-IRES-GFP vector, kindly provided by Christof von Kalle, NCT Heidelberg:

PrimerC:

GCTGGCGATGTTGAAAGTAACCCCGGTCCTATGAAGACCTTCAACATCTCTCAGC,

primerD: GGTTTATCGATTTAGTTCCTGGTGTACTTGAGGGGGAT.

To obtain the Sox2-E2F-blasticidin fusion fragment, a PCR was carried out under the following conditions: initial denaturation at 98°C for 1 min followed by 35 cycles of 98°C for 10 s, 50°C for 15 s, and 72°C for 45 s, followed by a 5 min at 72°C (primerA, primerD). The resulting fragment (Sox2-E2F-blasticidin) was gel-purified, NdeI- and ClaI-digested and inserted by directional cloning into the NdeI- and ClaI-digested Stemcca vector backbone

downstream of the internal ribosome entry site (IRES) element. All cloning procedures were performed with the help of Dr. Daniel Novak.
Cells were subjected to antibiotic selection starting at day three after transgene expression. Reprogramming process was stopped after indicated days and cells were used for further analysis in the absence of doxycycline.

3.2.7. Alkaline phosphatase staining

Cells were stained with the *Alkaline Phosphatase Staining Kit II* (Stemgent) according to the manufacturer's protocol. Briefly, cells were fixed and incubated with alkaline phosphatase substrate containing solution and the generation of red alkaline phosphatase-positive colonies was determined.

3.2.8. RNA extraction and cDNA synthesis

Total RNA was extracted using the RNeasy Mini Kit (Qiagen) or the ARCTURUS PicoPure RNA Isolation Kit (Life Technology), respectively, according to the manufacturer's protocol. Briefly, cells were lysed and RNA was purified with a column-based system. After washing and on-column DNAse treatment, RNA was eluted from the column using nuclease-free water. Concentration and integrity were measured using *NanoDrop 1000 Spectrophotometer V3.7.*
500 ng RNA was used to generate cDNA using the *first strand cDNA synthesis kit* according to the manufacturer's protocol. For all experiments, oligo-dT-Primers were used for cDNA-synthesis including the optional incubation step at 65°C and cDNA was diluted 1:10 in nuclease-free water before used for quantitative PCR.

3.2.9. Quantitative PCR (qPCR)

PCR was performed using SYBR Green in combination with the *Applied Biosystems® 7500 Real-Time PCR System* (Life Technologies) according to manufacturer's protocols. Used primer sequences are listed in **Table 2**. Expression of target genes was normalized to the housekeeping gene Gapdh after all cells were tested for low inter-sample-variance in Gapdh expression (≤2 cycles, data not shown). All primers were validated and primers with amplification efficiencies between 80 – 120 % were defined as functional. All samples were analyzed in technical triplicates and data was processed using the *7500 Software* and the delta(delta(Ct)) method. Graphs were generated using Prism Software and error bars show variance as 95 % confidence interval calculated in *7500 Software*.

	Amplified gene	Primer forward	Primer reverse
Murine	Oct4	TAGGTGAGCCGTCTTTCCAC	GCTTAGCCAGGTTCGAGGAT
	Sox2	TTAACGCAAAAACCGTGATG	GAAGCGCCTAACGTACCACT
	Nanog	TTGCTTACAAGGGTCTGCTACT	ACTGGTAGAAGAATCAGGGCT
	Ssea1	ACGGATAAGGCGCTGGTACTA	GGAAGCCATAGGGCACGAA
	Cdh2	CGTCCACCTTGAAATCTGCT	AAGGACAGCCCCTTCTCAAT
	Plastin3	TGGAGAGGGTCAGAAAGCAAA	AATCCACAACCGCCAAACTG
	Plat	AGTTCCTGCTGGGTGCTGTC	CGGGGACCACCCTGTATGTT
	Sall4	TCCAACATTTATCCGAGCACAG	TGGCAGACGAGAAGTTCTTTC
	Snai1	CACACGCTGCCTTGTGTCT	GGTCAGCAAAAGCACGGTT
	Snai2	TGGTCAAGAAACATTTCAACGCC	GGTGAGGATCTCTGGTTTTGGTA
	Snai3	CACTGCCACAGGCCGTATC	CTTGCCGCACACCTTACAG
	Sparc	CCAGGCAAAGGAGAAAGAAG	TTCAGACCGCCAGAACTCTT
	Twist1	CCCACCCCACTTTTTGACGA	GGGATGCCTTTCCTGTCAGT
	Mitf	CCAACAGCCCTATGGCTATGC	CTGGGCACTCACTCTCTGC
	Wnt5a	CTGGCAGGACTTTCTCAAGG	CTTCTAGCGTCCACGAACTCC
	Gapdh	TGTGAGGGAGATGCTCAGTG	TGTTCCTACCCCCAATGTGT
	Fst	GAGCAAGGAAGAGTGTTGCAG	CTCACACGTTTCTTTACAAGGGA
Human	GAPDH	GAAGGTGAAGGTCGGAGTC	GAAGATGGTGATGGGATTTC
	18S	GAGGATGAGGTGGAACGTGT	TCTTCAGTCGCTCCAGGTCT
	SNAI1	GAGGCGGTGGCAGACTAG	GACACATCGGTCAGACCAG
	SNAI2		
	SNAI3	GGAGACGCAGAGAGAAATCAAT	ACCTCGCTGACTTCCAAGG
	CD271	CGACAACCTCATCCCTGTCT	GCTGTTCCACCTCTTGAAGG
	DCT	GGTTCCTTTCTTCCCTCCAG	CCAACAGCACAAAAAGACCA
	MITF	GCTCACAGCGTGTATTTTTCC	TCTCTTTGGCCAGTGCTCTT
	TYRO	TTGTACTGCCTGCTGTGGAG	CAGGAACCTCTGCCTGAAAG
	TRP1	AGCAGTAGTTGGCGCTTTGT	TCAGTGAGGAGAGGCTGGTT
	CDH2	CTCCTATGAGTGGGAACAGGAACG	TTGGATCAATGTCATAATCAAGTGCTGTA
	CDH1	ATTCTGATTCTGCTGCTCTTG	AGTAGTCATAGTCCTGGTCTT
	ZEB2	TCCAGAAAAGCAGTTCCCTTC	CACACTGATAGGGCTTCTCG
	ZEB1	AGCAGTGAAAGAGAAGGGAATGC	GGTCCTCTTCAGGTGCCTCAG

Table 2 | Primers used for quantitative PCR
Table shows all primers that were used for cDNA amplification during quantitative PCR.

3.2.10. Immunoblotting

Proteins were extracted using radioimmunoprecipitation assay (RIPA) buffer (Invitrogen) including complete protease inhibitor cocktail (Roche). Protein yield was measured using the bicinchoninic acid (BCA) method (Thermo Scientific) prior to protein separation on 4-12 % Bis-Tris pre-cast polyacrylamide gels (Invitrogen) for 90 min at 150 V according to the manufacturers' protocol. Proteins were blotted to methanol-activated PVDF membranes for 12 h at 33 V and subsequently blocked for 1 h in 5 % BSA in PBS. After incubation with primary antibodies in blocking buffer over night at 4°C and 3 washing steps with TBST (each lasting at least for 10 min), secondary antibodies against either mouse- or rabbit-IgG labeled with horse-radish-peroxidase were incubated for 1-2 h at RT. After 3 additional washing steps signals were visualized using ECL™ Western Blotting Detection Reagents (GE Healthcare) according to the manufacturers' protocol and the gel imaging system *Image Quant™ LAS 4000* assuring to avoid detection of saturated signals. Quantification of proteins was performed using *ImageJ*.

3.2.11. Immunocytochemistry

Seeded cells were washed with PBS, fixed for 30 min using 4 % PFA. After several washing steps with PBS, unspecific binding sites were blocked with 2.5 % BSA in PBS, before cells were incubated with primary antibody. For not directly labeled primary antibodies, additional washing with PBS and incubation with a fluorescence-labeled secondary antibody followed. Cells were washed with PBS and nuclei were stained with PBS containing 1 µg/ mL of DAPI for 3 min. After mounting samples with DAKO mounting medium cells were analyzed using a fluorescence microscope (Nikon).

3.2.12. Flow cytometry

Induced pluripotent cells are generally cultured on a layer of post-mitotic MEFs as feeder cells. In order to reduce the feeder cell contamination in FACS, single cell suspension of pluripotent cells and feeder cells was cultured on a non-coated cell culture plate for 90 min. A portion of feeder cells attaches to the plate but pluripotent cells do not attach so that this "preplating" is used to enrich for pluripotent cells prior to FACS analysis. The remaining single cell suspension of reprogrammed cells was subjected to antibody staining using the *Mouse Pluripotent Stem Cell Transcription Factor Analysis Kit* (BD) according to the manufacturer's protocol. Briefly, cell suspension was fixed and stained by incubation with directly labeled antibodies against the target markers Oct4, Sox2 and Nanog. After incubation with primary antibodies cells were washed and resuspended in PBS containing 2 % FCS. Acquisition was performed using the *BD LSRFortessa*™ cell analyzer with

FACSDiva software with dead cell exclusion based on scatter profile **(Suppl. Figure 1b)**. *FlowJo7.6.5* software (Tree star) was used to analyze at least 100,000 events.

3.2.13. Proliferation assay

Cells were seeded in triplicates into black 96-well plates. After 72 h, medium was removed, 10 % *Alamar Blue REDOX indicator dye* (AbD Serotec) in medium was applied. Fluorescence was measured with excitation wavelength at 530-560 nm and emission wavelength at 590 nm after 4 h using the *Tecan Infinite® 200 PRO* plate reader. Fluorescence intensity was normalized to wells containing 10 % *Alamar Blue REDOX indicator dye* in medium only.

3.2.14. Migration and invasion assays

For all experiments regarding partial reprogramming, invasion capacity was assessed *in vitro* with the *CytoSelect™ 24-Well Cell Migration and Invasion Assay* (Cell Biolabs, Inc.) according to the manufacturer's protocol. Briefly, cells were seeded in starvation medium on top of a well containing an artificial basal membrane as a separation to FCS containing medium. After 24 h of incubation in a normal incubator cells that migrated through the membrane were detached and lysed with a lysis solution containing a fluorescent dye. Fluorescence emission correlates with number of cells and could be used to compare invasion potential of different cells.

For all experiments performed with human melanoma cell lines, migration and invasion potential was determined using the *Cultrex® 96 Well BME Cell Invasion Assay* (©2008, Trevigen, Inc.) according to the manufacturer's protocol. Briefly, cells were starved in serum-free MEF medium and transwell-chambers were coated with 0.1x basal membrane equivalent (BME) coating solution. After 24 h, $1x10^5$ cells per well were seeded on coated (invasion) and non-coated (migration) wells. After 24 h, cells that migrated into the bottom chamber were lysed and stained with a fluorescent dye. Fluorescence was measured at 485 nm excitation and 520 nm emission, respectively. Relative migratory and invasive potential was determined by comparing relative fluorescence units in order to cross-compare between different cell lines.

3.2.15. Whole genome expression array

All cells used in the hybridization-based whole genome expression microarray were cultured in mECS medium for seven days before extracting RNA to avoid medium-related alterations in gene expression. Total RNA extracted using the *ARCTURUS® PicoPure® RNA Isolation Kit* (Life Technology) was sent to the microarray unit of the *DKFZ Genomics and Proteomics Core Facility* who provided the Illumina expression profiling using whole genome BeadChip®

Sentrix arrays (mouseWG-6 v2). Differentially expressed genes were identified using *Chipster v2.12.0*. After quantile normalization of raw data using the Illumina normalization in *Chipster*, differentially expressed genes were compared between groups with indicated tests stated in figure legends. P-value cutoff was chosen with 0.05 if not otherwise indicated. Gene lists extracted after testing were imported into *MetaCore™ Data-mining and pathway analysis* (Thomson Reuters) for gene set enrichment analysis.

3.2.16. Tissue microarray analysis

All analyses involving human melanoma tissues were carried out according to the principles of the Declaration of Helsinki and were approved by the Medical Ethics Committee of the Medical Faculty Mannheim, University of Heidelberg. 37 melanocytic nevi and 26 primary melanomas were included in the tissue microarray (TMA) used in this study. TMA was generated at the core facility of the National Center for Tumor Diseases (NCT), Department of Pathology, University of Heidelberg. Each sample was included in duplicates to the TMA. Before TMA was analyzed, visualization of melanoma cells was performed by staining against S100B (Abcam).

Two blinded individuals applying a quantity/intensity- based IHC scoring system, which is displayed in **Figure 4**, performed scoring of tissue microarrays.

a

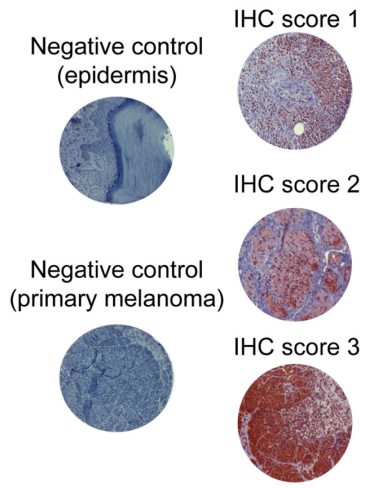

b

Percentage of positive cells	Score
0 %	0
1-25 %	1
26-50 %	2
51-75 %	3
76-100 %	4

Figure 4 | Tissue microarray analysis
Shown are samples of the tissue microarray used to catergorize melanoma patients according to the SNAI3 staining of their nevi and melanomas. **(a)** Left panel shows negative controls missing the primary antibody targeting SNAI3. Right panel shows different staining intensities. **(b)** The table shows the definition of quantity scores. IHC scores (see Figure 15) were calculated by multiplying intensity and quantity scores.
IHC=Immunohistochemistry

3.2.17. Immunohistochemistry

Tumors, which developed in vivo in NOD/SCID, C57B/6, or NSG mice, as well as human tissue from melanoma patients, were fixed in 4 % paraformaldehyde (PFA) for 24 h and were embedded in paraffin. 5 µm paraffin tissue sections were stained with hematoxylin and eosin. Additional staining against Ki67 (Abcam) or Snai3 (Sigma-Aldrich) was performed as indicated in figure legends.

TMA-slides were stained with indicating antibody (1:100) overnight. After washing with tris-buffered saline supplemented with tween-20 (0.05 %), slides were incubated with secondary, antibody (Dako EnVisionTM + System-HRP) for 60 min. After 15 min incubation with AEC and additional washing steps, samples were counterstained with hematoxylin and stabilized with mounting medium (Dako S3025) for storage and analysis.
All histological stainings were performed at the University Medical Center Mannheim with the help of Sayran Arif-Said.

3.2.18. Mouse experiments

After harvesting iPCCs, they were washed with PBS to remove FCS and medium supplements. Cells were resuspended in 100 µl – 300 µl PBS and cell suspensions were injected subcutaneously into both flanks of non-obese diabetic/severe combined immunodeficient (NOD/SCID) for teratoma assays or into non-obese diabetic/severe combined immunodeficient interleukin-2 receptor-γ chain null (NSG) mice for partially reprogrammed cells, respectively. Tumor development was observed and mice sacrificed by cervical dislocation whenever tumor size reached 1 cm (multiple tumors) or 1.5 cm (single tumors), respectively. Mice were sacrificed after 4 months the latest even without developing a tumor. Tumors were excised, fixed in 4 % PFA for 24 h and stored in PBS until they were embedded in paraffin for histological analysis.
For intravenous injections, single cell suspensions were washed once with PBS and filtered through a 40 µm-pore cell strainer. $2x10^5$ cells in 200 µl PBS were injected into the tail vein of C57BL/6 or NSG mice and mice were sacrificed 6 weeks after injections. Lungs were excised and fixed in Bouin's solution for 24 h. Lungs were stored in PBS until they were embedded in paraffin for hematoxylin and eosin (H&E) staining and histological analysis.
All animal experiments were conducted at the animal facility of the DKFZ (Heidelberg, Germany) in adherence to the standards of the German law for the care and use of laboratory animals.

3.2.19. Statistical analysis

Tests for all data except microarray data were performed using *GraphPad Prism version 5.00 (2007)* with indicated tests. Significance in two-tailed t-tests was assumed for $p \leq 0.05$ (*), $p \leq 0.01$ (**) or $p \leq 0.001$ (***), respectively.

4. Results

Reprogramming of cancer cells towards pluripotency provides an innovative tool to investigate cancer-associated processes from a novel perspective. Although reprogramming of cancer cells has been investigated using different cancer cell types, all induced alterations have only been assessed after complete conversion of tumor cells into the pluripotent state, which leaves the different stages during reprogramming aside. I established a novel *in vitro* model of partially reprogrammed melanoma cells that mimic the phenotype switch from highly proliferative, non-invasive to slowly proliferative, highly invasive cells.

The first section of this study describes the establishment of several assays that were used to evaluate pluripotency in reprogrammed cells. MEFs were reprogrammed *via* lentiviral transduction with defined transcription factors and subjected to gene expression analysis and *in vitro* differentiation. Next, two murine melanoma cell lines were reprogrammed and different assays were used for pluripotency confirmation including *in vivo* generation of teratomas. In the third section, the process of reprogramming melanoma cells is dissected by analyzing partially reprogrammed cells regarding their cellular characteristics.

4.1. Establishing different assays to confirm pluripotency in reprogrammed somatic cells

In order to establish the protocol for reprogramming somatic cells towards full pluripotency, MEFs were reprogrammed and subjected to a variety of pluripotency-validating assays. **Figure 5** shows a schematic overview of the technical set-up. MEFs were seeded in MEF medium and transduced with a polycistronic lentiviral construct encoding for Oct4, Sox2, Klf4 and c-Myc under the control of a doxycycline-inducible promoter (Stemcca-vector, **Suppl. Figure 1a**), together with a lentiviral vector encoding the constitutively active M2 reverse tetracycline controlled transactivator (M2). As a negative control, cells were transduced with M2 only in order to exclude that observed effects were due to the expression of the reverse transactivator or the presence of doxycycline. After transduction, culture conditions were changed from MEF medium to MEF-conditioned mESC medium and transcription of exogenous genes was induced by doxycycline administration. Cells were further cultured under stem cell promoting conditions (MEF-conditioned mESC medium) in the presence of doxycycline.

Figure 6a illustrates the continuous morphological change from a 2-dimensional monolayer of fibroblasts (non-reprogrammed cells, left panel) to 3-dimensional colonies evident at day 13 after transgene induction (right panel). At day seven, cells showed first signs of reprogramming with the appearance of spheroid cell clusters with blurred cell borders (day

nine) followed by formation of a colony with a clear and shiny border (day 11). 3-dimensional growth of reprogramming cells resulted in darker spots of dense cell clusters (day 13). At that stage, colonies were picked, resuspended in trypsin and single cells were replated on a layer of feeder cells (postmitotic MEFs). Doxycycline was withdrawn whenever colonies did not differentiate after picking and replating (between day 18-25 after transgene induction). After replating colonies for some passages, stable MEF-derived iPSCs (MEF-iPSCs) could be cultured on feeder cells in basic mESC medium in the absence of doxycycline and passaged as single cells. These cells were subjected to multiple assays to verify pluripotency.

First, cultivation of established MEF-iPSCs on feeder cells resulted in 3-dimensional growth of cells that displayed typical iPSC morphology of round shape, large nucleoli, and scant cytoplasm [113] **(Figure 6b)**. 24 hours after splitting, colonies were small and already showed shimmering borders typical for iPSCs **(Figure 6b,** left panel). Within four days cells grew 3-dimensionally and gave rise to large, packed, round-shaped iPSC-colonies **(Figure 6b,** middle panel). In addition, these colonies demonstrated alkaline phosphatase (AP) activity, which is a widely established sign for early reprogramming, indicating successful iPSC generation **(Figure 6b,** right panel). Lower magnification displays that

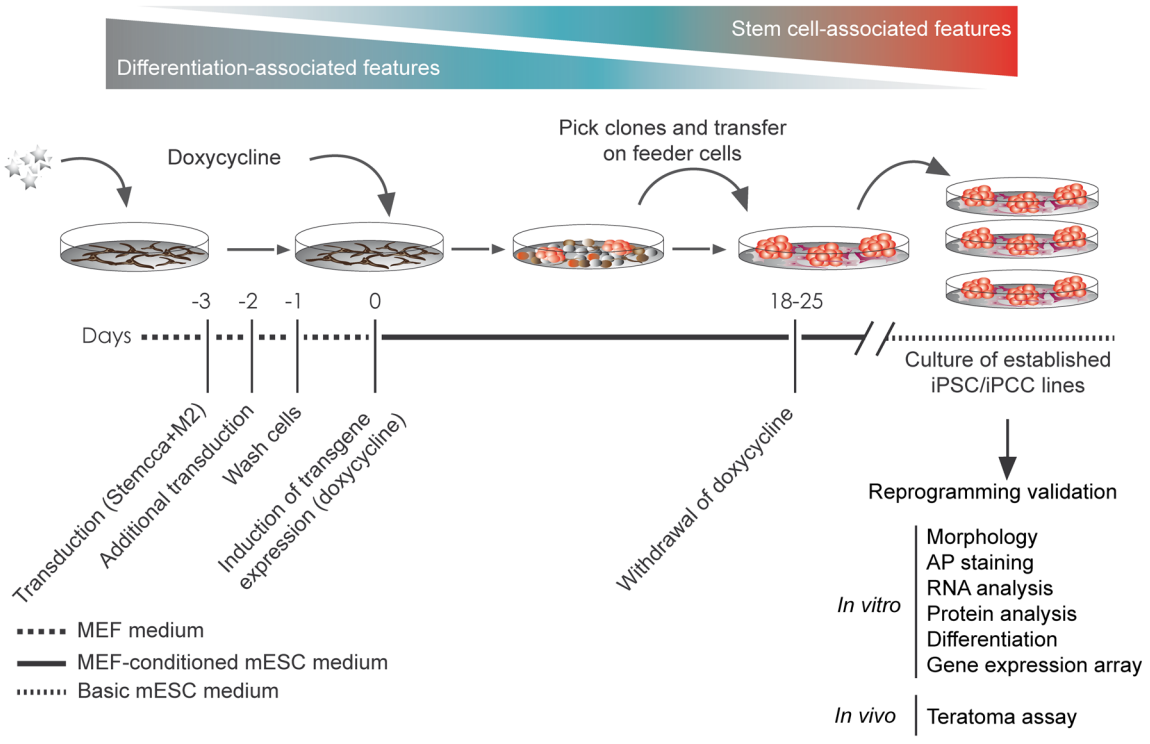

Figure 5 | Schematic overview of the reprogramming set-up using lentiviral transduction

Cells were transduced with M2 and doxycycline-inducible lentiviral vectors carrying the stem cell cassette while control cells were transduced with M2 only. Doxycycline administration induced transgene expression and upon colony formation, cells were picked and transferred to a dish coated with feeder cells (mitomycin-treated postmitotic MEFs) to be cultured as induced pluriotent stem cells (iPSCs) or induced pluripotent cancer cells (iPCCs). Pluripotency was validated using indicated *in vitro* and *in vivo* assays.

AP=alkaline phosphatase; M2=reverse tetracycline-responsible transactivator; MEFs=mouse embryonic fibroblasts; mESC=murine embryonic stem cells; RNA=ribonucleic acid

each colony was AP-positive and higher magnifications demonstrated clear boundaries between AP-positive colonies and feeder cells, which were clearly negative for this de-differentiation marker (**Figure 6b**, right panel, arrowheads). In order to prove concrete upregulation of known pluripotency-associated markers, cells were tested for expression of Oct4, Sox2 and Nanog. Endogenous Oct4, Sox2 and Nanog was prominently upregulated on RNA-level in reprogrammed cells whereas RNA of these genes was absent in parental cells **(Figure 6c)**. After reprogramming MEFs, the expression of endogenous Sox2 and Oct4 reached about 50 % of the expression level in murine embryonic stem cells (mESCs) and Nanog as one of the key players in the pluripotency circuit was upregulated almost 3-fold in MEF-iPSCs compared to mESCs. FACS analysis supported qPCR data by verifying protein expression of all three markers **(Figure 6d)**. 63.0 % of all single living cells were positive for SOX2. 59.6 % expressed NANOG, 66.8 % OCT4 and 46.7 % of all single living cells were OCT4/NANOG double positive. Next, I evaluated SOX2 expression in OCT4/NANOG double negative and OCT4/NANOG double positive subpopulations. Almost 90 % of cells that were negative for OCT4 and NANOG, did not show SOX2 expression indicating that this population was negative for all three markers and most likely consisted of feeder cells that were present due to the culture conditions for iPSCs. In line with that, almost 90 % of OCT4/NANOG double positive cells showed expression of SOX2 indicating a clear separation between triple negative and triple positive cells. Technical controls for FACS analysis indicated reliability since the isotype control did not show strong positive signals for the three markers **(Figure 6e)**. Of note, there was a subpopulation that was OCT4 positive but did not express NANOG (**Figure 6d**, second left panel). In order to determine whether this was due to alternating expression of NANOG within one iPSC-colony or caused by NANOG negative colonies, which retained in an intermediate state of reprogramming, immunocytochemical testing for NANOG protein was performed. It demonstrated expression and moreover nuclear localization of this transcription factor **(Figure 7a)**. As expected, post-mitotic feeder cells were negative for NANOG protein and showed nuclear DAPI staining only (indicated by white arrowheads, **Figure 7a** middle panel). NANOG protein was clearly expressed in all colonies and showed heterogeneous expression within individual colonies.

Taken together, qPCR and FACS data confirmed the stable state of pluripotency in MEF-iPSCs since analyses were conducted after cells were cultured without doxycycline, and thus without transgene expression, for at least five passages.

In addition to gene expression, also the differentiation potential of MEF-iPSCs was evaluated as a hallmark of pluripotency. Therefore, MEF-iPSC were cultured in hanging drops with approximately 50 cells per drop (50 µl MEF medium) for four days before they were pooled into 10 cm-culture plates in ten milliliters MEF-medium. Withdrawal of leukemia inhibiting

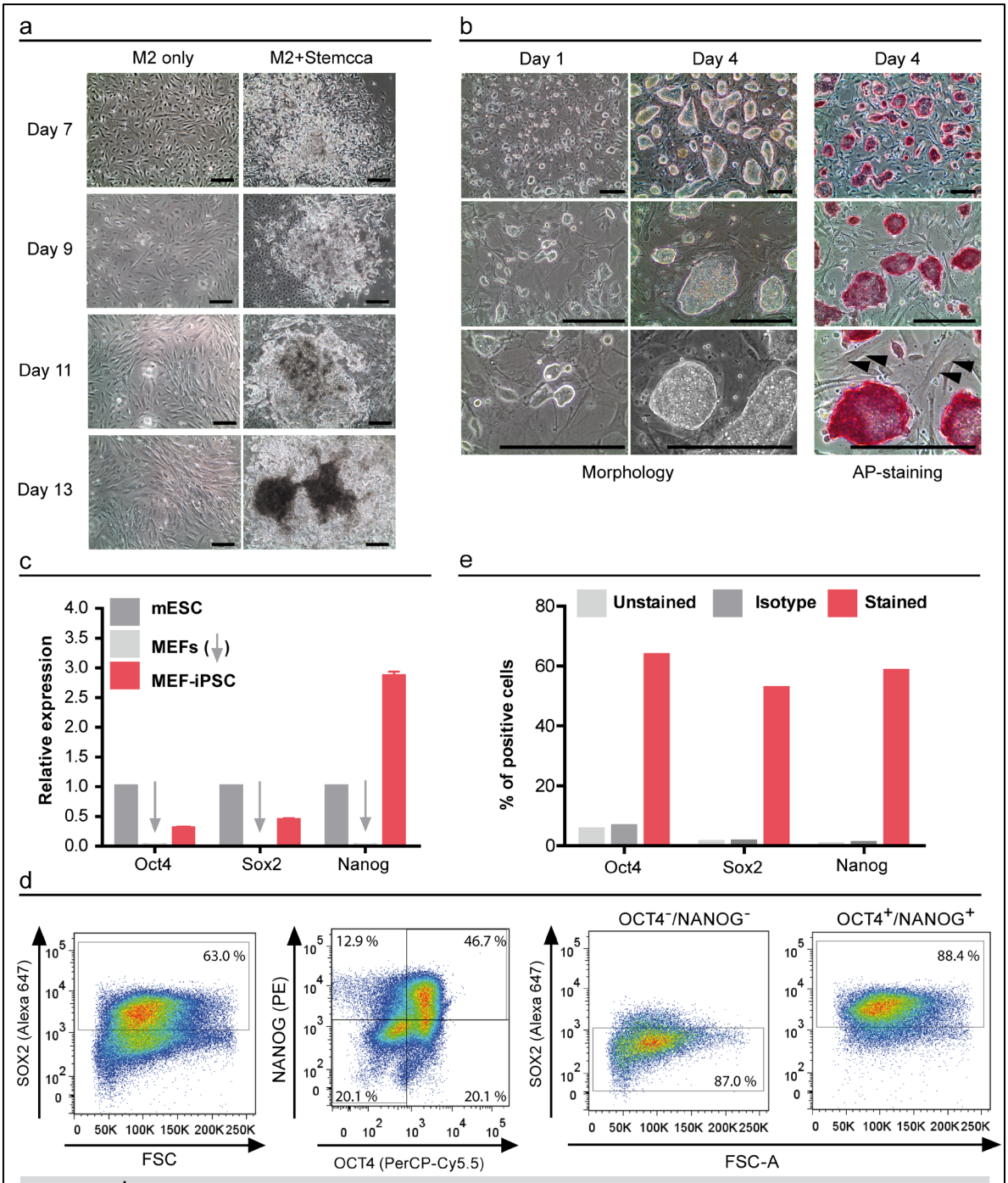

Figure 6 | Reprogramming murine embryonic fibroblasts

(a) Morphological alterations in MEFs during the reprogramming process at day seven, day nine, day 11 and day 13 after doxycycline administration (1 µg/ ml). Left panel displays M2-transduced control cells, right panel shows cells transduced with M2 and Stemcca. Bars=250 µm. **(b)** Morphology of MEF-iPSC-colonies one day (left panel) or four days (middle panel) after splitting and cultivation on feeder cells at passage five. Right panel shows AP staining of MEF-iPSCs at passage six. Arrow heads indicate fibroblasts. Bars=250 µm. **(c)** Endogenous expression of pluripotency-associated markers Oct4, Sox2 and Nanog using qPCR in original MEFs and corresponding MEF-iPSCs. Gapdh was used as endogenous control and mESCs as the reference sample. Graph displays mean and CI of technical triplicates. **(d)** FACS analysis of MEF-iPSCs regarding expression of pluripotency-associated markers OCT4, NANOG and SOX2. Left two panels show gating on single living cells, right two panels show gating on single, living, $Oct4^+/NANOG^+$ or $Oct4^-/NANOG^-$ cells. **(e)** Technical control of FACS showing percentage of marker-positive cells that were untreated, stained with isotype control antibodies or targeting antibodies at passage 16 (gated on single living cells).

AP=alkaline phosphatase; FACS=fluorescence activated cell sorting; Gapdh=glyceraldehyde 3-phosphate dehydrogenase; iPSC=induced pluripotent stem cells; M2=reverse tetracycline-responsible transactivator; MEF=murine embryonic fibroblasts; mESC=murine embryonic stem cell

factor (LIF) present in mESC medium and the addition of fetal calf serum (FCS) within MEF medium resulted in spontaneous differentiation of MEF-iPSCs. After cultivation in FCS-containing MEF medium for 23 days, this *in vitro* differentiation led to the appearance of MEF-iPSC-derived cardiomyocytes generating beating heart tissue, which could be identified by spontaneous contractions of cells **(Figure 7b)**.

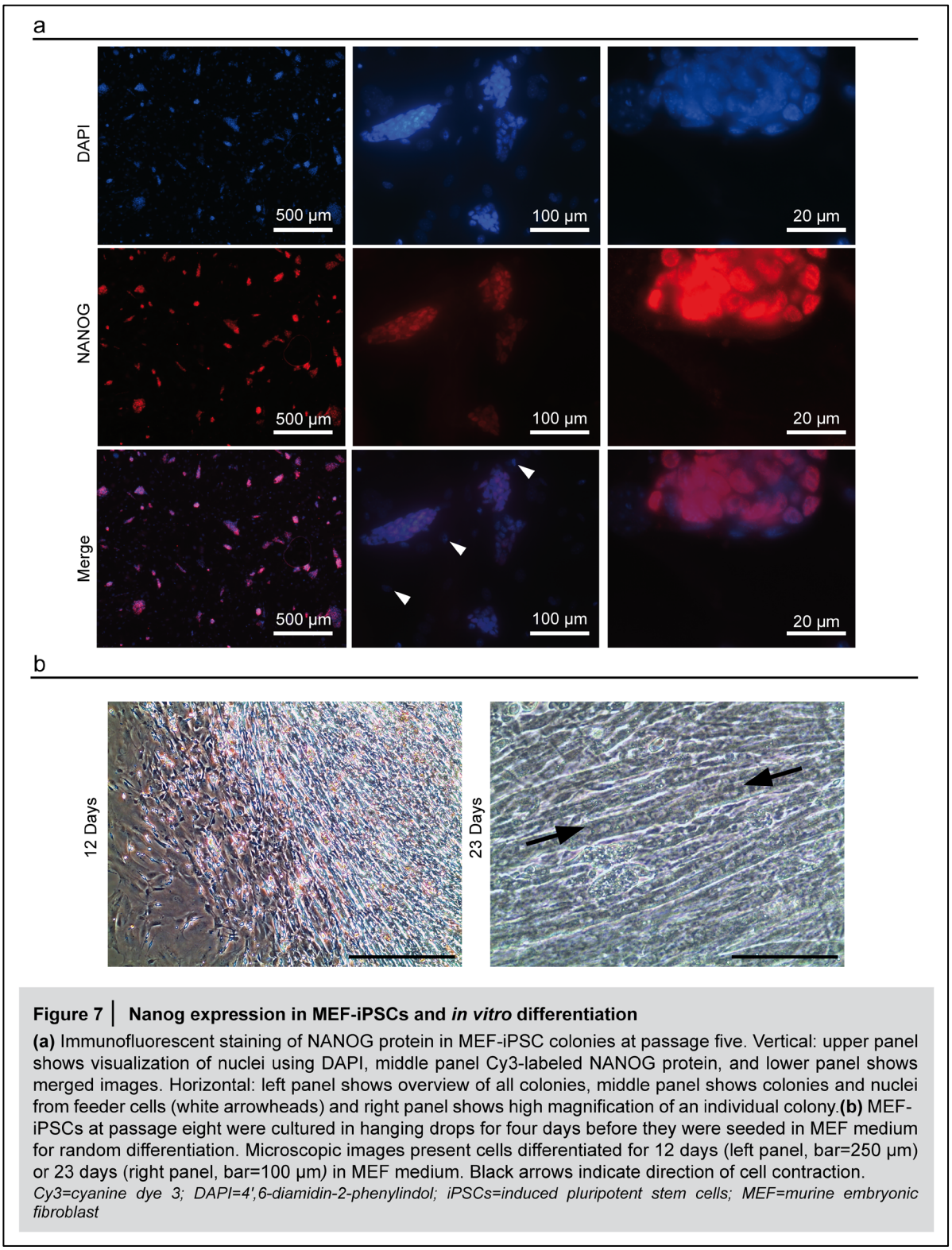

Figure 7 | Nanog expression in MEF-iPSCs and *in vitro* differentiation

(a) Immunofluorescent staining of NANOG protein in MEF-iPSC colonies at passage five. Vertical: upper panel shows visualization of nuclei using DAPI, middle panel Cy3-labeled NANOG protein, and lower panel shows merged images. Horizontal: left panel shows overview of all colonies, middle panel shows colonies and nuclei from feeder cells (white arrowheads) and right panel shows high magnification of an individual colony.**(b)** MEF-iPSCs at passage eight were cultured in hanging drops for four days before they were seeded in MEF medium for random differentiation. Microscopic images present cells differentiated for 12 days (left panel, bar=250 µm) or 23 days (right panel, bar=100 µm) in MEF medium. Black arrows indicate direction of cell contraction.
Cy3=cyanine dye 3; DAPI=4',6-diamidin-2-phenylindol; iPSCs=induced pluripotent stem cells; MEF=murine embryonic fibroblast

In summary, I successfully reprogrammed MEFs into MEF-iPSCs by using lentiviral vectors encoding for the four transcription factors Oct4, Sox2, Klf4 and c-Myc. MEF-iPSCs featured mESC-like morphology, alkaline phosphatase activity, endogenous expression of Oct4, Sox2 and Nanog, and they were differentiated into contracting cardiomyocytes indicating enhanced differentiation potential into non-fibroblast cells.

4.2. Reprogramming murine melanoma cell lines towards pluripotency

The process of reprogramming somatic cells towards a pluripotent stage is currently under thorough investigation and essential pathways have already been elucidated (see section 1.2.4). However, the reprogramming process can also be used to gain further insights into tumorigenesis and cancer progression (see section 1.2.5). Thus, a novel system to reveal further connections between pluripotency and cancerous features can be established by reprogramming cancer cells towards a pluripotent state (see section 1.2.6). In order to use this system for melanoma research, I aimed to reprogram two murine melanoma cell lines.

After establishing a variety of *in vitro* assays for proving pluripotency of reprogrammed cells, these assays were used to confirm successful reprogramming of two melanoma cell lines derived from the HGF/CDK4-melanoma mouse model (HCmel12 and HCmel17 cells, kindly provided by Prof. Thomas Tüting). These mice overexpress the hepatocyte growth factor (HGF) and carry an oncogenic mutation in the cyclin-dependent kinase 4 ($CDK4^{R24C}$). Due to these genetic modifications, these mice spontaneously develop a spectrum of primary melanomas with high penetrance during their first year of life [211,212]. HCmel17 and HCmel12 cell lines are derived from a spontaneous melanoma of these mice, and from a transplanted HGF/CDK melanoma, respectively.

According to the set-up for reprogramming MEFs **(Figure 5)**, HCmel12 and HCmel17 cells were seeded in their regular medium, transduced with a polycistronic lentiviral vector encoding for Oct4, Sox2, Klf4 and c-Myc under the control of a doxycycline-inducible promoter, together with a lentiviral vector encoding for a constitutively active M2. Upon doxycycline administration, both cell lines showed morphological changes during the first two weeks similar to those that were observed when MEFs were reprogrammed. **Figure 8a** displays representative microscopic images of HCmel17 cells during colony formation. Similar to MEFs, melanoma cells started losing their normal dendritic morphology at day seven after onset of reprogramming. Small round cells appeared, clustered to colonies (day nine), which finally showed blurred cellular boundaries (day 11). At day 13, large colonies consisting of densely packed cells were observed and after some passages of picking these colonies, cells were cultured on feeder cells in order to establish fully reprogrammed induced

pluripotent cancer cells (iPCCs). IPCC-lines were successfully established from both parental cell lines HCmel12 and HCmel17 (hereafter referred to as HCmel12-iPCCs and HCmel17-iPCCs, respectively). IPCC-colonies showed AP activity comparable to MEF-iPSCs **(Figure 8b)**. In addition, OCT4, SOX2 and NANOG protein was markedly increased as shown by FACS analysis **(Figure 8c-d)**. The percentage of SOX2 positive cells was increased from 1.56 % to 52.5 % and from 12.3 % to 76.4 % after reprogramming HCmel12 and HCmel17 cells, respectively (**Figure 8c**, right panel). Similar to MEF-iPSCs, HCmel-iPCCs showed separated positive and negative subpopulations regarding SOX2-expression**.** HCmel-iPCCs also showed OCT4/NANOG double positive cells (28.7 % or 34.6 % in HCmel12-iPCCs and HCmel17-iPCCs, respectively, **Figure 8c**). Comparable to MEF-iPSCs, more than 90 % of OCT4/NANOG double positive iPCCs also expressed SOX2 in both iPCC-lines indicating presence of a subpopulation that is positive for all three markers. In addition, 89.7 % and 72.0 % of NANOG/OCT4 double negative HCmel12-iPCCs and HCmel17-iPCCs, respectively, were also negative for SOX2 consistent with data derived from MEF-iPSCs **(Figure 8d)**. Thus, the negative population is most likely composed of remaining non-reprogrammed feeder cells due to the feeder-dependent culture method for iPCCs. In addition, immunocytochemical analysis of HCmel17-iPCC-colonies supported FACS data by showing nuclear staining of OCT4, SOX2 and NANOG **(Figure 8e)**. The heterogeneity of expression was in line with results from FACS analysis, since distribution was not homogenous within one iPCC colony.

After performing *in vitro* assays to validate the pluripotency of reprogrammed melanoma cells, the differentiation capacity of these cells was assessed *in vivo*. Upon subcutaneous injections of parental and reprogrammed cells into mice, the generated tumors were excised and subjected to histological analyses. Parental HCmel12 cells induced the generation of a rapidly growing pigmented melanoma, whereas the reprogrammed counterpart created a more solid, non-pigmented tumor **(Figure 9a)**. Histological analysis using hematoxylin and eosin (H&E) staining of paraffin-embedded tumor slices revealed that the HCmel12-derived melanoma consisted of a non-structured, homogenous tumor mass. Strikingly, the HCmel12-iPCCs-derived teratoma contained cells derived from different germ layers such as cartilage, epithelial cells and gland-like structures **(Figure 9a)**.

Parental cells of HCmel17 did not form tumors after injecting up to $1x10^6$ cells, whereas the reprogrammed counterpart generated a teratoma similar to the one derived from HCmel12-iPCCs after injecting two confluent wells of a 6-well plate **(Suppl. Figure 2)**.

The time needed for a tumor to reach a diameter of 1.5 cm varied extremely between HCmel12 with 19 days and HCmel12-iPCCs with more than 30 days **(Figure 9b)**. Of note, the number of injected iPCCs was different than that of parental cells because pluripotent cells are generally injected as clumps without previous single cell suspension and thus,

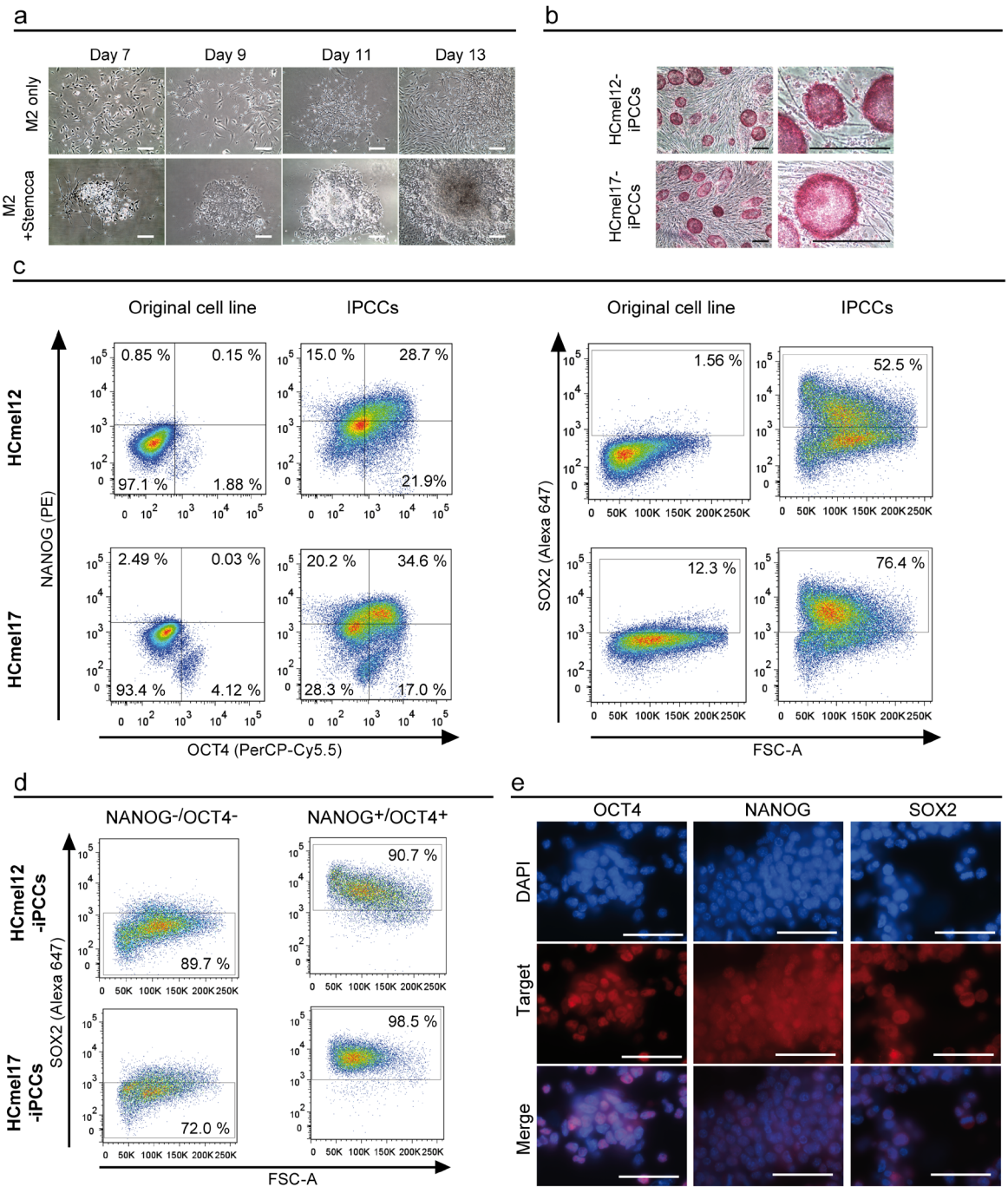

Figure 8 | Colony-formation and expression of pluripotency-associated markers in melanoma cells after reprogramming

(a) Morphological alterations in HCmel17 cells during the reprogramming process on day seven, day nine, day 11 and day 13 after doxycycline administration (1 µg/ ml). Upper panel shows control cells transduced with M2 only, whereas lower panel shows reprogramming-associated colony formation, bars=250 µm. **(b)** AP-staining of HCmel12- and HCmel17-iPCCs at passage 16 (five days after splitting), bars=250 µm. **(c)** FACS analysis of parental HCmel cell lines and HCmel-iPCCs for expression of pluripotency-associated markers OCT4, NANOG and SOX2, gated on single living cells. **(d)** FACS analysis of SOX2 expression in HCmel-iPCCs, gated on single living $OCT4^+/NANOG^+$ or $OCT4^-/NANOG^-$ negative iPCCs, respectively. **(e)** Representative fluorescence images of HCmel17-iPCCs seeded on coverslips and stained with fluorophore-labeled antibodies against indicated target protein. Upper panel shows nuclear visualization with DAPI, middle panel shows Cy3-labeled target protein and lower panel shows merged channels, bar=20 µm.

AP=alkaline phosphatase; Cy=Cyanine fluorophore; DAPI=4',6-diamidin-2-phenylindol; FACS=fluorescence activated cell sorting, FSC-A=forward scatter (area); iPCCs=induced pluripotent cancer cells, iPSCs=induced pluripotent stem cells, M2=reverse tetracycline transactivator; PE=phycoerythrin; PerCP=Peridinin-Chlorophyll, Stemcca=Stem cell cassette

counting is unreasonable. However, an 80 % confluent well of a 6-well plate generally contains more than 1x10^6 iPCCs. Therefore, despite lower cell number (5x10^5 cells), parental HCmel12 cells generated the melanoma faster than HCmel12-iPCCs created the teratoma. This indicates that reprogramming induced a reduction in proliferation capacity as well as changes in the cellular differentiation status. Decreased proliferation was confirmed by analysis of Ki67 expression on paraffin embedded tumor slices of the HCmel12-derived melanoma and the HCmel12-iPCC-derived teratoma. This marker is widely used to show proliferation since it is only expressed during G1-, S-, G2- and M-phase of the cell cycle. The melanoma derived from HCmel12 cells showed homogenous expression of Ki67, whereas the teratoma displayed a Ki67-positive area surrounding the tumor with Ki67-negative parts in the center, separated by a sharp border (**Figure 9c,** right panel, black arrowheads).

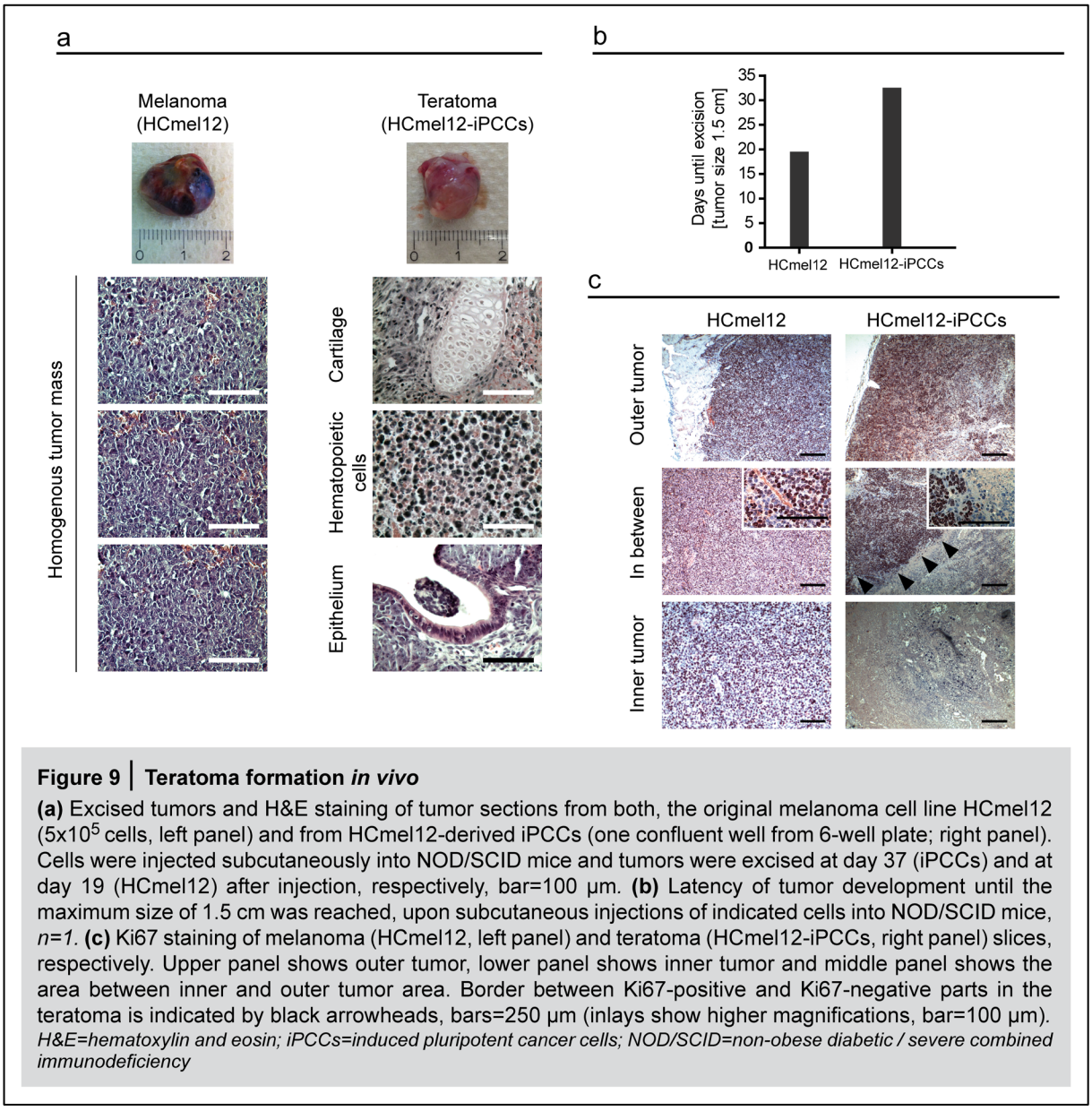

Figure 9 | Teratoma formation *in vivo*

(a) Excised tumors and H&E staining of tumor sections from both, the original melanoma cell line HCmel12 (5x10^5 cells, left panel) and from HCmel12-derived iPCCs (one confluent well from 6-well plate; right panel). Cells were injected subcutaneously into NOD/SCID mice and tumors were excised at day 37 (iPCCs) and at day 19 (HCmel12) after injection, respectively, bar=100 µm. **(b)** Latency of tumor development until the maximum size of 1.5 cm was reached, upon subcutaneous injections of indicated cells into NOD/SCID mice, *n=1.* **(c)** Ki67 staining of melanoma (HCmel12, left panel) and teratoma (HCmel12-iPCCs, right panel) slices, respectively. Upper panel shows outer tumor, lower panel shows inner tumor and middle panel shows the area between inner and outer tumor area. Border between Ki67-positive and Ki67-negative parts in the teratoma is indicated by black arrowheads, bars=250 µm (inlays show higher magnifications, bar=100 µm).
H&E=hematoxylin and eosin; iPCCs=induced pluripotent cancer cells; NOD/SCID=non-obese diabetic / severe combined immunodeficiency

In vitro assays in combination with *in vivo* differentiation confirmed successful reprogramming of melanoma cells towards full pluripotency **(Figure 8-9)**. Next, differences between global gene expression signatures of parental melanoma cells, melanoma cell-derived iPCCs and control MEF-iPSCs were examined using total RNA for a hybridization-based expression microarray **(Figure 10a)**. Total RNA was used in technical triplicates and microarray data were subjected to analysis using *Chipster* software. Gene expression data were quantile normalized (*Illumina quantile normalization*) and filtered for differentially expressed genes (empirical Bayes test, $p \leq 0.05$). Visualization using heatmap presentation demonstrated strong similarities between both iPCC-lines and vast differences between parental melanoma cell lines and their reprogrammed counterparts. Strikingly, the similarity between iPCCs and MEF-iPSCs was higher than the similarity between melanoma cells and their pluripotent equivalent indicated by the hierarchical cluster that shows Pearson distance. However, gene expression patterns between MEF-iPSCs and tumor-derived iPCCs revealed substantial differences so that iPCCs clustered together but with some distance to normal MEF-derived iPSCs. Heatmap presentation shows that some genes downregulated in MEF-iPSCs were still expressed in iPCCs and *vice versa* **(Figure 10a)**. The melanocyte-associated gene set "*upregulation of MITF in melanoma*" was among the top ten pathways of commonly downregulated pathway maps in reprogrammed melanoma cells compared to their parental cell lines (map #6, **Suppl. Table 1**) with typical differentiation markers like Sox10, Tyrp2, Tyrp1 and Mlana being significantly downregulated **(Figure 10b)**.

All gene ontology processes that were up- or downregulated after full reprogramming of melanoma cells are summarized in **Table 3**. Of note, the enrichment of processes involved in basic system development and differentiation indicated the complete conversion of differentiated cells into a cell type with higher developmental potential. **Figure 10c** illustrates one of the networks enriched in differentially expressed genes when HCmel17 cells were

-log (p-value)	Pathway map
>25 (HCmel17) >35 (HCmel12)	System development
>24 (HCmel17) >30 (HCmel12)	Anatomical structure development
>24 (HCmel17) >30 (HCmel12)	Developmental processes
>25 (HCmel17) >30 (HCmel12)	Multicellular organismal developmental process
>24 (HCmel17) >25 (HCmel12)	Cell differentiation
>20 (HCmel17) >25 (HCmel12)	Single organism developmental process
>20 (HCmel17) >25 (HCmel12)	Cellular development process
>20 (HCmel17) >24 (HCmel12)	Anatomical structure morphogenesis
>15 (HCmel17) >24 (HCmel12)	Single– multicellular organism process
>15 (HCmel17) >24 (HCmel12)	Organ development

Table 3 | Gene set enrichment analysis of HCmel12- and HCmel17-iPCCs
Gene set enrichment analysis of pathway maps involving genes up- or downregulated after reprogramming HCmel12 and HCmel17 melanoma cells towards pluripotency. Table shows significant enrichment (p-value) of differentially regulated genes in indicated pathways. Upper -log(p) represents enrichment in HCmel17 cells, lower -log(p) enrichment in HCmel12 cells cells.
Analysis tools: Chipster, Metacore

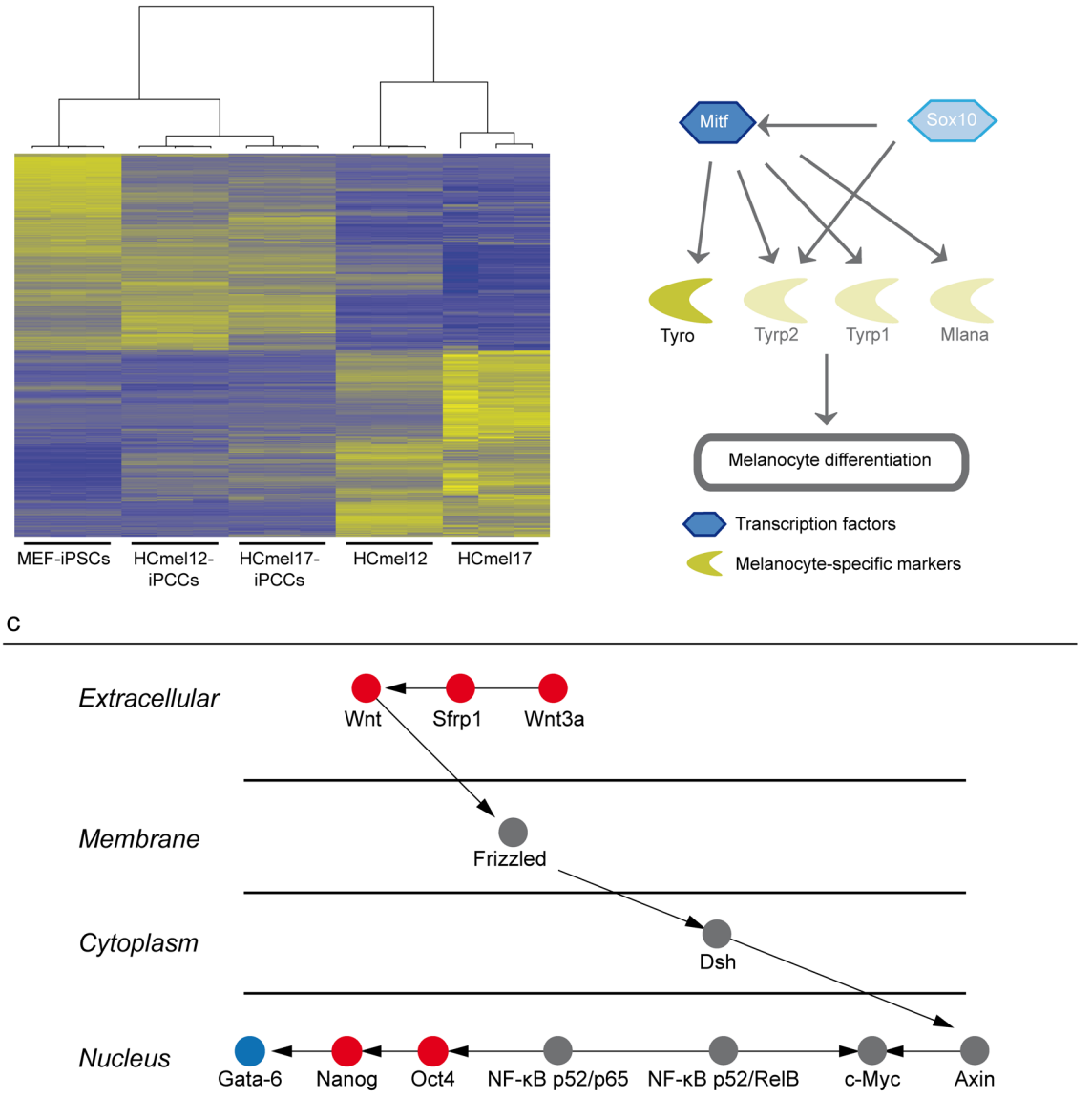

Figure 10 | Whole-genome expression analysis of melanoma cell line- derived iPCCs

Total RNA from HCmel12 (P11), HCmel17 (P10), MEF-iPSC (P16), HCmel12-iPCCs and HCmel17-iPCCs cultured on feeder cells (P24 or P25, respectively) was used for hybridization based gene expression microarray in technical triplicates. **(a)** Heatmap presentation displays differentially up- and downregulated genes determined by several groups test (empirical Bayes) with a p-value threshold of 0.05 (p-value adjustment with BH-method). Each row stands for a gene and each column represents a sample, n=3. Yellow indicates upregulation, blue indicates downregulation. Clustering was performed using *Chipster* and is displayed as Pearson distance. **(b)** Selected genes derived from pathway #6 *Upregulation of MITF in melanoma* (Suppl. Table 1) that is enriched in genes that are differentially regulated. Fade blue and yellow indicate downregulation of genes after reprogramming. **(c)** Representative network of differentially regulated genes in HCmel17-iPCCs compared to HCmel17. Network #6 *Signal transduction: WNT signaling* was among the most relevant networks (Suppl. Table 2). Displayed is are genes involved in this network. Red circles indicate upregulation, blue circles downregulation and grey indicates not-altered gene expression.

Axin=axis inhibition protein; BH=Benjamini and Hochberg; Dsh=Dishevelled; iPCCs=induced pluripotent cancer cells; Gata6=Transcription factor GATA-6; iPSCs=induced pluripotent stem cells; MEF=murine embryonic fibroblasts; NF-κB=nuclear factor kappa-light-chain-enhancer of activated B cells protein complex; *P=culture passage; Sfpr1=Secreted frizzled-related protein 1; Wnt3a=Wingless-type MMTV integration site family member 3a*

compared to HCmel17-iPCCs (see also **Suppl. Table 2**). Consistent with data from qPCR and FACS analyses, the hybridization-based microarray detected upregulation of Nanog and Oct4 mRNA indicated by red circles, even in the absence of transgene expression. Interestingly, also the canonical Wnt-signaling pathway showed upregulation of specific genes that are known to be involved in established pluripotency, including Wnt and Wnt3a [213]. In addition, the mesoderm-lineage specifier Gata6 was significantly downregulated, illustrated by the blue circle, which indicates successful repression of lineage specifiers in combination with enhanced pluripotency-associated gene expression **(Figure 10c)**.

In summary, two melanoma cell lines were successfully reprogrammed. Both reprogrammed melanoma cell lines showed criteria of full pluripotency *in vitro* as well as *in vivo* demonstrated by gene expression and teratoma formation. Of note, differences between MEF-iPSCs and HCmel-iPCCs regarding global gene expression were observed indicating that iPCCs are still distinguishable from normal iPSCs. However, iPCCs are distinguishable from their parental melanoma cells lines and showed strong similarities with MEF-iPSC. This indicates that forced expression of four transcription factors resulted in resetting the complete molecular signature of HCmel cells. In line, subcutaneously injected reprogrammed HCmel-iPCCs showed decreased proliferation indicating that pushing melanoma cells towards a pluripotent state alters their gene expression patterns and affects their cellular phenotype.

4.3. Partial reprogramming of HCmel17 cells

Having observed decreased proliferation by reduced Ki67 expression after reprogramming melanoma cells towards full pluripotency, the question arose, whether cellular changes were exclusively evident in the pluripotent state of melanoma cells or already detectable at earlier stages during reprogramming.

Therefore, I established a novel protocol that allows to study a pure population of cells transduced with both, M2 and the reprogramming factors **(Figure 11)**. HCmel17 cells stably co-expressing the M2 coupled to the fluorophore mCherry were generated (cells are hereafter referred to as HCmel17-M2) and sorted for mCherry expression with purity higher than 85 % using FACS **(Suppl. Figure 3)**. In order to enable selection of transgene-expressing cells, we substituted c-Myc from the doxycycline-inducible Stemcca-vector with a blasticidin resistance cassette (Stemca-blasti, **Figure 12a)** since c-Myc was endogenously expressed in HCmel17-M2 cells **(Suppl. Table 3)**.

HCmel17-M2 cells were seeded in 6-well plates in their regular medium and transduced with the Stemcca-blasti vector. Following another transduction 24 hours later, cells recovered overnight before they were used for further experiments. After three days of transgene expression induced by doxycycline administration in mESC medium, blasticidin was added to

select Oct4, Sox2 and Klf4-expressing cells. This protocol was established for investigating cellular functions at defined steps during reprogramming **(Figure 11)**.

After ten, 12 and 18 days, cells were subjected to different analyses. All assays were performed in the absence of doxycycline in order to inhibit further reprogramming and maintain the particular de-differentiation status. As a control, HCmel17-M2 cells were transduced with the Stemcca-blasti vector but not induced with doxycycline so that cells did not express transgenes. These control cells were cultured in the absence of doxycycline throughout all experiments.

By day ten after transgene induction cells showed morphological alterations, e.g. clustering of small cells into groups with barely visible cellular borders (**Figure 12b**, right panel). Bigger clusters and colony formation were evident at day 12 and 18. In addition, AP-activity as a general indicator of early reprogramming and de-differentiation was detectable already at day ten with increasing activity at day 12 and 18 after transgene expression (**Figure 12c**, right panel). This indicated successful reprogramming in the absence of c-Myc. Cells that were cultured in the absence of doxycycline kept their normal morphology (**Figure 12b**, left panel)

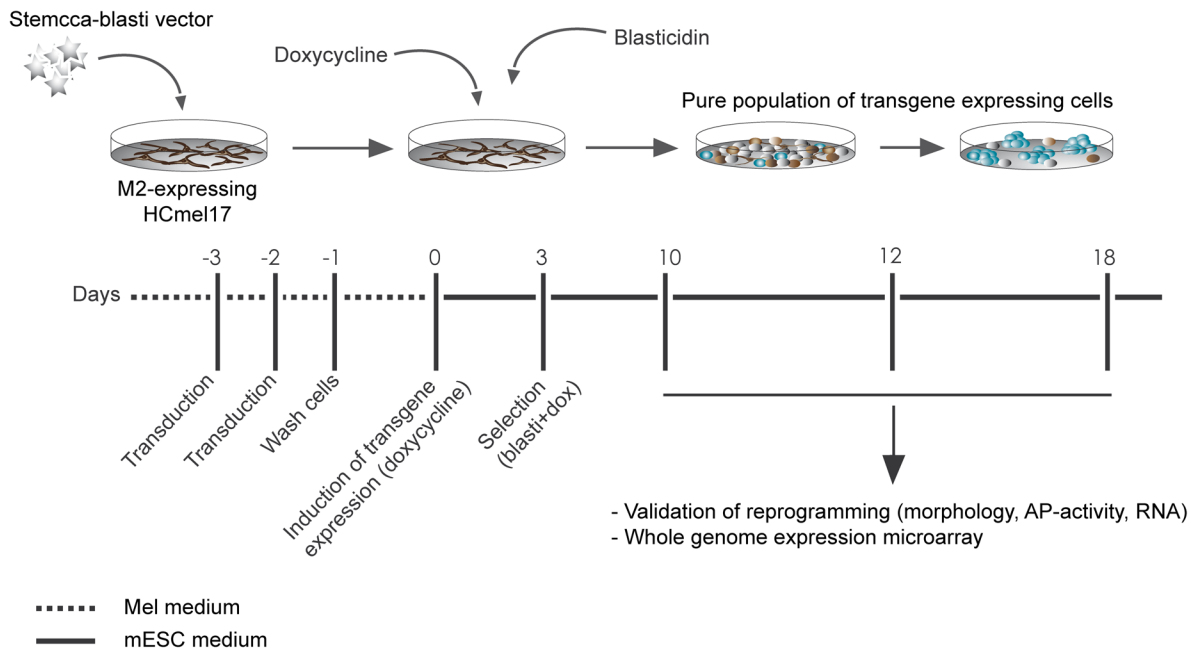

Figure 11 | Schematic overview of the set-up for dissecting the reprogramming process in HCmel17 cells

HCmel17 cells stably expressing M2 were transduced with a doxycycline-inducible Stemcca-vector carrying a blacticidin resistance cassette (Oct4, Sox2, Klf4, blasticidin). After three days of transgene expression *via* doxycycline administration, cells were subjected to blasticidin selection and cultured in the presence of doxycycline and blasticidin for the remaining time. Time points of harvesting cells and analyzing partially reprogrammed cells were day ten, day 12 and day 18 after induction.

AP=alkaline phosphatase; blasti=blasticidin; dox=doxycycline; mESC=murine embryonic stem cell, M2=M2-rtTA; Stemcca=stem cell cassette

and remained AP-negative indicating that AP-activity was a result of transgene expression (**Figure 12c,** left panel).

Consistent with the indication of general de-differentiation, expression of Mitf, the key differentiation factor of the melanocytic lineage, was downregulated during the process of reprogramming **(Figure 12d)**. Mitf levels decreased by more than 50 % by day 12 compared to basal level expression of this transcription factor in non-reprogrammed control cells. Accordingly, expression of Sall4, which is a downstream target of Oct4, Nanog and Sox2 [147] and thus, an indicator of reprogramming, was increased in reprogrammed cells compared to control cells. These results demonstrated not only de-differentiation but also directed reprogramming towards pluripotency **(Figure 12d)** [214]. Since Sall4 is not expressed in non-reprogrammed control cells, expression levels were normalized to MEF-iPSCs explaining the low increase in expression level (0.2 %). However, when comparing non-reprogrammed cells to reprogrammed cells at day 12 or day 18, a clear elevation of Sall4 expression was observed.

In order to analyze global changes in gene expression and to further validate the stability of this biological process, non-reprogrammed control cells and cells reprogrammed for ten, 12 and 18 days were subjected to a hybridization-based gene expression microarray in independent biological triplicates. Completely reprogrammed HCmel17-iPCCs as well as MEF-iPSCs from previous experiments were included into the analysis. **Figure 12e** shows the heatmap of all significantly expressed genes ($p \leq 0.005$). Every row represents a gene (292 genes in total) and every column one sample.

Biological replicates from each sample clustered closely together indicating a biologically stable process of de-differentiation during partial reprogramming. MEF-iPSCs and HCmel17-iPCCs grouped together with some distance to partially reprogrammed cells. Non-reprogrammed control cells (-Dox) represented the group with the largest distance compared to all non-parental cells. The shift from up- to downregulated and from down- to upregulated genes reflected the gradual change of global gene expression during reprogramming. Interestingly, the gene expression signature in cells partially reprogrammed for ten to 18 days revealed a group with significant difference in gene expression when compared to their parental cell line or to their fully reprogrammed counterparts **(Figure 12e).** Gene set enrichment analysis of genes downregulated in partially reprogrammed cells (12 days) compared to non-reprogrammed cells included processes related to *positive regulation of cell differentiation* indicating the switch from a differentiated melanoma cell towards a more de-differentiated type of cell **(Suppl. Table 4)**.

In summary, these results indicate that HCmel17 cells were successfully reprogrammed to different stages of de-differentiation. Notably, this complex biological process could be reproduced with high accuracy.

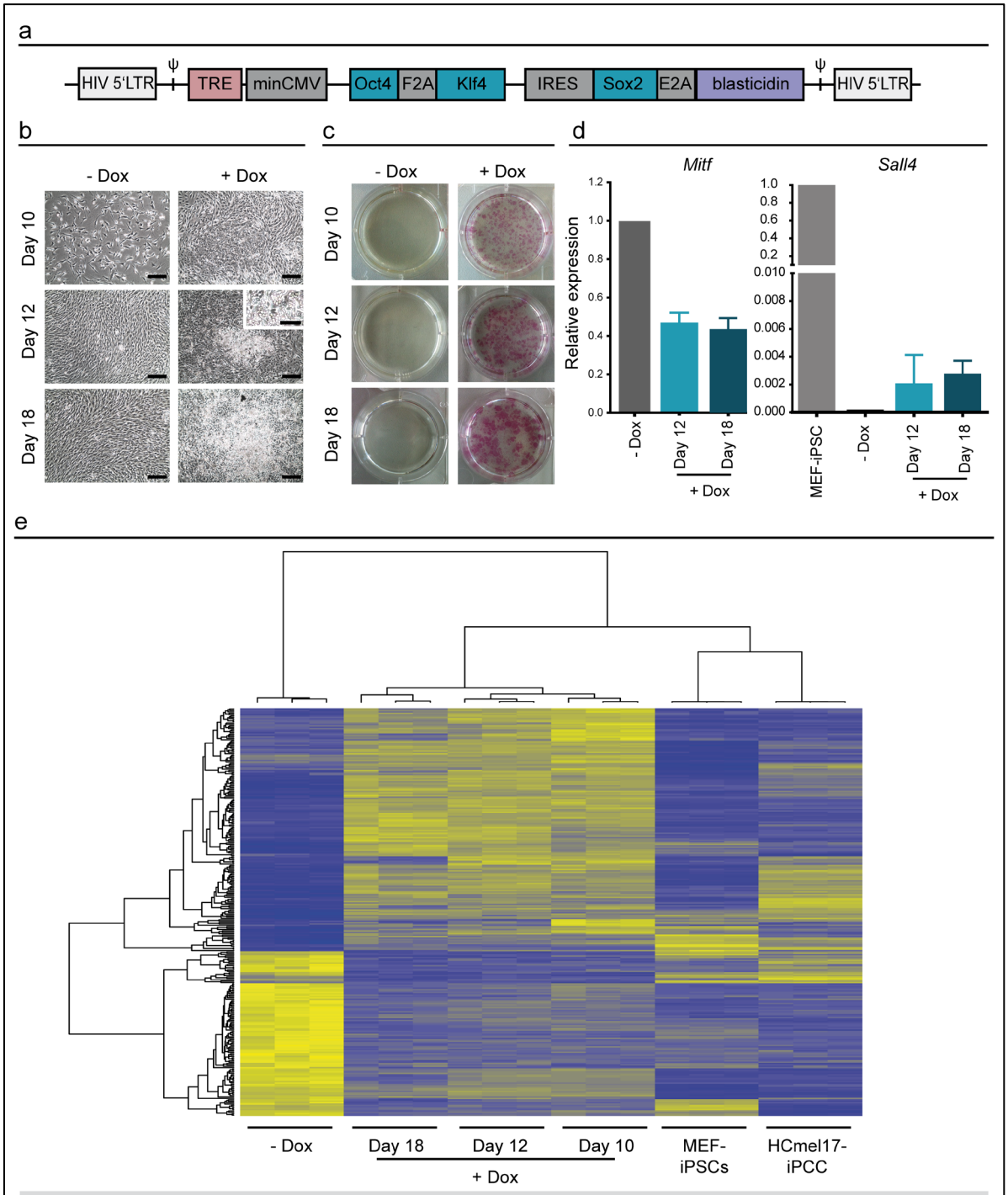

Figure 12 | Partial reprogramming of HCmel17 cells

(a) Scheme of the Stemcca vector carrying a blasticidin selection cassette instead of the c-myc under the control of a tetracycline-responsible element (TRE). **(b)** Light-microscopic images of partially reprogrammed HCmel17 cells (right) and their non-reprogrammed counterparts (left) on indicated days after transgene expression; bar=250 µm, inlay bar=125 µm. **(c)** AP staining of partially reprogrammed HCmel17 cells (right) and their non-reprogrammed counterparts (left) on indicated days after transgene expression. **(d)** Mitf and Sall4 mRNA expression in partially reprogrammed cells detected by qPCR. Gapdh was used as endogenous control; reference samples were non-reprogrammed cells (Mitf) or MEF-iPSCs (Sall4). Graph shows mean and CI of technical triplicates). **(e)** Heatmap displays differentially up- and downregulated genes determined by several groups test (empirical Bayes) with a p-value threshold of 0.005 (p-value adjustment with Holm-method). Each row stands for a gene (292 genes are shown) and each column represents a sample, n=3. Yellow indicates upregulation, blue indicates downregulation.

AP=alkaline phosphatase; CI=confidence interval; Dox=doxycycline; iPCC=induced pluripotent cancer cells; iPSC=induced pluripotent stem cells; MEF=murine embryonic fibroblast, qPCR=quantitative polymerase chain reaction; Stemcca=stem cell cassette

Next, I wanted to identify cellular processes that were strongly affected by partial reprogramming. Gene set enrichment analysis of both, up- and downregulated genes ($p \leq 0.05$) at day 12 after induction of transgene expression compared to non-reprogrammed HCmel17 cells revealed that the majority of processes affected by partial reprogramming were involved in cell adhesion and cytoskeleton remodeling **(Table 4)**. Since cell adhesion and cytoskeleton remodeling are of huge importance in cancer cells' acquisition of invasive potential, I aimed to further investigate this functionally in partially reprogrammed melanoma cells. Therefore, the invasion through an artificial basal membrane was examined in three independent experiments in technical triplicates **(Figure 13a)**. Cells were seeded in serum-free medium on top of an artificial basal membrane and invasion through this layer towards serum-containing medium was measured. Strikingly, the invasive capacity of HCmel17 cells increased significantly in a transient manner showing a threefold increase after 12 days of reprogramming ($p \leq 0.05$) with a subsequent significant decrease at day 18 after induction of transgene expression ($p \leq 0.05$).

Other cell lines were subjected to partial reprogramming by transducing them with M2-mCherry and Stemcca-blasti. MEFs, a hepatocellular carcinoma cell line (Hepa1.6, kindly provided by Prof. Klingmüller) and an additional melanoma cell line (Ret2, kindly provided by Prof. Umansky) were used. **Figure 13b** illustrates the percentage of invasion capacity through an artificial basal membrane comparing cells reprogrammed for 12 days to non-reprogrammed control cells. Strikingly, only cell lines that generated AP-positive

-log (p-value)	Pathway
>7	FGF signaling in pancreatic cancer
>7	Development: TGFβ-dependent induction of EMT
>6	Stimulation of TGFβ-signaling in lung cancer
>6	TGF,WNT and cytoskeleton remodeling
>6	Development: regulation of EMT
>5	Cell adhesion: Plasmin signaling
>5	Cell adhesion: ECM remodeling
>5	Blood coagulation: GPCRs in platelet aggregation
>5	Cytoskeleton remodeling
>5	Neurophysiological process: Receptor-mediated axon growth repulsion

Table 4 | Gene set enrichment analysis of pathways in partially reprogrammed HCmel17 cells
Gene set enrichment analysis of pathways comprising differentially regulated genes in HCmel17 cells after 12 days of reprogramming. Table shows top 10 pathways with significant enrichment (p-value) of genes up- and down-regulated after 12 days of reprogramming. *Analysis tools: Chipster (quantile normalization using Illumina software version 3, two-groups test=empirical Bayes, p-value adjustment method=BH, p-value≤0.05); Metacore (p-value for gene set enrichment in pathways shown in table).*

ECM=extracellular matrix; EMT= epithelial-to-mesenchymal-transition; FGF=fibroblast growth factor; GPCRs=g-protein coupled receptors; PI3K=phosphoinositide 3-kinase; TGFß=transforming growth factor β

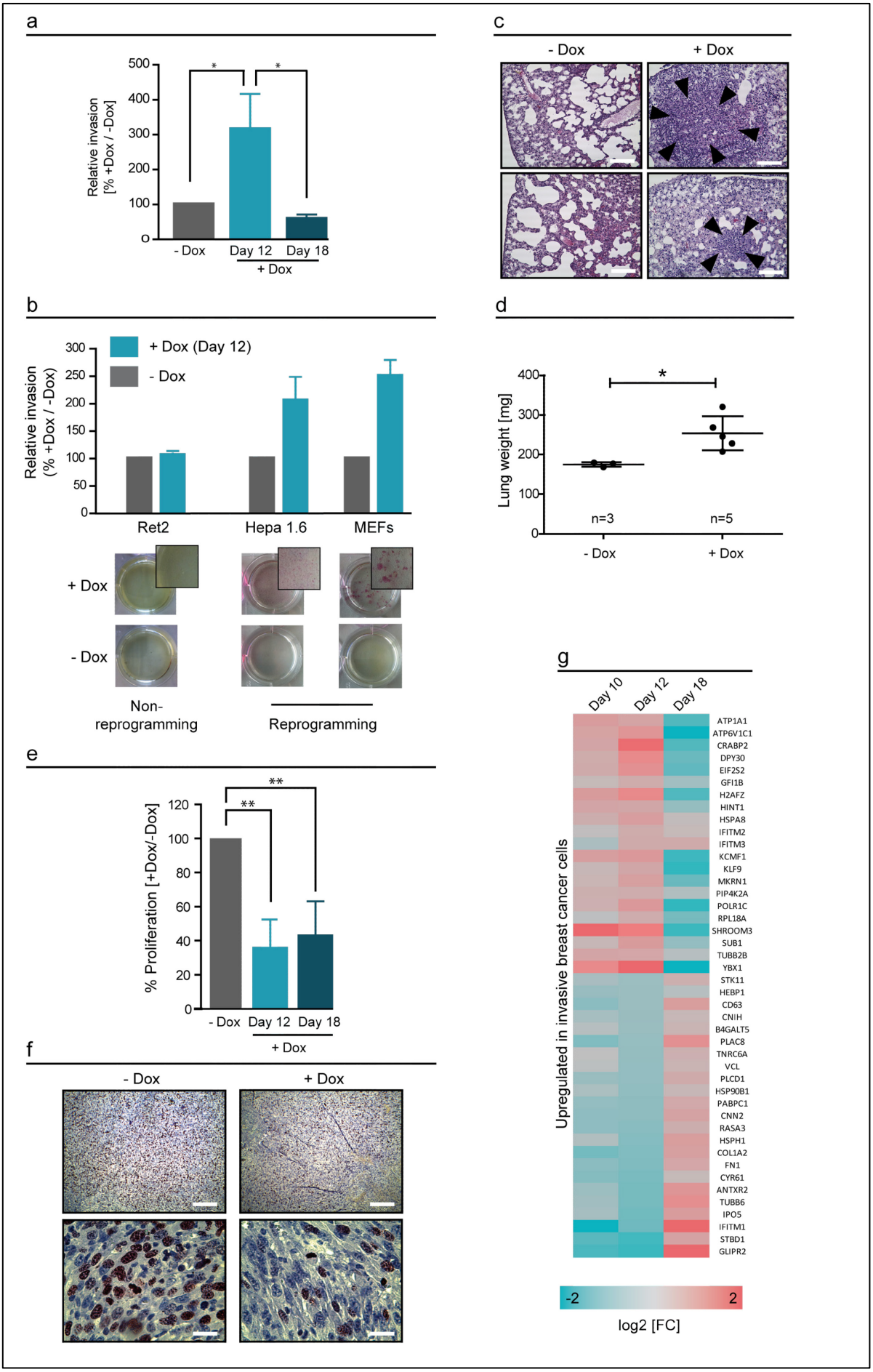
a
Relative invasion [% +Dox / -Dox]
500
400
300
200
100
0
*
*
- Dox
Day 12
Day 18
+ Dox
b
Relative invasion (% +Dox / -Dox)
300
250
200
150
100
50
0
+ Dox (Day 12)
- Dox
Ret2
Hepa 1.6
MEFs
+ Dox
- Dox
Non-reprogramming
Reprogramming
c
- Dox
+ Dox
d
Lung weight [mg]
400
300
200
100
0
*
n=3
n=5
- Dox
+ Dox
e
% Proliferation [+Dox/-Dox]
120
100
80
60
40
20
0
**
**
- Dox
Day 12
Day 18
+ Dox
f
- Dox
+ Dox
g
Day 10
Day 12
Day 18
Upregulated in invasive breast cancer cells
ATP1A1
ATP6V1C1
CRABP2
DPY30
EIF2S2
GFI1B
H2AFZ
HINT1
HSPA8
IFITM2
IFITM3
KCMF1
KLF9
MKRN1
PIP4K2A
POLR1C
RPL18A
SHROOM3
SUB1
TUBB2B
YBX1
STK11
HEBP1
CD63
CNIH
B4GALT5
PLAC8
TNRC6A
VCL
PLCD1
HSP90B1
PABPC1
CNN2
RASA3
HSPH1
COL1A2
FN1
CYR61
ANTXR2
TUBB6
IPO5
IFITM1
STBD1
GLIPR2
-2
2
log2 [FC]

Figure 13 | Partial reprogramming alters invasion and proliferation capacity of HCmel17 cells
(a) Invasion capacity of partially reprogrammed HCmel17 cells through an artificial basal membrane was assessed and is displayed as percentage of invasion (non-reprogrammed cells were used as reference sampel); graph shows mean and SD, n=3. **(b)** Invasion capacity of different cells is displayed. The melanoma cell line Ret2, the hepatocellular carcinoma cell line Hepa 1.6 and MEFs were reprogrammed for 12 days and invasion through an artificial basal membrane was determined. Photographic images of AP-staining at the time point of harvesting the cells are placed below the bars. Graph shows mean and SD from technical triplicates. **(c)** $5x10^5$ HCmel17 cells were injected i.v. into C57BL/6 mice and mice were sacrified after 6 weeks. Displayed is the histological H&E staining of excised lungs from these mice; bar=50 µm, arrowheads indicate lung-infiltrating tumor cells. **(d)** Lung weight of intravenously injected mice six weeks after injection. Displayed are mean and SD of lung weight, p≤0.05, n=3 (-Dox), n=5 (+Dox). **(e)** Proliferation evaluation of partially reprogrammed cells at day 12 and 18 (2000 cells seeded, proliferation measurement after 72 h, alamarBlue incubation=4 h, n=4, graph displays mean and SD of biological replicates). **(f)** At day 12 of reprogramming, $5x10^5$ cells (-Dox) and $1x10^6$ (+Dox) were injected subcutaneously into NSG mice and mice were sacrificed when tumors reached maximum size of 1.5 cm (-Dox: 76 days; +Dox: 70 days). Images show immunohistochemistry staining against Ki67; bar upper panel=250 µm, bar lower panel=25 µm. **(g)** Displayed are genes that were shown to be upregulated in invasive breast cancer cells [216] and that are differentially regulated at day 12 after reprogramming with log2 [FC] > 0.5 (Day 12 + Dox *vs.* - Dox; p≤0.05). Heatmap shows fold changes of gene expression at indicated days after transgene induction in comparison to non-reprogrammed control cells.
AP=alkaline phosphatase; Dox=doxycycline; FC=fold change; H&E=hematoxylin and eosin; i.v.=intravenous; MEFs=murine embryonic fibroblasts; n=biological replicates; NSG=NOD-scid IL2rγ$^{-/-}$; p.i.=post injection; SD=standard deviation; significance tested using two-tailed t-test

colonies by day 12 upon transgene expression showed increased invasive potential. Hep1.6 displayed a two-fold increase in invasion compared to control cells and MEFs increased their invasive potential almost three-fold. Both cell lines showed AP-activity. In contrast, Ret2 cells displayed neither morphological changes nor AP-activity after transgene expression for 12 days although cells were viable despite blasticidin selection indicating intact transgene expression. Strikingly, no changes regarding their invasive potential was observed **(Figure 13b)**. These data demonstrated that increased invasive potential of partially reprogrammed murine cell lines depended on successful reprogramming but transgene expression alone was not sufficient to induce this invasive phenotype.

In order to confirm the higher invasive potential of partially reprogrammed HCmel17 cells *in vivo*, a tail vein assay in syngeneic C57BL/6 mice was performed. $5x10^5$ HCmel17 cells, reprogrammed for 12 days or non-reprogrammed, were injected intravenously into C57BL/6 mice and mice were sacrificed six weeks after injection. To analyze extravasation potential of cells, lungs of all animals were excised, weighted and fixed for histological analysis. Metastases could be identified in lungs derived from mice injected with partially reprogrammed cells (**Figure 13c**, right panels, arrowheads), whereas lungs from control animals showed normal lung histology without infiltrating tumor cells (**Figure 13c,** left panel). In line with that, the weight of lungs derived from mice injected with partially reprogrammed cells was significantly higher (253.8 mg ± 43.19 mg, n=5, p≤0.05) when compared to lung weight of animals injected with control cells (175.0 mg ± 5.766 mg, n=3, **Figure 13d**).

After showing increased invasive potential of partially reprogrammed cells *in vitro* and *in vivo*, proliferation changes during the process of reprogramming were analyzed. In order to

investigate if and how proliferation was influenced by partial reprogramming, cells were harvested at day 12 or 18 after onset of reprogramming and seeded in 96-well plates to be subjected to proliferation analysis. Partial reprogramming for 12 or 18 days resulted in significantly decreased proliferation compared to non-reprogrammed counterparts **(Figure 13e)**. Already at day 12, proliferation was decreased by more than 60 % with a slight increase at day 18. In order to test this alteration *in vivo*, $1x10^6$ of partially reprogrammed cells (day 12) or $5x10^5$ non-reprogrammed control cells were injected subcutaneously into mice. After excision of tumors with a size of 1.5 cm (-Dox: 76 days; +Dox: 70 days), they were subjected to immunohistochemical analysis of Ki67 expression, a widely established proliferation marker. The tumor derived from partially reprogrammed cells demonstrated fewer Ki67-positive cells compared to the tumor derived from control cells indicating decreased proliferation **(Figure 13f)**, which is consistent with data derived from *in vitro* analysis.

In summary, partially reprogrammed HCmel17 cells at day 12 after transgene induction demonstrated increased invasion capacity with decreased proliferation *in vitro* and *in vivo*. *In vitro* findings further showed that the elevated invasion capacity was a transiently occurring phenomenon that was reversed at day 18.

Taken together, the analysis of global gene expression signatures revealed that cytoskeleton remodeling was among the top ten pathway maps enriched in differentially expressed genes on day 12 of reprogramming. In addition, these cells demonstrated significantly increased invasive potential *in vitro* and *in vivo*.

Interestingly, it was shown that breast cancer cells use the cytoskeleton remodeling process as the major route in order to gain invasive potential, in contrast to cells from other cancer types that favor proteolytic invasion [215]. In order to analyze the expression of genes, which are associated with highly invasive breast cancer cells, these gene sets were extracted from the whole genome expression analysis of partially reprogrammed cells compared to non-reprogrammed control cells ([216], **Figure 13g**). Genes that are upregulated in invasive breast cancer cells and differentially regulated after partial reprogramming could be separated into two groups: about half of them were also upregulated at day 12 after reprogramming, whereas the other half showed the opposite expression pattern with decreased expression at day 10 and 12 and increased expression at day 18. The first group of genes showing increased expression in highly invasive breast cancer cells as well as in partially reprogrammed cells (day 12) included genes that are known to play important roles in cytoskeleton remodeling during development and in cancer progression, i.e. Shroom3 [217], Atp1a1 [218], and Atp6v1c1 [219]. Also a major constituent of microtubules, Tubb2b, was upregulated indicating that cytoskeleton remodeling is a key event not only in invasive breast cancer but also in partially reprogrammed HCmel17 cells. In contrast, genes that were

shown to be upregulated in invasive breast cancer cells but downregulated at day ten and 12 of partial reprogramming included well known factors that drive EMT in somatic and tumorigenic cells, i.e. Glipr-2 [220] and fibronectin (fn1, [221]).
Strikingly, between day 12 and 18 the upregulation of invasion-related genes demonstrated a strong switch, whereas day ten and 12 share similar expression of invasion-related genes **(Figure 13g)**. This expression profile of invasion-related genes, which showed a clear switch in expression between day 12 and 18, was in agreement with observed functional changes.

4.4. Identification of potential invasion-related genes

Since HCmel17 melanoma cells reprogrammed for 12 days showed a significant increase in their invasive potential *in vitro* and *in vivo*, expression of invasion-related genes became focus of investigation. **Figure 14a** displays the fold change expression of neural crest-related genes, which have been previously shown to be linked to invasion [75], during the process of reprogramming including fully reprogrammed HCmel17-iPCCs. Strikingly, partial reprogramming for 12 days and accelerated invasion potential did not correlate with expression of neural crest-related markers. Independent of the involvement of these genes within the neural crest signaling cascade, i.e. induction, specification, EMT/invasion, genes were mainly downregulated while cells were converted to a pluripotent state. Nes was the only gene that was expressed slightly higher at day ten and 12 compared to non-reprogrammed cells or cells reprogrammed for 18 days, respectively **(Figure 14a)**. In addition, markers, which were shown to be up- or downregulated after the phenotype switch from proliferative to highly invasive melanoma cells in previous studies [77,100,222], did not correlate with the phenotypic change of melanoma cells that were reprogrammed for 12 days **(Figure 14b)**. Downregulation of Ror1, Zeb2, Snai2 and Phf19 was demonstrated to correlate with increased invasion, as was the upregulation of Ror2 and Zeb1 [77,100,222]. In contrast, in melanoma cells partially reprogrammed for 12 days, which show increased invasion in combination with decreased proliferation, these genes were not significantly altered between day 12 and 18 **(Figure 14b)**. Of note, Zeb1 and Snai2 were strongly downregulated in completely reprogrammed HCmel17-iPCCs.
In addition, Mmps, which were previously shown to be to related to melanoma cell invasion [85,87–90], were not upregulated at day 12 after reprogramming. In contrast, expression of Mmp3, Mmp2 and Mmp14 was strongly decreased during the process of reprogramming with maximum decrease in completely reprogrammed HCmel17-iPCCs compared to non-reprogrammed control cells **(Figure 14c)**.
Next, I aimed to identify novel genes, which expression correlated with this transient invasive phenotype. Therefore, *Chipster software* was used to filter genes, which were significantly

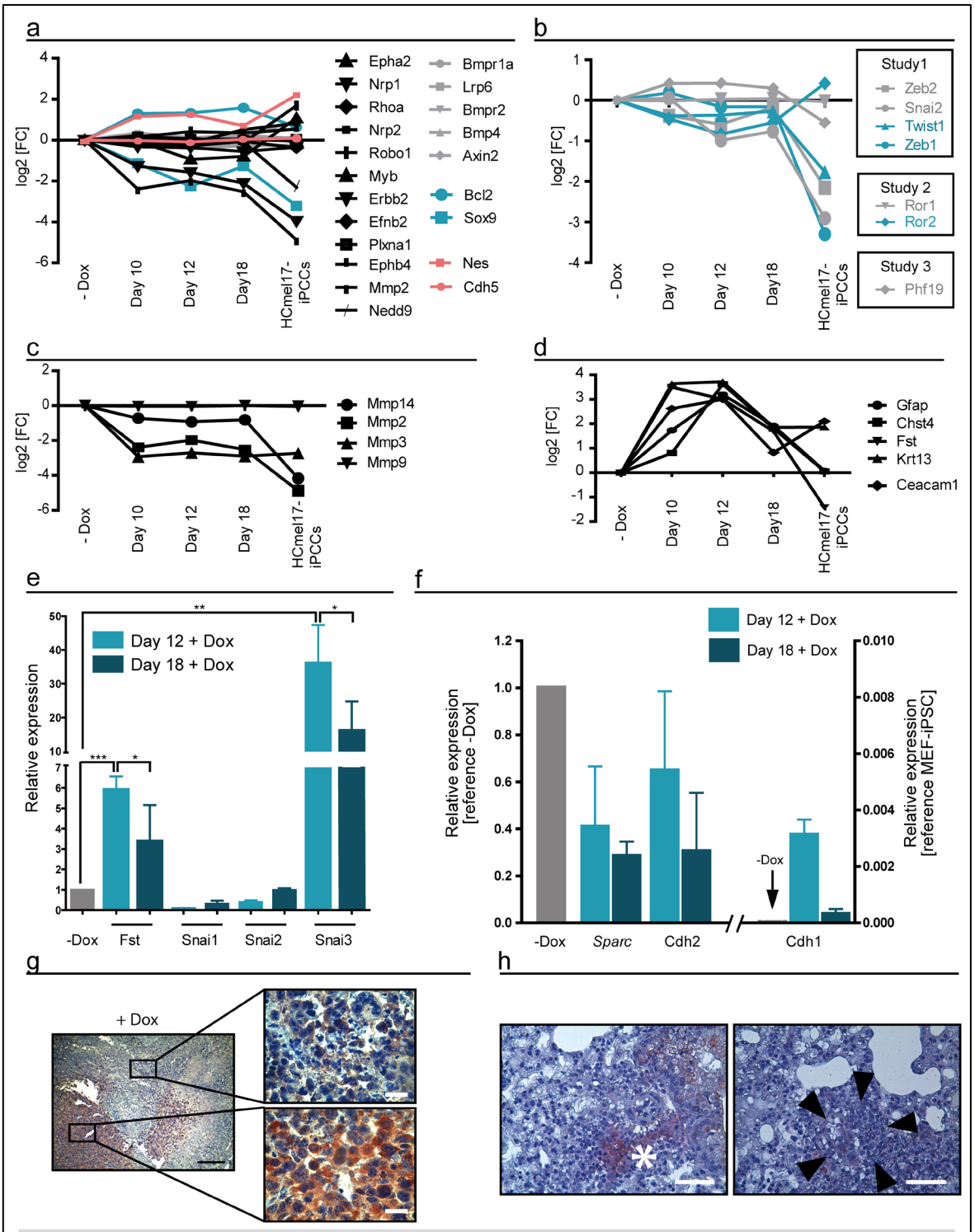

Figure 14 | Identification of SNAI3 as a novel invasion-related marker in melanoma

(a) Displayed is the log2 [FC] of genes that are involved in neural crest signaling [75] at indicated time points during reprogramming. They are grouped based on their involvement with the neural crest program: induction (grey), specification/survival (blue), EMT/migration (black), and red represents genes that are not specifically associated with any of these steps. **(b)** Displayed is the log2 [FC] of genes, which were shown to correlate with the phenotype switch in melanoma cells, at indicated time points during reprogramming. They are grouped based on their expected expression pattern. Blue indicates that genes were shown to be upregulated, grey indicates that genes were shown to be downregulated after phenotype switching. **(c)** Displayed is the log2 [FC] of Mmps, which have been linked to melanomagenesis, at indicated time points during reprogramming. **(d)** Displayed is the log2 [FC] of genes, which were significantly upregulated at day 12 ($p \leq 0.005$; log2 [FC] ≥ 3.00) and downregulated at day 18 ($p \leq 0.005$; log2 [FC] ≤ 2.00), correlating to

the invasive phenotype of partially reprogrammed cells. **(e)** Validation of gene expression of Follistatin (Fst) and all members of the Snai-TF-family using qPCR (Gapdh was used as endogenous control and non-induced cells served as the reference sample. Graph displays mean and CI; n=3). **(f)** Gene expression of known EMT-related markers using qPCR (Gapdh was used as endogenous control; non-induced cells served as the reference sample for Sparc and Cdh2 plotted on the left y-axis; MEF-iPSCs served as the reference sample for Cdh1 plotted on the right y-axis. Graph displays mean and CI of technical triplicates). **(g)** Immunohistochemical visualization of SNAI3 in tumors excised from mice after s.c. injection of non-reprogrammed or partially reprogrammed HCmel17 cells (day 12). Tumor was excised on day 70 after injection of $1x10^6$ cells (+dox), embedded in paraffin and stained for SNAI3; bar=250 µm (left panel); bar=25 µm (right panel). **(h)** Anti-SNAI3 staining of lungs removed from mice injected with cells partially reprogrammed for 12 days. Left: white asterisk indicates SNAI3-positive lung-infiltrating tumor cells; right: black arrowheads indicate SNAI3-negative lung-infiltrating tumor cells; bar=50 µm.
CI=confidence interval; dox=doxycyclin; EMT=epithelial-to-mesenchymal transition; FC=fold change; iPCCs=induced pluripotent cancer cells; iPSCs=induced pluripotent stem cells; s.c.=subcutaneous; TF=transcription factor; significance=tested using two-tailed t-test

upregulated at day 12 compared to their parental cells ($p \leq 0.05$; $FC \geq 3.00$) followed by decreased expression at day 18 ($p \leq 0.05$, $FC \leq 2.00$; **Figure 14d**). Next to Carcinoembryonic antigen-related cell adhesion molecule 1 (Ceacam1), Follistatin (Fst) was among the top five genes**.** Since a closely related protein of Fst (Fstl-1) was connected to invasive potential and Snai1-induced EMT in cancer cells [223], I aimed to elucidate the role of SNAI-family members in this invasive phenomenon. First, I validated Fst expression by qPCR showing an increase at day 12 after induction of partial reprogramming and subsequent downregulation at day 18 being consistent with expression data derived from the microarray **(Figure 14e)**. In addition, expression of Snai1 (Snail), Snai2 (Slug) and Snai3 was analyzed. Neither of the first two members, which are known regulators of EMT processes in cancer cells, showed increased expression, which would explain the invasive potential of HCmel17 cells reprogrammed for 12 days. Strikingly, the third member of this transcription factor-family, Snai3, was highly upregulated in HCmel17 cells reprogrammed for 12 days in combination with subsequent downregulation at day 18 **(Figure 14e)**.

In addition, other well-known genes, which are deregulated when melanoma cells acquire an EMT-induced invasive phenotype including Sparc and Cdh2 and Cdh1, were analyzed by qPCR **(Figure 14f)**. Neither Sparc nor Cdh2 was upregulated at day 12. In addition, Cdh1 that is frequently downregulated upon EMT induction in carcinomas to promote invasion was upregulated at day 12.

In order to find out whether Snai3 is also expressed *in vivo* its expression was analyzed in tumors derived from partially reprogrammed cells (day 12) that had been subcutaneously injected into mice. Representative microscopic images are displayed in **Figure 14g**. Partially reprogrammed cells that exhibited highly upregulated Snai3 expression *in vitro* showed areas of high SNAI3 protein expression as well as SNAI3 negative areas *in vivo* indicating a heterogeneous expression of this marker in tumors. Moreover, the expression of SNAI3 in lung metastases from the tail vein assay was analyzed. Interestingly, not all lung infiltrating

tumor cells showed positive signals for SNAI3 in established metastases (**Figure 14h,** arrowheads) but rare tumor cells showed expression of SNAI3 (**Figure 14h,** white asterisk).
In summary, the model of partial reprogramming and subsequent *in vitro* as well as *in vivo* analyses revealed a phenotype switch of melanoma cells with increased invasion and decreased proliferation at day 12 after transgene induction. This phenotype switch was independent of neural crest-related gene expression. In addition, expression of genes that have been suggested to label the phenotype switch in melanoma cells did not correlate with observed functional alterations. This indicates that my system of partially reprogrammed tumor cells can be used to identify novel pathways that might drive the phenotype switch in melanoma cells. Importantly, this *in vitro* system can be used to find genes that are expressed according to the observed phenotype and thus, allows to identify novel biomarkers for the phenotype switch. Here, I demonstrate that Snai3 is regulated in correlation with the functional changes after the phenotype switch indicating a role for this transcription factor in acquisition of invasive potential in melanoma cells.

4.5. SNAI3 as a putative marker for invasive potential in melanoma

4.5.1. SNAI3 expression and its relevance in the clinic

The SNAI transcription factor family is heavily involved in the acquisition of invasive properties during normal development but also in tumor progression. Its novel member, SNAI3 has just recently been identified in humans and thus, its role in cancer is completely unknown. Hints from microarray analyses indicated a role of SNAI3 in the phenotype switch of partially reprogrammed cells, why I further analyzed SNAI3 expression *in vivo* in order to explore whether it correlates with invasive potential of melanoma cells. Therefore, paraffin embedded primary tissues from melanoma patients were stained for SNAI3. **Figure 15a** shows representative images of SNAI3 expression in a melanocytic nevus and a primary melanoma in different magnifications. SNAI3 was present in normal human keratinocytes in the epidermis consistent with data published in the human protein atlas (**Figure 15a**, left panel, arrowheads, [224]). Melanocytic nevus cells were hardly stained for SNAI3, whereas the primary tumor showed diverse SNAI3 expression with strongest signals in deeper regions of the tumor (**Figure 15a**, right panel). These results indicate a role of SNAI3 in invasiveness of melanoma cells since its expression was mainly detected on invasive sides of tumors (in deeper regions of primary melanoma). To elucidate the expression of SNAI3 in a bigger cohort of patients, its expression was analyzed using a tissue microarray (TMA) containing human benign intradermal melanocytic nevi (n=37) and biopsies collected from primary

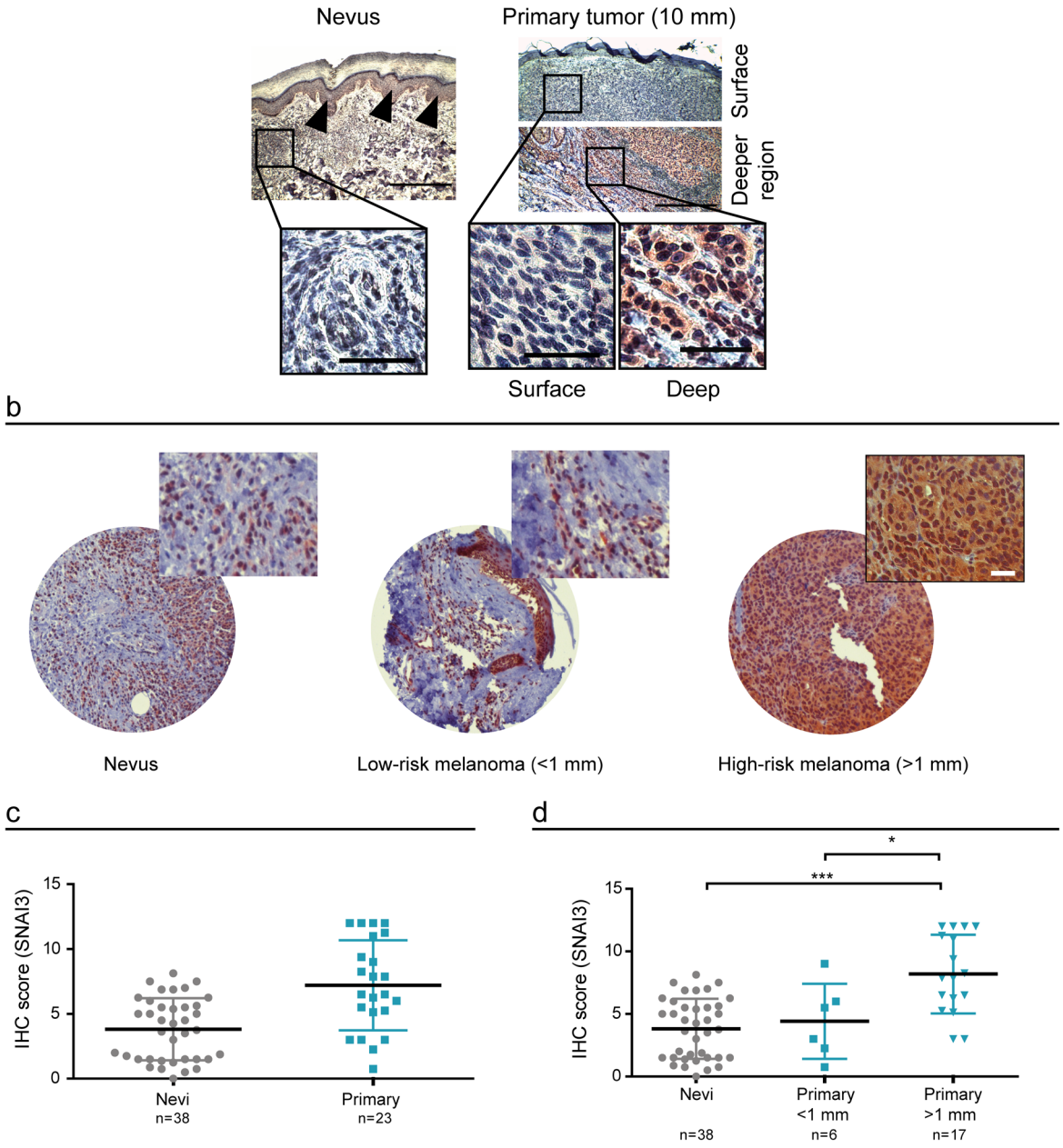

Figure 15 | SNAI3 expression correlates with tumor thickness

(a) Immunohistochemical analysis of SNAI3 expression in paraffin-embedded tumor samples from patients (left panel: melanocytic nevus; right panel: primary melanoma); upper panel: bar=500 µm; lower panel: bar=50 µm. **(b)** Tissue microarray samples of a nevus (left panel), a low-risk (middle panel) and a high-risk primary melanoma (right panel) stained for SNAI3; bar=25 µm. **(c)** Immunohistochemical score of SNAI3 staining of melanocytic nevi and all primary tumors. Mean and SD for indicated n are presented. **(d)** Immunohistochemical score of SNAI3 staining for melanocytic nevi and primary tumors with low risk and high risk to metastasize are displayed. Mean and SD for indicated n are shown.

IHC=immunohistochemistry score; SD=standard deviation; significance tested using two-tailed t-test

melanomas (n=26). SNAI3 was detected in parts of nevi (**Figure 15b**, left panel) and primary melanomas of low risk (≤1mm tumor thickness, **Figure 15b**, middle panel) or high risk (≥1mm tumor thickness, **Figure 15b**, right panel), respectively. In addition to another independent researcher, I measured expression intensity and quantity in a blind setting using a defined immunohistochemical (IHC) score **(Figure 4)**. Strikingly, SNAI3 expression and depth of primary melanomas (Breslow score) correlated and a significant increase in the IHC score for SNAI3 was observed in all pooled primary melanomas compared to nevi **(Figure 15c)**. In order to discover at what exact step of melanomagenesis SNAI3 expression increases, comparative analysis was performed between low-risk and high-risk primary melanomas **(Figure 15d)**. The significant difference between nevi and high-risk melanoma regarding the IHC score was further increased, which indicates that high-risk melanoma are tumors, which retain the highest IHC score for SNAI3 in the pool of primary melanomas. Remarkably, the IHC score is also significantly increased comparing low-risk with high-risk melanomas **(Figure 15d)**.

4.5.2. SNAI3-overexpression in human melanoma cells lines

To further elucidate SNAI3's particular role in melanomagenesis, gain of function studies were performed. Therefore, four human melanoma cell lines were transduced with an expression vector encoding for human SNAI3, or with the pLX304 control vector (pLX), respectively. Both vectors carried a blasticidin resistance cassette and cells were used for overexpression confirmation and functional assays after selecting with blasticidin for at least ten days at defined concentrations **(Table 1)**. Next to melanoma cell lines, immortalized human fibroblasts were examined in parallel as an additional, non-tumorigenic control.

Overexpression of SNAI3 was validated in authenticated human melanoma cells lines A375, Mewo, SKmel28, SKmel30 and human immortalized fibroblasts on RNA level using qPCR **(Figure 16a)**. Gapdh was used as the endogenous control and data were normalized to immortalized human keratinocytes as SNAI3 is known to be expressed in these cells [224]. The pLX-transduced control cells showed expression levels of SNAI3 that were just above the detection threshold. Strikingly, transduction with the overexpression vector resulted in a 3,000-30,000-fold increase of SNAI3 mRNA in all cell lines tested compared to keratinocytes. Immunoblot analysis validated overexpression in three out of four cell lines with α-ACTININ serving as the loading control **(Figure 16b)**. SKmel28 did not show any SNAI3 protein expression in neither pLX-transduced or SNAI3-OE vector-transduced cells. Immortalized human fibroblasts did not grow after transduction with the SNAI3 construct and therefore could not be used for protein extraction or other analyses.

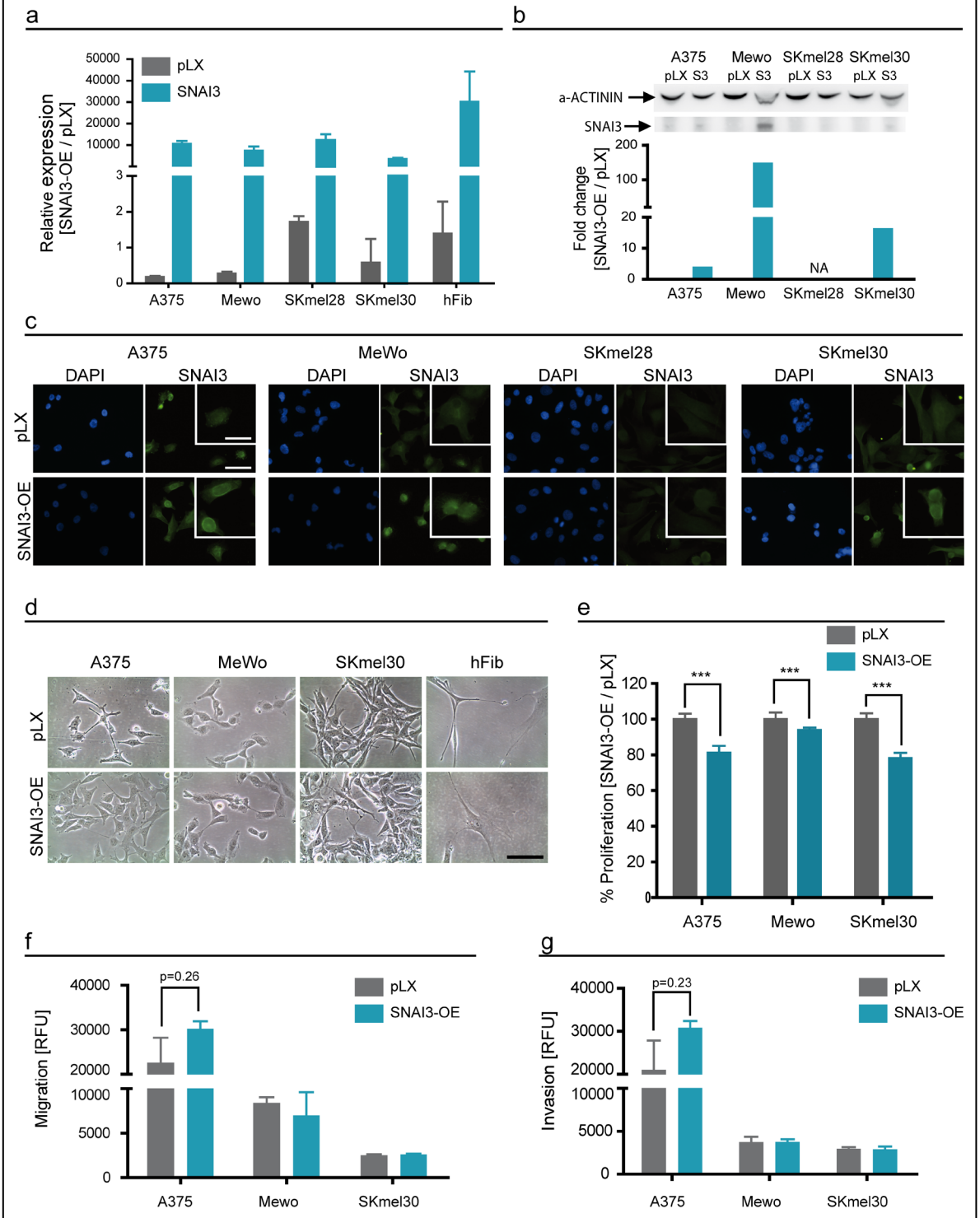

Figure 16 | SNAI3 overexpression in human melanoma cell lines

(a) Expression of SNAI3 in melanoma cells lines and in human fibroblasts (hFib): displayed is relative expression of SNAI3 in cells transduced with the control vector pLX and cells transduced with a SNAI3-OE vector measured by qPCR. Relative expression was determined using Gapdh as the endogenous control. Data were normalized to immortalized human keratinocytes. Graph displays mean and CI for technical triplicates. **(b)** Immunoblot of SNAI3 overexpression in melanoma cell lines: alpha-ACTININ served as a loading control for 40 µg total protein loaded. SNAI3 protein was detected at the expected size of 32 kDa and protein expression levels were quantified using *ImageJ*. Expression was normalized to each loading control and pLX-transduced cells were used as a reference for fold change calculations. **(c)** Fluorescence-microscopic images of indicated cell lines stained for SNAI3 protein. Cells were fixed, stained with

anti-SNAI3 antibody overnight with a dilution of 1:400 and then incubated with a secondary antibody against rabbit IgG labeled with Atto488 (green). DAPI was used for visualization of nuclei (blue). Upper panel shows cells transduced with the control vector pLX, lower panel shows cells transduced with the SNAI3-OE construct, bars=50 µm (inlay bars=25 µm). **(d)** Microscopic images of melanoma cell lines transduced with pLX vector or the SNAI3-OE vector; bar=100 µm. **(e)** Proliferation of melanoma cell lines transduced with the control vector pLX or with the SNAI3-OE construct (4000 cells were seeded and grown for 72 h, alamarBlue incubation=3 h, graph displays mean and SD of technical replicates, n=6). **(f)** Migration capacity of melanoma cells was determined using a transwell chamber system. Cells were seeded in serum-free medium and FCS was used as chemoattractant. Migration capacity was measured after 24 h. Graph shows mean and SD of technical triplicates. **(g)** Invasion capacity of melanoma cells was determined using a transwell chamber system with 0.5x BME coating. Cells were seeded in serum-free medium and FCS was used as chemoattractant. Invasion capacity was measured after 24 h. Graph shows mean and SD of technical triplicates.
BME=basement membrane extract; CI=confidence interval; DAPI=4',6-diamidin-2-phenylindol; FCS=fetal calf serum; hFib=human fibroblasts; NA=not available; qPCR= quantitative polymerase chain reaction; RFU=relative fluorescence unit; S3=SNAI3; SD=standard deviation; significance tested using two-tailed t-test

Quantification of immunoblots using *ImageJ* revealed a four to 100-fold increase of SNAI3 protein in melanoma cell lines with Mewo cells showing the strongest overexpression, and A375 and SKmel30 a slight expression when transduced with SNAI3-OE vector **(Figure 16b)**. When transduced with the control vector pLX, only A375 cells showed little expression of SNAI3 on protein level supporting qPCR data that demonstrated mRNA quantity, which was just above detection level for all cells lines. Of note, little protein presence in pLX control cells lead to strong variances regarding the quantification of fold-changes. In order to confirm protein expression, immunocytochemical analysis was performed. Cells were seeded in 8-well chamber-slides and incubated under normal growth conditions for 12 hours. After staining using an anti-SNAI3 antibody overnight they were incubated with an Atto488-labeled secondary antibody (green). Representative pictures are shown in **Figure 16c**. In line with results derived from immunoblot analysis, A375 cells demonstrated slight SNAI3 expression when transduced with the control vector pLX but showed stronger staining of SNAI3 when transduced with the SNAI3-OE construct. Expression data derived from immunoblot analysis could also be verified for SKmel28 since SNAI3-staining showed barely any SNAI3 expression with no difference between cells transduced with the control vector or the SNAI3-OE construct. Fluorescence images of Mewo cells revealed a strong expression of SNAI3 when transduced with the SNAI3-OE construct compared to control cells and SKmel30 also demonstrated stronger staining for SNAI3 when transduced with the SNAI3-OE construct. In summary, immunocytochemical analysis confirmed data derived from immunoblot analysis and showed overexpression of SNAI3 on protein level in three out of four cell lines. Due to lack of SNAI3 expression when transduced with the SNAI3-OE construct, SKmel28 cells were excluded from further analyses.

After confirmation of SNAI3 overexpression in the three cell lines A375, Mewo and SKmel30, these cells were used to investigate changes in cellular functions. Morphological alterations upon SNAI3 overexpression were not observed in any of the cell lines **(Figure 16d)**. Of note,

fibroblasts showed morphological changes towards a senescent-like phenotype with swollen cytoplasm and a visible nucleus. They did not proliferate after SNAI3 transduction and were not further analyzed.

Next, proliferation, migration and invasion capacity of cells overexpressing SNAI3 were investigated in order to identify its functional impact on melanoma cells. Proliferation capacity was assessed and is displayed as percentage of proliferation in pLX-transduced control cells. All melanoma cell lines showed significantly reduced proliferation **(Figure 16e)** but they could be continuously cultured in regular medium.

Migration as well as invasion potential was assessed using a combined transwell-chamber system. Therefore, cells were seeded into the top chamber of the transwell-system in serum-deprived medium and migration through established pores (migration) or through additional coating containing basal membrane equivalent (invasion) towards serum-containing medium in the bottom chamber was measured. Exclusively A375 showed a tendency to increased migration as well as increased invasion potential when SNAI3 was overexpressed but Mewo and SKmel30 cell lines did not exhibit altered migratory **(Figure 16f)** or invasive capacities **(Figure 16g)**. However, this increase in migration and invasion in A375 cells was not significant.

In order to test for de-differentiation and to detect potential differences in gene expression of invasion-related genes, qPCR analysis was performed for de-differentiation-associated, EMT-related, or invasion-related genes **(Figure 17)**. All expression data were normalized to Gapdh as the endogenous control. Normal human melanocytes (NHM) served as the reference sample for differentiation-related markers (DCT, MITF, TYRO) in order to cross-compare expression between cell lines. The melanocyte-specific genes DCT, MITF and TYRO were absent or barely expressed in A375 and Mewo cells even without overexpressing SNAI3 so that no alteration of expression could be detected **(Figure 17a)**. SNAI3-overexpression in SKmel30 cells resulted in reduced expression of all three differentiation-associated factors. Of note, with about four percent of expression levels compared to NHM, TYRO and DCT could only be detected at very low levels in pLX-transduced control cells so that the reduction caused by SNAI3-overexpression is not necessarily biologically relevant. In contrast, MITF was reduced compared to NHM from about 25 % to 10 % and this might indicate a de-differentiation of cells upon SNAI3 overexpression.

Except for the differentiation markers, all expression data were normalized to the pLX-transduced control cells **(Figure 17b)**. Interestingly, the other family members of the SNAI family (SNAI1 and SNAI2) were not affected regarding their expression levels in A375 and Mewo cells, whereas in SKmel30 cells, SNAI1 was strongly reduced to about 20 % and

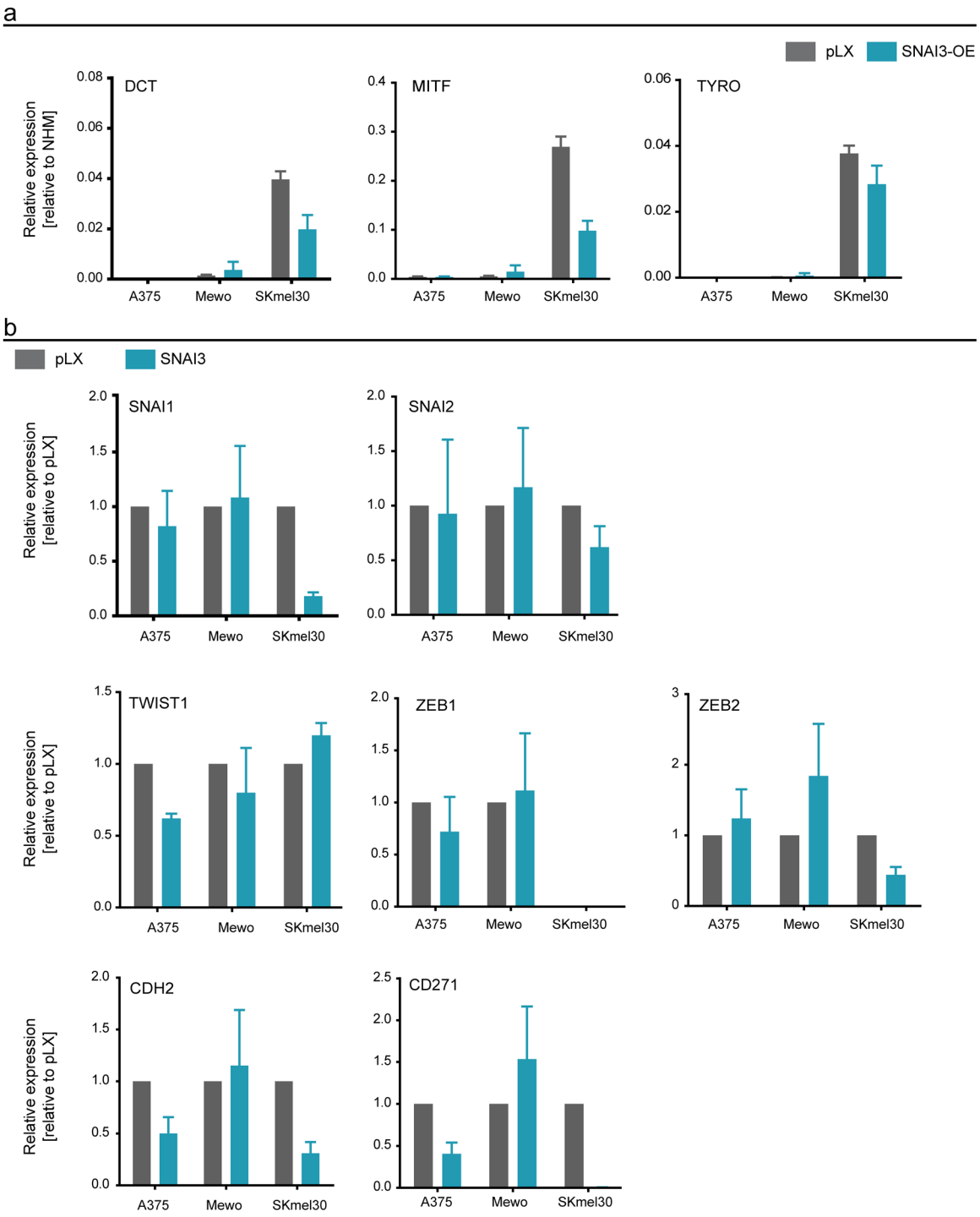

Figure 17 | Expression of invasion-related genes in SNAI3-overexpressing melanoma cells

Gene expression of a panel of genes detected by qPCR. Gapdh was used as endogenous control for all samples. **(a)** Expression of melanocyte-specific markers that were normalized to NHMs as the reference sample. Graph displays mean and CI, n=3. **(b)** Expression of EMT-, de-differentiation- and invasion-associated markers normalized to control cells transduced with pLX as the reference sample. Graph displays mean and CI; n=3.

CI=confidence interval; EMT=epithelial-to-mesenchymal-transition, GAPDH=glyceraldehyde 3-phosphate dehydrogenase; n=technical triplicates; NHM=normal human melanocytes; qPCR=quantitative PCR

SNAI2 showed a moderate downregulation to 60 % compared to pLX-transduced control cells. In addition, ZEB2 was heterogeneously expressed in these three melanoma cells lines upon SNAI3-overexpression whereas ZEB1 remained at the same expression levels after exogenous SNAI3 expression. Another known EMT- and invasion-related marker, TWIST1, did not show enhanced expression upon SNAI3-overexpression. Analysis of other de-differentiation-related markers (CD271, CDH2) revealed that there was no clear direction the cells were driven to regarding their phenotypic status in line with results from functional assays. CDH2 was decreased in A375 and SKmel30 but did not show deregulation in Mewo cells upon SNAI3-overexpression. Expression of CD271 was downregulated in A375 and SKmel30 but did not show any de-regulation in Mewo after SNAI3-overexpression **(Figure 17b)**. These data are in line with the absence of functional differences when SNAI3 was overexpressed in human melanoma cell lines.

Taking all data into account, this study shows that overexpression of SNAI3 in human melanoma cell lines is not sufficient to induce the enhanced invasion capacity observed in murine melanoma cells upon partial reprogramming. However, SNAI3 expression possesses clinical relevance due to its correlation with tumor thickness and a significant increase in expression comparing low-risk to high-risk primary melanomas.

5. Discussion

Reprogramming of cancer cells towards pluripotency has been studied in recent years [184,185,187,225,226]. However, the stepwise conversion of malignant cells with possible changes of cellular functions during the process of reprogramming has not been investigated. Here, I demonstrate that partial reprogramming of murine melanoma cells is a time-dependent and reproducible *in vitro* model that mimics the phenotype switch from highly proliferative and less invasive into less proliferative and highly invasive melanoma cells. In addition, this *in vitro* model led to the identification of SNAI3 as a novel invasion-related marker with potential prognostic value for melanoma patients.

5.1. Murine melanoma cells can be reprogrammed towards full pluripotency

A range of *in vitro* assays confirmed pluripotency in HCmel12- and HCmel17-iPCCs. Cellular morphology, alkaline phosphatase activity and expression of pluripotency-associated markers including Oct4, Sox2 and Nanog, verified the pluripotent state of melanoma cell-derived iPCCs **(Figure 8)**. In addition, whole genome expression analysis revealed a gene expression signature comparable to that of MEF-iPS control cells and a strong separation from parental cells **(Figure 10)**. This indicates that the conversion of HCmel cells into a pluripotent state results in a switch of transcriptome identity as previously shown for reprogrammed cancer cells [184]. In addition, *in vivo* differentiation demonstrated the capacity of HCmel12- and HCmel17-iPCCs to differentiate into cells derived from different germ layers by generation of teratomas upon subcutaneous injections **(Figure 9a, Suppl. Figure 2)**. This is in agreement with other studies showing that reprogramming cancer cells to a pluripotent state enables them to terminally differentiate into different cell types [185].
Moreover, all pluripotency validating assays were performed after established iPCCs have been cultured for at least five passages in the absence of doxycycline. This approves the stability of their pluripotent state independent from exogenous transgene expression. Taken together, these data are in agreement with previously published studies showing the conversion of murine melanoma cells into a pluripotent state with an increase of Sox2 and Oct4 expression and successful teratoma formation [141]. Thus, I successfully reprogrammed two melanoma cell lines towards pluripotency with subsequent differentiation into cells from different germ layers. The fact that parental HCmel17 cells did not induce melanoma generation *in vivo* upon subcutaneous injections can be explained by variances in the procedure of injection. However, HCmel17-M2 cells transduced with Stemcca-blasti in

the absence of doxycycline generated tumors upon subcutaneous injections confirming the tumor initiating capacity of these cells (**Figure 13f**, left panel).

The observed reduction of Ki67 expression in HCmel-iPCC-derived teratomas indicates diminished proliferation. Thus, reprogramming towards pluripotency has effects on cellular functions that are essential for tumor formation, i.e. proliferation. This further supports other studies showing that reprogrammed cancer cells, which are subsequently differentiated into different lineages, show reduced proliferation with abrogation of tumorigenicity *in vivo* [186,187]. In agreement with this, HCmel-iPCCs generated differentiated cells from different lineages *in vivo* supporting the hypothesis that upon reprogramming, cancer cells lose their original morphology and can be converted into terminally differentiated cell types as demonstrated by other reprogrammed cancer cells that were successfully differentiated *in vitro* (**Figure 9a,** [186]). Data from the current study further indicate that the proliferation capacity of cancer cells can be altered experimentally by converting them into a pluripotent state.

Since reprogramming is a complex process involving successive picking and replating of colonies, contamination with other cells is possible. In order to confirm identity of HCmel cells before and after reprogramming, cell lines were authenticated using microsatellite markers for genotyping and showed 100 % consensus, which proves genetic identity of parental and reprogrammed cells (section 3.1.5). Although methylation status of particular loci as another method to prove altered gene expression regulation [141,185,186] has not been investigated in this study, global gene expression signatures confirm the conversion of HCmel melanoma cells towards a pluripotent state **(Figure 10)**.

5.2. Partial reprogramming of melanoma cells is a stable process with time-dependent changes in gene expression

In order to dissect the reprogramming process of melanoma cells, this process was evaluated regarding its stability and biological reproducibility. The examination of the timeline for reprogramming HCmel17 cells revealed colony-formation within seven to 13 days **(Figure 12b)**. This is consistent with the reprogramming time line of HCmel17 cells using the Stemcca vector **(Figure 8)**, where cells showed similar morphological changes within the same time frame. This indicates that the absence of exogenous c-Myc in HCmel17-M2 cells transduced with Stemcca-blasti did not result in delayed reprogramming. The endogenous expression level of c-Myc in HCmel17-M2 cells transduced with Stemcca-blasti without doxycycline administration was identical to that of established HCmel17-iPCCs **(Suppl. Table 3)** and therefore sufficient to reprogram HCmel17-M2 cells without exogenous expression of this factor. This is in agreement with other studies showing that endogenous

expression of particular reprogramming factors enables reprogramming with less than four factors [141,227,228].

Strikingly, reprogramming of melanoma cells represents a stable and reproducible process that comprises gradual changes of global gene expression correlating to the time of transgene expression **(Figure 12e)**, which is in line with detailed analyses of the reprogramming process in MEFs that revealed reproducible and defined steps throughout reprogramming [151]. Although regulation of particular genes, such as downregulation of Thy-1, is known as a reliable indicator during reprogramming of MEFs, the exact same markers cannot be used to measure reprogramming in melanoma cells due to the lineage-dependent absence of these genes in melanoma cells compared to MEFs [150]. However, Mitf as a driver of melanocytic differentiation was downregulated by day 12 of reprogramming indicating successful de-differentiation **(Figure 12d)**. Whether this key player in melanocytic development is downregulated as early as three days after transgene expression, comparable to Thy-1 in fibroblasts, remains subject of investigation [150].

Importantly, melanoma cells show a gradual change in global gene expression between day ten, day 12 and day 18 and all partially reprogrammed cells cluster closer to their pluripotent equivalent than to their parental cell lines indicating that the transcriptional profile of melanoma cells is already lost after ten days of reprogramming **(Figure 12e)**. This is in line with descriptions of the reprogramming process of normal fibroblasts [150]. In addition, HCmel17-derived iPCCs cluster closer to MEF-iPSCs than to the partially reprogrammed HCmel17 cells demonstrating that essential steps take place between day 18 and full attainment of the pluripotent state. This is a difference compared to MEFs reprogrammed with Oct4, Sox2, Klf4, and c-Myc, since they show stable gene expression changes at day nine and onwards, and enter stable pluripotency already at day 12 [151]. Of note, early morphological changes were detected at similar time points during reprogramming of MEFs and HCmel17 cells **(Figure 6a, 8a)**. Therefore, it is likely that early events are similarly regulated but acquisition of full pluripotency is delayed in melanoma cells-derived iPCCs**.** This delay in reprogramming can be explained by the fact that HCmel17 cells harbor mutations that might affect reprogramming efficiency. In depth analysis is required to identify underlying mechanisms.

Non-reprogrammed control cells have been cultured in the same medium like reprogramming cells and did not show a gene expression signature comparable to partially reprogrammed cells **(Figure 12e)**, excluding possible influences of growth factors within the medium to cause changes in gene expression. Also, doxycycline treatment as well as blasticidin selection did not cause reprogramming-associated changes since cells reprogrammed for different periods (ten, 12, 18 days) showed significantly deregulated gene expression when

compared to each other, demonstrating that gene expression alterations are truly caused by transgene expression and subsequent reprogramming of the cells.

The change in gene expression during reprogramming indicates a gradual conversion of melanoma cells into iPCCs *via* expression of transgenes. The analysis of pluripotency-associated marker expression further confirms true reprogramming (AP, Sall4; **Figure 12c-d**). The fact that murine melanoma cells are reprogrammed in a reproducible way with a time-dependent change in gene expression profiles reveals that this *in vitro* model can be used as a tool to further investigate melanoma cells on their route to acquire pluripotency. This can help to understand molecular events and find novel markers that are associated with disease progression, since particularly in melanoma, de-differentiation is associated with metastatic spread, poor prognosis and drug resistance [66,229].

Due to their capability to reprogram within days, mouse cells were chosen for this technical approach. However, it will be interesting to assess whether human melanoma cells show comparable expression changes in a similarly stable shift towards pluripotency. Comparable analysis might reveal underlying mechanisms that are conserved between species. It is also of interest whether reprogramming-induced gene expression changes can also be observed in a two-wave pattern in melanoma cells as it is reported for MEFs [151]. Therefore, deeper analyses of epigenetic modifications including DNA-methylation, changes in chromatin structures and histone modifications will be needed to fully dissect this process in melanoma cells [151,153]. Nevertheless, I illustrate for the first time the stable and time-dependent conversion of murine melanoma cells towards a pluripotent state and provide a novel platform for investigating changes in melanoma cells associated with directed de-differentiation.

5.3. Partial reprogramming induces a transient phenotype switch in HCmel17 cells

Partial reprogramming of melanoma cells revealed a transiently occurring phenotype switch that was accompanied by elevated invasive potential in combination with decreased proliferation. Gene set enrichment analysis of up- and downregulated genes at day 12 after induction of transgene expression revealed that the majority of pathways affected by partial reprogramming were involved in cell adhesion and cytoskeleton remodeling **(Table 4)**. This is in agreement with morphological alterations and 3-dimensional growth of melanoma cells during the reprogramming process **(Figure 12b)** that has also been described for other cells when reprogrammed [150]. Cell adhesion and cytoskeleton remodeling-related processes are also strongly involved in mediating cellular motility and tumor cell invasion [86,87,91]. In line with this, functional analyses in the current study disclosed significantly enhanced invasion capability through basal membrane equivalent *in vitro* and significantly increased

lung colonization *in vivo* at day 12 of reprogramming **(Figure 13a, d)**. This increase in invasion combined with decreased proliferation at day 12 after transgene induction mimics the phenotype switch in melanoma cells from highly proliferative to highly invasive cells [97,98,102]. Decreased proliferation of partially reprogrammed cells *in vitro* was determined by alamarBlue - a vital dye, which is metabolically reduced by cellular enzymes to a fluorescent product that can be measured using standard fluorescence plate readers. Although this assay is widely established as an adequate measurement of cellular proliferation [230–232], the appearance of metabolic changes in partially reprogrammed cells, which may affect the results of alamarBlue reduction, cannot be ruled out. However, further *in vivo* analysis supported *in vitro* data by demonstrating reduced Ki67 expression in tumors derived from partially reprogrammed cells, confirming diminished proliferation **(Figure 13e, f)**.

So far, only the cultivation of melanoma cells in neural crest medium has been shown to induce phenotype switching *in vitro* [78]. Since phenotype switching of melanoma cells has a strong impact on disease progression, novel *in vitro* systems are desirable [222]. Here, I present partial reprogramming as such a novel system to investigate the phenotype-switch. Of note, day-to-day investigations of changes in invasive capacity during the reprogramming process are of further interest to define the day of maximal invasiveness and the pace of phenotype switching. Examining the stability and doxycycline-dependency of the invasive phenotype upon abortion of transgene expression might also help understanding the underlying mechanisms behind the phenotype switch.

5.4. Increased invasion potential in partially reprogrammed cells is not caused exclusively by transgene expression

Partial reprogramming of multiple cell lines gave further insight into its effect on invasive properties. Enhanced invasion potential after partial reprogramming was not only observed in HCmel17 cells but also confirmed in MEFs and Hep1.6 cells. This indicates, that elevated invasion capacity upon partial reprogramming is not a melanoma or a cancer-associated phenomenon only. Interestingly, this switch towards a highly invasive status is reprogramming-dependent since transgene expression alone without effective reprogramming does not induce elevated invasion potential (i.e. Ret2 cells, **Figure 13b**). Reasons for the inability to initiate reprogramming in Ret2 cells remain undetermined. One possible explanation is that their high degree of genomic aberrations prevents them from entering reprogramming. Furthermore functionality of transgenes could be post-transcriptionally or post-translationally modified so that Oct4, Sox and Klf4 cannot induce gene expression alterations efficiently. However, silencing of the complete expression cassette as described for transgenes in general [233] does not cause the inability to

reprogram Ret2 cells, as they were successfully selected using blasticidin **(Table 1)** and upon nine days of selection (day 12 after reprogramming) viable Ret2 cells were detected.
In summary, expression of the Stemcca-blasti in four different cell lines revealed that induction of reprogramming and not transgene expression alone caused enhanced invasion capacity after 12 days. This rules out that ectopic expression of Oct4, Sox2, and Klf4 solely promotes malignant properties of partially reprogrammed cells, especially as previous studies showed that forced Oct4 expression in normal cells *in vivo* caused dysplasia in epithelial tissues [135].

5.5. Partially reprogrammed HCmel17 cells show heterogeneous expression of established invasion-related markers

The transiently elevated invasion potential in partially reprogrammed melanoma cells can give insight into gene expression patterns involved in invasion-associated programs. This section discusses the expression signature of neural crest-related genes in the context of partial reprogramming. In addition, established mesenchymal markers, which are linked to enhanced migratory and invasive potential in development and disease, and their expression during reprogramming will be discussed.

5.5.1. Partially reprogrammed HCmel17 cells do not hijack portions of the neural crest program to acquire invasive properties

Since the cultivation of melanoma cells in neural crest medium has been shown to induce the phenotype switch *in vitro* [78] and expression of neural crest- associated genes results in higher plasticity and enhanced metastatic potential [75], I examined the expression of neural crest-related genes during reprogramming **(Figure 14a)**. Gene sets were chosen in accordance to a study, which demonstrated that malignant melanoma cells hijack portions of the embryonic neural crest invasion program using a chick embryo transplant model [75]. Interestingly, partially reprogrammed melanoma cells appear to use a different program to acquire a highly invasive state since none of the neural crest-related genes shows a strong increase in expression after 12 days of reprogramming. However, a slight increase at day ten and 12 is observed for Nestin (Nes). This is in agreement with data from a study showing that co-expression of Nestin and Sox2 in melanoma cells correlates with disease progression [177]. However, the increase in Nestin upon partial reprogramming is relatively low (log2 [FC]=1.25) and since all other neural crest-related markers are not upregulated at day 12, it indicates that partially reprogrammed cells did not use modulation of the neural crest gene expression signature to acquire enhanced invasive potential. In accordance, another study demonstrated that neural crest-related gene expression signature is rather associated with a group of melanoma cells exhibiting low metastatic potential [80]. Of note,

reprogramming is not the simple reversion of differentiation pathways and does not necessarily induce expression of markers, which are important during early steps of normal differentiation, but rather adapts other mechanisms including mesenchymal-to-epithelial transition (MET) [156,157,234,235]. Thus, expression of neural crest-related markers during the process of reprogramming is not required for HCmel17 cells to acquire pluripotency. However, whether or not neural crest-related genes are expressed at time points during reprogramming that have not been evaluated in this study (earlier than day ten, later than day 18) remains to be investigated.

In summary, comparison of gene expression signatures derived from partially reprogrammed melanoma cells and neural crest cells revealed that neural crest signaling pathways are not involved in invasion-acquisition *via* partial reprogramming.

5.5.2. Mesenchymal markers are not elevated in highly invasive HCmel17 cells

In general, partial reprogramming of melanoma cells induces two types of fate switching. On one hand, cells need to undergo MET-like processes to induce reprogramming, which are defined by expression of epithelial markers and downregulation of mesenchymal markers [234]. On the other hand, partial reprogramming for 12 days leads to higher invasion indicating upregulation of motility-supporting mesenchymal markers [236–238]. These contradicting processes are represented by heterogeneous expression of several different gene-sets at day 12 after reprogramming.

In somatic cells of non-epithelial origin expression of particular cadherins is required for successful reprogramming [157,234]. Therefore, it is expected that melanoma cells also increase cadherins, especially Cdh1, when converted into a pluripotent state. Although melanocytes are derived from the non-epithelial neural crest, they express Cdh1 under physiological conditions in order to maintain intact connections to keratinocytes leading to controlled growth and limited motility. Expression of Cdh1 is also recapitulated in cell culture of human melanocytes [239]. However, the expression is diminished after malignant transformation of melanocytes into melanoma cells [240] and partially re-established at more advanced melanoma stages *in vivo* [239,241]. Consistent with this, Cdh1 is absent in parental HCmel17 cells but is increased at day 12, although still 250-fold lower expressed than in MEF-iPSCs. This is in line with the downregulation of Sparc and Snai2 **(Figure 14e, f)**, which may facilitate higher Cdh1 levels since both transcription factors repress Cdh1-expression in the context of melanoma [236,238]. In addition, Cdh2 downregulation is observed during partial reprogramming in line with occurring MET during reprogramming of somatic cells [157]. Its role in invasion-related processes suggests Cdh2 as a maker for invasive cells, contradicting its decreased expression in combination with elevated invasion

potential observed in partially reprogrammed cells **(Figure 14f)**. Overall, the expression pattern of Cdh1 and Cdh2 is contrary to the observed invasion potential of partially reprogrammed cells. Whether or not partially reprogrammed cells at day 12 after transgene induction are at the stage of complete MET remains subject of investigation.

Expression analysis of other EMT-related genes that are linked to mesenchymal phenotypes (Snai2, Zeb1, Zeb2 and Twist1) reveals a non-specific expression pattern showing that these general EMT-related markers are not essential for acquisition of invasive capacity in partially reprogrammed melanoma cells **(Figure 14b,e)**. These data contradict recent studies stating that a change in EMT-related gene clusters in melanoma cells induces invasive properties in melanoma cells [77]. They describe a switch from Zeb2/Snai2-positive to Zeb1/Twist1-positive melanoma cells when they acquire invasive properties. In contrast, in the current study, Zeb1 and Twist1 are not upregulated but rather downregulated in HCmel17 cells at day 12 of reprogramming despite their high invasion capacity **(Figure 14b)**. It will be of interest whether this decrease in Twist1 and Zeb1 is caused by decreased MEK/ERK signaling upon partial reprogramming since Zeb1 is induced by hyperactivated RAF-signaling [77]. Further in-depth analysis of the phosphorylation status of mediators within the MAPK signaling cascade might reveal the role of its activation in gaining invasive potential.

Snai1 and Snai2 are widely excepted to regulate EMT, trigger invasion in cancer cells and drive metastasis [77,242,243]. Partially reprogrammed melanoma cells exhibit these enhanced migratory and invasive features with increased lung extravasation ability although they express only moderate levels of Snai1 and Snai2 **(Figure 14e)**. However, the expression of Snai1 and Snai2 correlates with MET processes accompanied by downregulated mesenchymal markers during reprogramming [151]. In addition, it will be of interest, whether exogenous Sox2 and Oct4 from the Stemcca-blasti vector suppress the EMT mediator Snai1 during partial reprogramming, since it was shown that Snai1 is directly suppressed by these pluripotency-associated genes during reprogramming of MEFs [157]. Snai1 is known to be absent in the majority of melanoma samples but Snai2 was shown to play an essential role in melanoma progression induced by EMT-like conversions of melanoma cells [77,236,244]. In the present study, Snai1 and Snai2 are present at moderate levels during the process of partial reprogramming (Ct values between 23-26 cycles, **Suppl. Table 5**) but correlate inversely with the transient increase in invasion capacity of partially reprogrammed cells. This is of great interest and indicates that melanoma cells can recruit other pathways to develop an invasive phenotype, which are not accompanied by increased expression of Snai2.

Taken together, partially reprogrammed cells do not imply mesenchymal gene expression to gain motility indicating that increased epithelial markers do not necessarily label non-invasive cells as proposed by several studies [172,238] but can also correlate with invasion capacity

of melanoma cells. Whether this is due to correlative or causative reasons remains to be determined.

The high heterogeneity regarding the expression of particular gene sets can be explained by different hypotheses: First, melanoma cells harbor a repertoire of different mechanisms to induce invasion that are each dependent on certain gene expression patterns but are independent from each other resulting in contradicting expression data regarding particular markers.

Second, induction of reprogramming induces expression of epithelial markers and melanoma cells acquire enhanced invasion despite this reprogramming-induced upregulation of epithelial markers. It remains unclear whether partial reprogramming and acquisition of invasive properties are organized in a hierarchical manner so that one process dominates the other one regarding gene expression signatures and thus hides important regulators of invasion.

Of note, the expression of controversially discussed melanoma stem cell markers Cd133 and Rank did not correlate with invasive potential of partially reprogrammed cells [63,72] **(Suppl. Figure 4)**. The high invasion potential of partially reprogrammed cells did also not correlate to Jarid1b expression, which has been shown to be dynamically expressed and to label a slowly proliferating population required for continuous melanoma growth [73]. Assuming a true capability of these markers to label melanoma-initiating cells [63,73], this data implicate that underlying mechanisms behind melanoma initiation and melanoma progression might be distinctive. Melanoma stem cell markers might label cells with higher tumorigenic potential but they are not necessarily linked to higher invasion capacity and disease progression. Interestingly, partial reprogramming led to transiently increased Cd271 expression **(Suppl. Figure 4)**. Although Cd271 has been discussed as a melanoma stem cell marker [66,70] it was also linked to de-differentiation of melanoma cells [245]. It is likely that the correlative expression pattern of Cd271 and the transiently enhanced invasion potential of partially reprogrammed cells is rather linked to Cd271's role in de-differentiation than to its melanoma stem cell-labeling properties. Taken together, the regulation of enhanced invasion in partially reprogrammed cells did not imply expression of melanoma stem cell markers.

5.6. The invasion mode of partially reprogrammed cells is linked to amoeboid-like migration rather than MMP-driven proteolytic migration

It is unlikely that the enhanced invasive property of partially reprogrammed cells is caused by proteolytic degradation of extracellular matrix. MMPs, which have been shown previously to

be involved in melanoma cell invasion [85,87–90] were not upregulated at day 12 after reprogramming **(Figure 14c).** In contrast, a strong downregulation of Mmp3, Mmp2 and Mmp14 was observed during the process of reprogramming with maximum decrease in completely reprogrammed HCmel17-iPCCs. Moreover, MMPs in general were absent in the list of genes upregulated after reprogramming for 12 days **(Suppl. Table 6)**. These data indicate that proteolytic degradation is not a main mode of promoting invasion upon partial reprogramming. Of note, Mmps are primarily regulated by posttranslational modifications and not *via* changes in expression [246], so that microarray-derived expression data used in the present study leave open the possibility of enhanced Mmp-activation despite decreased expression. However, the vast decrease, especially of Mmp2 and Mmp14 mRNA (log2 [FC]≤-3), suggests a proteolysis-independent mode of action.

Another invasion mode of cancer cells is the so called “amoeboid mode”, which is associated with a small spherical shape of cells [91,95]. Strikingly, this morphology is found in the small round shape of partially reprogrammed HCmel17 cells and the loss of HCmel17-characteristic processes after partial reprogramming (inlay in **Figure 12b**). Also, cytoskeleton remodeling is among the top ten pathways that are enriched in differentially regulated genes upon partial reprogramming **(Table 4)**. Thus, the expression of particular genes, known to be involved in the amoeboid mode of invasion [86,91,95,247], was analyzed to examine whether amoeboid-related invasion was associated with increased lung colonization and enhanced invasion capability *in vitro* **(Suppl. Figure 5)**. Of note, Tesk1 and Limk2, two mediators of cytoskeleton remodeling, were shown to be roadblocks for reprogramming MEFs towards the pluripotent state and their knockdown promotes cellular reprogramming [162]. Interestingly, Tesk1 expression was not altered and Limk2 was even increased at day 12 of reprogramming **(Suppl. Figure 5)**. Thus, downregulation of these molecules might be required for cytoskeleton remodeling during full reprogramming of somatic cells but the invasive phenotype of melanoma cells upon partial reprogramming does not involve downregulation of Tesk1 and Limk2 expression. However, cytoskeleton remodeling-associated programs are activated at day 12 demonstrated by gene set enrichment analysis **(Table 4)**.

In addition, partially reprogrammed melanoma cells and highly invasive breast cancer cells share a subset of genes that are differentially regulated (**Figure 13g**, [216]). Here, the cytoskeleton remodeling-associated genes were concomitantly regulated (i.e. Shroom3 [217], Atp1a1 [218], and Atp6v1c1), whereas upregulation of general mesenchymal markers observed in invasive breast cancer cells (i.e. Glipr-2 [220] and Fibronectin/Fn [221]), was not required for partially reprogrammed cells to become invasive. This is in line with unchanged or decreased expression of additional mesenchymal markers discussed above.

Breast cancer cells are known to use the cytoskeleton-influencing Cofilin signaling pathway to respond to environmental stimuli and enhance motility [215]. Members of the Cofilin pathway are also described to play an essential role in other tumor types including melanoma [248]. Analysis of gene set enrichment within processes involved in cytoskeleton remodeling pathways reveals the melanoma-associated MAPK signaling pathway as the process with the highest enrichment in deregulated genes upon partial reprogramming and concomitant increase in invasion **(Table 5)**. Interestingly, the Cofilin-pathway is integrated in the MAPK-signaling cascade **(Suppl. Figure 6)**. Breast cancer cells are described to de-regulate the Cofilin-pathway in order to permit initiation of actin polymerization, which drives the motility cycle and ultimately leads to acquisition of invasive properties (reviewed in [215]). Expression data derived from partially reprogrammed HCmel17 cells indicate deceased Cofilin activity due to its decreased expression **(Suppl. Figure 6)**. In addition, Limk was upregulated, which inactivates Cofilin *via* phosphorylation. However, recent studies revealed that the activity of Cofilin cannot be measured appropriately by determining the expression level or the phosphorylation status of Cofilin due to different regulatory mechanisms, which are independent from each other and do not all depend on phosphorylation [249,250]. Thus, expression data that just describe the presence of total Cofilin, are not sufficient to predict its signaling activity. In addition, it was demonstrated that not the expression of single genes within the Cofilin pathway but rather the net outcome of Cofilin signaling is crucial for induction of cellular motility [216]. This might also explain the assumed contradiction of increased Limk2 expression during partial reprogramming despite its role as roadblocks for reprogramming, which further supports the hypothesis, that the overall net outcome of the Cofilin signaling cascade is superior to the deregulation of single genes involved in this pathways [215].

In summary, the role of differentially regulated genes involved in Cofilin signaling indicates that this pathway might be involved in the complex mode of cellular invasion, which could not be explained by neural crest– or EMT–

p-value	Processes within pathway #9
4.1^{-31}	MAPK cascade
4.80^{-28}	Positive regulation of cell migration
8.86^{-25}	Protein phosphorylation
4.69^{-23}	Angiogenesis
1.54^{-21}	Phosphorylation
6.99^{-19}	Response to hypoxia
3.70^{-18}	Actin cytoskeleton organization
6.44^{-18}	Positive regulation of peptidyl-serine phosphorylation
9.38^{-18}	Wound healing
1.79^{-16}	Regulation of early endosome to late endosome transport

Table 5 | Gene enrichment analysis of processes within the cytoskeleton remodeling pathway
Displayed are the top 10 processes involved in the pathway *cytoskeleton remodeling* (#9 from enrichment analysis, Table 2) that are enriched in de-regulated genes after 12 days of reprogramming.
Analysis tools: Metacore (processes are derived from pathway #9 in Table 2; p-value for gene set enrichment in processes are shown in table).
MAPK=mitogen-activated protein kinase

related signaling changes. Direct analysis of polymerization and bundling of actin filaments as the net-outcome of Cofilin signaling might help to further elucidate whether Cofilin-deregulation causes enhanced invasion upon partial reprogramming. In addition, experimental depletion of Cofilin in HCmel17 cells and subsequent partial reprogramming will uncover whether the invasion increase at day 12 depends on this actin-binding protein.

Taken together, it remains to be elucidated whether this invasion-program associated with partial reprogramming of murine melanoma cells is also present in human melanoma cells *in vitro* and *in vivo*. However, this study shows that the experimental *in vitro* system of partial reprogramming can be used to identify novel processes that might be connected to invasive properties of melanoma cells.

5.7. SNAI3 is a novel invasion-related marker for melanoma with potential for clinical application

Analysis of gene expression at day 12 and 18 revealed that Carcinoembryonic antigen-related cell adhesion molecule 1 (Ceacam1) was also among the top five genes, which were highly upregulated at day 12 **(Figure 14d)**. Previous studies found that this adhesion molecule shows gradually increasing expression from melanocytic nevi to metastatic specimens and is therefore a prognostic marker for melanoma progression [251]. Moreover, Ceacam1 is also functionally involved in resistance against anti-melanoma therapy and promotes melanoma cell invasion [252]. This further indicates possible causative roles for genes, which expression correlates with the transient phenotype switch in HCmel17 cells upon partial reprogramming. Thus, I propose this *in vitro* model as a novel system to identify unknown candidate genes that are expressed in accordance to the transiently enhanced invasion capability and might be functionally involved in melanoma progression.

Strikingly, Snai3 is expressed in correlation with the elevated invasion potential of melanoma cells when they were subjected to partial reprogramming **(Figure 14e)**. Since this transcription factor has been discovered as recently as 2002, its function in carcinogenesis has not been investigated yet. Presence of SNAI3 was confirmed on protein level *in vivo* in subcutaneous tumors derived from partially reprogrammed cells **(Figure 14g)** and in lung-infiltrating melanoma cells derived from mice intravenously injected with partially reprogrammed cells **(Figure 14h)**.

Visualization of SNAI3 in human tissues reveals that nevi are barely stained, whereas primary melanomas show non-homogenous staining with more prominent staining in deeper areas **(Figure 15a)**. The differential expression in mouse and in human melanoma tissue

indicates controlled SNAI3-expression during melanomagenesis making this transcription factor an interesting biomarker.

In the present study, the quantitative analysis of a tissue microarray using defined IHC scores reveals significantly increased SNAI3 expression in primary melanoma compared to nevi. Strikingly, SNAI3 expression *in vivo* correlates with staging of patients suffering from primary melanomas. SNAI3 staining significantly increases from low-risk to high-risk primary melanomas. These data indicate that SNAI3 rather correlates with deeper growth of primary melanomas than with initiation of malignant transformation of melanocytes in benign nevi. Data from SNAI3 visualization in human tissues are in line with increased SNAI3 expression in partially reprogrammed murine cells, which comprise increased invasion capability *in vitro* and *in vivo* **(Figure 14e)**. Of note, it remains to be determined whether SNAI3 expression is required for enhanced invasion capability of partially reprogrammed cells or whether it simply labels invasive melanoma cells rather than being actively involved in inducing invasive properties. Experimental depletion of SNAI3 in parental HCmel17 cells and subsequent induction of partial reprogramming will uncover whether SNAI3 is required for reprogramming and for the highly invasive phenotype of partially reprogrammed melanoma cells.

In melanoma, a variety of biomarkers has been identified during the last decades using high throughput screening (reviewed in [253] and [254]). All biomarkers identified using cell lines and high throughput analysis of gene expression require confirmation in independent data sets and verification in clinically relevant settings [253]. SNAI3, which I identified using a cell line-based *in vitro* assay, demonstrates clinical relevance by being differently expressed within primary tumors with prominence in invasive regions. This brings SNAI3 a step closer to clinical application. Importantly, in melanoma a drastic drop of five-year relative survival is observed between stage 0 and IV. 89 % to 95 % with localized stage I survive five years after diagnosis, whereas only 9 % to 19 % with distant stage IV melanoma reach this time point [255]. Thus, the conversion from a low-risk to a high-risk primary melanoma defines disease progression and this underlines the need for biomarkers, which distinguish between these stages of primary melanomas, i.e. SNAI3.

In mice, SNAI3 expression was high in experimental primary melanomas but strong expression was not maintained in lung-infiltrating melanoma cells **(Figure 14g-h)**, implying a switch of expression signature as melanoma cells metastasize. This is in agreement with previous studies showing the reversible adjustment of expression of other genes in metastasizing melanoma cells, e.g. Brn2 and pigmentation-related genes [102]. The study also disclosed that circulating melanoma cells show the expression pattern of highly invasive cells disseminating from the primary melanoma. Thus, it is of great interest whether SNAI3-positive melanoma cells are present in the circulating of melanoma patients. This analysis will define whether SNAI3 also has the potential to be used as a serum biomarker. In

addition, paired SNAI3 expression analyses of primary melanomas and their associated metastases, are required in order to determine SNAI3's potential to label invasive cells in a reversible manner in human as demonstrated experimentally in murine cells.

In summary, I demonstrate that partial reprogramming reveals the novel biomarker SNAI3 that correlates with tumor thickness and distinguishes between low-risk and high-risk melanomas. This proves that partial reprogramming of melanoma cells is a suitable *in vitro* model to identify biomarkers for melanoma progression and patient stratification.

5.8. Exogenous expression of SNAI3 in human melanoma cells is not sufficient to enhance invasive properties *in vitro*

Although expression of SNAI3 correlates with the transiently occurring invasive phenotype switch in melanoma cells upon partial reprogramming and to tumor thickness in human melanoma, its ectopic expression in human melanoma cells is not sufficient to enhance invasion capacity *in vitro*.

Four melanoma cell lines and immortalized human fibroblasts were stably transduced with an empty control vector (pLX) or a SNAI3-encoding vector in order to examine the effect of ectopic SNAI3 expression on cellular functions. Interestingly, fibroblasts overexpressing SNAI3 displayed an elongated cell body indicating a senescence–like morphology [256] together with decreased proliferation so that these cells could not be cultured for more than one passage **(Figure 16d)**. The fact that cells do not proliferate but can be cultured for longer than 14 days without passaging indicates senescence rather than increased cell death upon SNAI3 expression. However, whether senescence-associated mechanisms are truly activated upon SNAI3-overexpression in fibroblasts remains to be determined. Of note, inhibited proliferation upon SNAI3-overexpression is not caused by blasticidin selection since pLX-transduced cells were cultured under the exact same selection-condition and they kept their normal morphology and could be cultured under normal conditions for at last seven passages (data not shown). This indicates that SNAI3 has an effect on proliferation or senescence of fibroblasts, whereas in contrast, melanoma cell lines overexpressing SNAI3 did not discontinue to proliferate and could be cultured for at least seven passages after blasticidin selection. In addition, in melanoma cell lines, SNAI3-overexpression does not induce morphological changes comparable to senescence-triggered elongation of the cell body showing that the effect of SNAI3 regarding senescence differs when it is overexpressed in normal fibroblasts or in melanoma cells. This difference might be caused by the fact that fibroblasts are non-malignant cells and SNAI3 expression only induces senescence-like morphology in normal cells, or that the effect is lineage dependent. SNAI3 overexpression in normal melanocytes will elucidate the dependence of morphological alterations on the

melanocytic lineage. This is technically challenging since normal human melanocytes are difficult to transduce and thus, fibroblasts were used as non-malignant control cells in this study.

Although morphology is not affected by SNAI3 overexpression, proliferation was slightly decreased to 80 % in two out of the three analyzed melanoma cell lines **(Figure 16e)**. However, it remains to be investigated whether this change of proliferation in SNAI3 expressing melanoma cells is biologically relevant since the maximum decrease was limited to 20 %. Interestingly, SNAI3 overexpression in melanoma cells does not enhance migration through defined pores or invasion through a basal membrane equivalent *in vitro* using chemotactic attraction with FCS. The migration and invasion capacity of Mewo and SKmel30 cells were not affected by SNAI3 expression and the trend of increased migration and invasion in A375 cells could be explained by biological variance indicated by high standard deviation for pLX-transduced control cells **(Figure 16f-g)**. Invasion and migration are dependent on chemotactic stimuli and it has been described that different chemoattractants result in different outcomes [257,258]. Whether different starving conditions including glucose depletion affect the invasion capacities of human melanoma cells *in vitro* needs to be further investigated.

In general, the overexpression of a single gene might not lead to functional changes since the acquisition of migratory and invasive capacities is a complex progress and can be induced by a variety of different molecular mechanisms. Thus, the inability of SNAI3 overexpression to induce enhanced invasion capacity *in vitro* does not prove that it is dispensable for invasion in human melanoma cells. It remains to be investigated whether other factors might act synergistically with SNAI3 in order to promote invasive programs.

In summary, SNAI3 overexpression in human melanoma cells is not sufficient to enhance migratory or invasive properties *in vitro*. However, the correlation of SNAI3 expression in human melanoma samples to disease progression supports the high clinical relevance as a biomarker, which distinguishes between low-risk and high-risk primary melanomas.

6. Conclusion

This study was set out to dissect the reprogramming process of murine melanoma cells on their route to pluripotency in order to investigate the role of directed de-differentiation on melanoma cells' function. It revealed that reprogramming is a time-dependent and reproducible process in murine HCmel17 melanoma cells. Furthermore, it discovered that partial reprogramming induces a transiently occurring phenotype switch of melanoma cells, which describes the conversion of highly proliferative and less invasive to less proliferative and highly invasive cells. This study further aimed to identify novel markers, which correlate with the metastatic potential of melanoma cells. These markers are of great importance because of the extremely high increase of mortality once a melanoma has metastasized. Using the model of partial reprogramming, I identified SNAI3 as a novel invasion-related marker that correlates with tumor thickness and distinguishes between low-risk and high-risk melanomas.

In summary, two main conclusions are emphasized. First, neural crest-related gene expression, which has been previously shown to be heavily involved in enhanced invasion capacity of melanoma cells using different *in vitro* models [75,259], was not recruited during partial reprogramming. This is in agreement with another study showing that expression of neural crest-related genes is not increased in highly invasive human melanoma cells [80]. Therefore, invasive properties might be promoted by independent programs in melanoma cells, which further highlights their tremendous plasticity. Taken together, these results underline the need for careful interpretation of artificial *in vitro* systems since they might mimic biological phenomenons but do not necessarily provide insight into the underlying mechanisms that are recruited *in vivo*. This study demonstrates that different *in vitro* assays can show identical biological outcomes (enhanced invasion) without mediating it through the same molecular routes (neural crest-dependent vs. neural crest-independent pathways). Whether or not one or more of these assays give physiologically relevant insights into gene expression changes remains subject of investigation.

The second major conclusion of this study is that the analysis of primary tumors and metastases, in respect to biomarkers that label invasive melanoma cells, is of great importance. Studies often compare gene expression between primary tumors and metastases to identify targets, which are more strongly expressed in metastases. Using these genes to find molecular mechanisms that promote disease progression and metastases implies a major challenge. Melanoma cells possess the ability to alter their

proliferation and invasion capacity in response to environmental signals [97]. Most likely, a reversible phenotype switch enables melanoma cells to disseminate from the primary tumor and establish metastases at secondary sites, which exhibit the heterogeneity of the primary tumor [96,102]. Thus, highly invasive melanoma cells are most probably present on the invasive border of primary tumors and in the circulation to home to distant organs. Within the established metastasis only a minority of cells are expected to be highly invasive, because at secondary tumor sites, proliferation is superior to invasive properties in order to establish a novel melanoma-metastasis. This has been elegantly shown by a study proving the reversible expression of differentiation/proliferation- associated and invasion-associated genes when melanoma cells become metastatic [102]. Strikingly, the expression of SNAI3, which I identified as a novel invasion-associated marker, distinguishes between low-risk and high-risk melanomas in patients. This increased expression in primary tumors with high risk to metastasize indicates a link between SNAI3 expression and invasive potential of melanoma cells. *In vitro*, partially reprogrammed murine melanoma cells strongly expressed SNAI3 in tumors that formed after subcutaneous injections, but only few melanoma cells were SNAI3-positive in experimental lung metastases. This indicates a possible switch of SNAI3 expression after dissemination from primary tumors. However, this has to be thoroughly investigated by SNAI3 expression analysis in human melanoma metastases.

In summary, this study offers novel insight into melanoma cell reprogramming and the role of directed de-differentiation on invasive capacity of melanoma cells. It contributes to our understanding of the concept of melanoma phenotype switching by establishing a novel *in vitro* system. Moreover, SNAI3 was identified as a novel invasion-related marker with potential for clinical application as it allows to distinguish between human melanomas with low and high risk to metastasize.

7. References

[1] Rigel, D.S.; Friedman, R.J.; Kopf, A.W. The Incidence of Malignant Melanoma in the United States: Issues as We Approach the 21st Century. *J. Am. Acad. Dermatol.*, **1996**, *34*, 839–847.

[2] Ferlay, J.; Soerjomataram, I.; Ervik, M.; Dikshit, R.; Eser, S.; Mathers, C.; Rebelo, M.; Parkin, D.; Forman, D.; Bray, F. GLOBOCAN 2012 v1.0, Cancer Incidence and Mortality Worldwide: IARC CancerBase No. 11 [Internet]. Lyon, France: International Agency for Research on Cancer.

[3] Jhappan, C.; Noonan, F.P.; Merlino, G. Ultraviolet Radiation and Cutaneous Malignant Melanoma. *Oncogene*, **2003**, *22*, 3099–3112.

[4] American Cancer Society. Cancer Facts & Figures 2014. *Atlanta Am. Cancer Soc.*, **2014**.

[5] Yaar, M.; Gilchrest, B. a. Ageing and Photoageing of Keratinocytes and Melanocytes. *Clin. Exp. Dermatol.*, **2001**, *26*, 583–591.

[6] Carsberg, C.J.; Warenius, H.M.; Friedmann, P.S. Ultraviolet Radiation-Induced Melanogenesis in Human Melanocytes Effects of Modulating Protein Kinase C. *J. Cell Sci.*, **1994**, *107*, 2591–2597.

[7] Brenner, M.; Hearing, V.J. The Protective Role of Melanin Against UV Damage in Human Skin. *Photochem. Photobiol.*, **2008**, *84*, 539–549.

[8] Cichorek, M.; Wachulska, M.; Stasiewicz, A.; Tymińska, A. Skin Melanocytes: Biology and Development. *Postępy dermatologii i Alergol.*, **2013**, *30*, 30–41.

[9] Le Douarin, N.M.; Creuzet, S.; Couly, G.; Dupin, E. Neural Crest Cell Plasticity and Its Limits. *Development (Cambridge, England)*, **2004**, *131*, 4637–4650.

[10] Dorsky, R.I.; Moon, R.T.; Raible, D.W. Control of Neural Crest Cell Fate by the Wnt Signalling Pathway. *Lett. to Nat.*, **1998**, *396*, 370–373.

[11] Sieber-Blum, M.; Cohen, A.M. Clonal Analysis of Quail Neural Crest Cells. *Dev. Biol.*, **1980**, *80*, 96–106.

[12] Gilbert, S. The Neural Crest. In *Developmental Biology*; 2000, S.A., Ed.; Associates, Sinauer: Sunderland (MA), **2000**.

[13] Erickson, C. a.; Duong, T.D.; Tosney, K.W. Descriptive and Experimental Analysis of the Dispersion of Neural Crest Cells along the Dorsolateral Path and Their Entry into Ectoderm in the Chick Embryo. *Dev. Biol.*, **1992**, *151*, 251–272.

[14] Ernfors, P. Cellular Origin and Developmental Mechanisms during the Formation of Skin Melanocytes. *Exp. Cell Res.*, **2010**, *316*, 1397–1407.

[15] Vance, K.W.; Goding, C.R. The Transcription Network Regulating Melanocyte Development and Melanoma. *Pigment Cell Res.*, **2004**, *17*, 318–325.

[16] Sauka-Spengler, T.; Bronner-Fraser, M. A Gene Regulatory Network Orchestrates Neural Crest Formation. *Nat. Rev. Mol. Cell Biol.*, **2008**, *9*, 557–568.

[17] Dhillon, a S.; Hagan, S.; Rath, O.; Kolch, W. MAP Kinase Signalling Pathways in Cancer. *Oncogene*, **2007**, *26*, 3279–3290.

[18] Cargnello, M.; Roux, P.P. Activation and Function of the MAPKs and Their Substrates, the MAPK-Activated Protein Kinases. *Microbiol. Mol. Biol. Rev.*, **2011**, *75*, 50–83.

[19] Matallanas, D.; Birtwistle, M.; Romano, D.; Zebisch, A.; Rauch, J.; von Kriegsheim, A.; Kolch, W. Raf Family Kinases: Old Dogs Have Learned New Tricks. *Genes Cancer*, **2011**, *2*, 232–260.

[20] Davies, H.; Bignell, G.R.; Cox, C.; Stephens, P.; Edkins, S.; Clegg, S.; Teague, J.; Woffendin, H.; Garnett, M.J.; Bottomley, W.; Davis, N.; Dicks, E.; Ewing, R.; Floyd, Y.; Gray, K.; Hall, S.; Hawes, R.; Hughes, J.; Kosmidou, V.; Menzies, A.; Mould, C.; Parker, A.; Stevens, C.; Watt, S.; Hooper, S.; Wilson, R.; Jayatilake, H.; Gusterson, B. a; Cooper, C.; Shipley, J.; Hargrave, D.; Pritchard-Jones, K.; Maitland, N.; Chenevix-Trench, G.; Riggins, G.J.; Bigner, D.D.; Palmieri, G.; Cossu, A.; Flanagan, A.; Nicholson, A.; Ho, J.W.C.; Leung, S.Y.; Yuen, S.T.; Weber, B.L.; Seigler, H.F.; Darrow, T.L.; Paterson, H.; Marais, R.; Marshall, C.J.; Wooster, R.; Stratton, M.R.; Futreal, P.A. Mutations of the BRAF Gene in Human Cancer. *Nature*, **2002**, *417*, 949–954.

[21] Long, G. V; Menzies, A.M.; Nagrial, A.M.; Haydu, L.E.; Hamilton, A.L.; Mann, G.J.; Hughes, T.M.; Thompson, J.F.; Scolyer, R. a; Kefford, R.F. Prognostic and Clinicopathologic Associations of Oncogenic BRAF in Metastatic Melanoma. *J. Clin. Oncol.*, **2011**, *29*, 1239–1246.

[22] Goydos, J.; Mann, B.; Kim, H.; Gabriel, E.; Alsina, J.; Germino, F.; Shih, W.; Gorski, D. Braf and Nras Mutations in Melanoma. *J. Am. Coll. Surg.*, **2005**, *200*, 362–370.

[23] Tsao, H.; Zhang, X.; Benoit, E.; Haluska, F.G. Identifcation of PTEN/MMAC1 Alterations in Uncultured Melanomas and Melanoma Cell Lines. *Oncogene*, **1998**, *16*, 3397–3402.

[24] CDKN2A cyclin-dependent kinase inhibitor 2A http://www.ncbi.nlm.nih.gov/gene/1029.

[25] Al-Kaabi, A.; Bockel, L.W. van; Pothen, A.J.; Willems, S.M. p16 INK4A and p14 ARF Gene Promoter Hypermethylation as Prognostic Biomarker in Oral and Oropharyngeal Squamous Cell Carcinoma : A Review. *Hindawi Publ. Corp.*, **2014**, *2014*, 8 pages.

[26] Young, R.J.; Waldeck, K.; Martin, C.; Foo, J.H.; Cameron, D.P.; Kirby, L.; Do, H.; Mitchell, C.; Cullinane, C.; Liu, W.; Fox, S.B.; Dutton-Regester, K.; Hayward, N.K.; Jene, N.; Dobrovic, A.; Pearson, R.B.; Christensen, J.G.; Randolph, S.; McArthur, G. a; Sheppard, K.E. Loss of CDKN2A Expression Is a Frequent Event in Primary Invasive Melanoma and Correlates with Sensitivity to the CDK4/6 Inhibitor PD0332991 in Melanoma Cell Lines. *Pigment Cell Melanoma Res.*, **2014**, *27*, 590–600.

[27] Bollag, G.; Hirth, P.; Tsai, J.; Zhang, J.; Ibrahim, P.N.; Cho, H.; Spevak, W.; Zhang, C.; Zhang, Y.; Habets, G.; Burton, E. a; Wong, B.; Tsang, G.; West, B.L.; Powell, B.; Shellooe, R.; Marimuthu, A.; Nguyen, H.; Zhang, K.Y.J.; Artis, D.R.; Schlessinger, J.; Su, F.; Higgins, B.; Iyer, R.; D'Andrea, K.; Koehler, A.; Stumm, M.; Lin, P.S.; Lee, R.J.; Grippo, J.; Puzanov, I.; Kim, K.B.; Ribas, A.; McArthur, G. a; Sosman, J. a; Chapman, P.B.; Flaherty, K.T.; Xu, X.; Nathanson, K.L.; Nolop, K. Clinical Efficacy of a RAF Inhibitor Needs Broad Target Blockade in BRAF-Mutant Melanoma. *Nature*, **2010**, *467*, 596–599.

[28] Chapman, P.B.; Hauschil, A.; Robert, C.; Larkin, J.M.G.; Haanen, J.B.A.G.; Ribas, A.; Hogg, D.; Hamid, O.; Ascierto, P.A.; Testori, A.; Lorigan, P.; Dummer, R.; Sosman, J.A.; Garbe, C.; Maio, M.; Nolop, K.B.; Nelson, B.J.; Joe, A.K.; Flaherty, K.T.; McArthur, G.A. Updated Overall Survival (OS) Results for BRIM-3, a Phase III Randomized, Open-Label, Multicenter Trial Comparing BRAF Inhibitor Vemurafenib (vem) with Dacarbazine (DTIC) in Previously Untreated Patients with BRAFV600E-Mutated Melanoma. *2012 ASCO Annu. Meet.*, **2012**.

[29] Hauschild, A.; Grob, J.-J.; Demidov, L. V; Jouary, T.; Gutzmer, R.; Millward, M.; Rutkowski, P.; Blank, C.U.; Miller, W.H.; Kaempgen, E.; Martín-Algarra, S.; Karaszewska, B.; Mauch, C.; Chiarion-Sileni, V.; Martin, A.-M.; Swann, S.; Haney, P.; Mirakhur, B.; Guckert, M.E.; Goodman, V.; Chapman, P.B. Dabrafenib in BRAF-Mutated Metastatic Melanoma: A Multicentre, Open-Label, Phase 3 Randomised Controlled Trial. *Lancet*, **2012**, *380*, 358–365.

[30] Nazarian, R.; Shi, H.; Wang, Q.; Kong, X.; Koya, R.C.; Lee, H.; Chen, Z.; Lee, M.-K.; Attar, N.; Sazegar, H.; Chodon, T.; Nelson, S.F.; McArthur, G.; Sosman, J. a; Ribas, A.; Lo, R.S. Melanomas Acquire Resistance to B-RAF(V600E) Inhibition by RTK or N-RAS Upregulation. *Nature*, **2010**, *468*, 973–977.

[31] Kaplan, F.M.; Mastrangelo, M.J.; Aplin, A.E. The Wrath of RAFs: Rogue Behavior of B-RAF Kinase Inhibitors. *J. Invest. Dermatol.*, **2010**, *130*, 2669–2671.

[32] Montagut, C.; Sharma, S. V; Shioda, T.; McDermott, U.; Ulman, M.; Ulkus, L.E.; Dias-Santagata, D.; Stubbs, H.; Lee, D.Y.; Singh, A.; Drew, L.; Haber, D. a; Settleman, J. Elevated CRAF as a Potential Mechanism of Acquired Resistance to BRAF Inhibition in Melanoma. *Cancer Res.*, **2008**, *68*, 4853–4861.

[33] Johannessen, C.M.; Boehm, J.S.; Kim, S.Y.; Thomas, S.R.; Wardwell, L.; Johnson, L. a; Emery, C.M.; Stransky, N.; Cogdill, A.P.; Barretina, J.; Caponigro, G.; Hieronymus, H.; Murray, R.R.; Salehi-Ashtiani, K.; Hill, D.E.; Vidal, M.; Zhao, J.J.; Yang, X.; Alkan, O.; Kim, S.; Harris, J.L.; Wilson, C.J.; Myer, V.E.; Finan, P.M.; Root, D.E.; Roberts, T.M.; Golub, T.; Flaherty, K.T.; Dummer, R.; Weber, B.L.; Sellers, W.R.; Schlegel, R.; Wargo, J. a; Hahn, W.C.; Garraway, L. a. COT Drives Resistance to RAF Inhibition through MAP Kinase Pathway Reactivation. *Nature*, **2010**, *468*, 968–972.

[34] Poulikakos, P.I.; Zhang, C.; Bollag, G.; Shokat, K.M.; Rosen, N. RAF Inhibitors Transactivate RAF Dimers and ERK Signalling in Cells with Wild-Type BRAF. *Nature*, **2010**, *464*, 427–430.

[35] Nakamura, A.; Arita, T.; Tsuchiya, S.; Donelan, J.; Chouitar, J.; Carideo, E.; Galvin, K.; Okaniwa, M.; Ishikawa, T.; Yoshida, S. Antitumor Activity of the Selective Pan-RAF Inhibitor TAK-632 in BRAF Inhibitor-Resistant Melanoma. *Cancer Res.*, **2013**, *73*, 7043–7055.

[36] Emery, C.M.; Vijayendran, K.G.; Zipser, M.C.; Sawyer, A.M.; Niu, L.; Kim, J.J.; Hatton, C.; Chopra, R.; Oberholzer, P. a; Karpova, M.B.; MacConaill, L.E.; Zhang, J.; Gray, N.S.; Sellers, W.R.; Dummer, R.; Garraway, L. a. MEK1 Mutations Confer Resistance to MEK and B-RAF Inhibition. *Proc. Natl. Acad. Sci.*, **2009**, *106*, 20411–20416.

[37] Smalley, K.S.M.; Lioni, M.; Dalla Palma, M.; Xiao, M.; Desai, B.; Egyhazi, S.; Hansson, J.; Wu, H.; King, A.J.; Van Belle, P.; Elder, D.E.; Flaherty, K.T.; Herlyn, M.; Nathanson, K.L. Increased

Cyclin D1 Expression Can Mediate BRAF Inhibitor Resistance in BRAF V600E-Mutated Melanomas. *Mol. Cancer Ther.*, **2008**, *7*, 2876–2883.

[38] US Food and Drug Administration. Trametinib. *http://www.fda.gov/Drugs/InformationOnDrugs/ApprovedDrugs/ucm354478.htm*, **2013**.

[39] Flaherty, K.T.; Robert, C.; Hersey, P.; Nathan, P.; Garbe, C.; Milhem, M.; Demidov, L. V; Hassel, J.C.; Rutkowski, P.; Mohr, P.; Dummer, R.; Trefzer, U.; Larkin, J.M.G.; Utikal, J.; Dreno, B.; Nyakas, M.; Middleton, M.R.; Becker, J.C.; Casey, M.; Sherman, L.J.; Wu, F.S.; Ouellet, D.; Martin, A.-M.; Patel, K.; Schadendorf, D. Improved Survival with MEK Inhibition in BRAF-Mutated Melanoma. *N. Engl. J. Med.*, **2012**, *367*, 107–114.

[40] US Food and Drug Administration. Trametinib and Dabrafenib. *http://www.fda.gov/Drugs/InformationOnDrugs/ApprovedDrugs/ucm381451.htm*, **2014**.

[41] Flaherty, K.T.; Infante, J.R.; Daud, A.; Gonzalez, R.; Kefford, R.F.; Sosman, J.; Hamid, O.; Schuchter, L.; Cebon, J.; Ibrahim, N.; Kudchadkar, R.; Burris, H. a; Falchook, G.; Algazi, A.; Lewis, K.; Long, G. V; Puzanov, I.; Lebowitz, P.; Singh, A.; Little, S.; Sun, P.; Allred, A.; Ouellet, D.; Kim, K.B.; Patel, K.; Weber, J. Combined BRAF and MEK Inhibition in Melanoma with BRAF V600 Mutations. *N. Engl. J. Med.*, **2012**, *367*, 1694–1703.

[42] Larkin, J.; Ascierto, P. a.; Dréno, B.; Atkinson, V.; Liszkay, G.; Maio, M.; Mandalà, M.; Demidov, L.; Stroyakovskiy, D.; Thomas, L.; Merino, L.D.L.C.; Dutriaux, C.; Garbe, C.; Sovak, M. a.; Chang, I.; Choong, N.; Hack, S.P.; McArthur, G. a.; Ribas, A. Combined Vemurafenib and Cobimetinib in BRAF -Mutated Melanoma. *N. Engl. J. Med.*, **2014**, 140929070023009.

[43] Villanueva, J.; Vultur, A.; Lee, J.T.; Somasundaram, R.; Cipolla, A.K.; Wubbenhorst, B.; Xu, X.; Phyllis, A.; Kee, D.; Santiago-walker, A.E.; Letrero, R.; Andrea, K.D.; Pushparajan, A.; Hayden, J.E.; Brown, K.D.; Laquerre, S.; Mcarthur, G.A.; Sosman, J.A.; Nathanson, K.L.; Herlyn, M. Acquired Resistance to BRAF Inhibitors Mediated by a RAF Kinase Switch in Melanoma Can Be Overcome by Cotargeting MEK and IGF-1R/PI3K. *Cancer Cell*, **2010**, *18*, 683–695.

[44] Beadling, C.; Jacobson-Dunlop, E.; Hodi, F.S.; Le, C.; Warrick, A.; Patterson, J.; Town, A.; Harlow, A.; Cruz, F.; Azar, S.; Rubin, B.P.; Muller, S.; West, R.; Heinrich, M.C.; Corless, C.L. KIT Gene Mutations and Copy Number in Melanoma Subtypes. *Clin. Cancer Res.*, **2008**, *14*, 6821–6828.

[45] Antonescu, C.R.; Chapman, P.B.; Roman, R.; Teitcher, J.; Panageas, K.S.; Busam, K.J.; Lutzky, J.; Pavlick, A.C.; Fusco, A.; Cane, L.; Bouvier, N.; Bastian, B.C.; Schwartz, G.K. KIT as a Therapeutic Target. *J. Am. Med. Assoc.*, **2014**, *305*, 2327–2334.

[46] Todd, J.; Becker, T.; Kefford, R.; Rizos, H. Secondary c-Kit Mutations Confer Acquired Resistance to RTK Inhibitors in c-Kit Mutant Melanoma Cells. *Pigment Cell Melanoma Res.*, **2013**, *26*, 518–526.

[47] Topalian, S.L.; Hodi, S.; Gettinger, S.N.; Brahmer, J.R.; Smith, D.C.; Mcdermott, D.F.; Powderly, J.D.; Carvajal, R.D.; Sosman, J.A.; Atkins, M.B.; Leming, P.D.; Spigel, D.R.; Antonia, S.J.; Horn, L.; Drake, C.G.; Pardoll, D.M.; Chen, L.; Sharfman, W.H.; Anders, R.A.; Taube, J.M.; Mcmiller, T.L.; Xu, H.; Korman, A.J.; Jure-Kunkel, M.; Agrawal, S.; McDonald, D.; Kollia, G.D.; Gupta, A.; Wigginton, J.M.; Sznol, M. Safety, Activity, and Immune Correlates of Anti–PD-1 Antibody in Cancer. *N. Engl. J. Med.*, **2012**, *366*, 2443–2454.

[48] Hamid, O.; Robert, C.; Daud, A.; Hodi, F.S.; Hwu, W.-J.; Kefford, R.; Wolchok, J.D.; Hersey, P.; Joseph, R.W.; Weber, J.S.; Dronca, R.; Gangadhar, T.C.; Patnaik, A.; Zarour, H.; Joshua, A.M.; Gergich, K.; Elassaiss-Schaap, J.; Algazi, A.; Mateus, C.; Boasberg, P.; Tumeh, P.C.; Chmielowski, B.; Ebbinghaus, S.W.; Li, X.N.; Kang, S.P.; Ribas, A. Safety and Tumor Responses with Lambrolizumab (anti-PD-1) in Melanoma. *N. Engl. J. Med.*, **2013**, *369*, 134–144.

[49] Robert, C.; Thomas, L.; Bondarenko, I.; O'Day, S.; Weber, J.; Garbe, C.; Lebbe, C.; Baurain, J.-F.; Testori, A.; Grob, J.; Davidson, N.; Richards, J.; Maio, M.; Hauschild, A.; Miller, W.H.; Gascon, P.; Lotem, M.; Harmankaya, K.; Ibrahim, R.; Francis, S.; Chen, T.; Humphrey, R.; Hoos, A.; Wolchok, J.D. Ipilimumab plus Dacarbazine for Previously Untreated Metastatic Melanoma. *N. Engl. J. Med.*, **2011**, *364*, 2517–2526.

[50] Food and Drug Administration. Anti-CTLA Antibody Ipilimumab. *http://www.fda.gov/newsevents/newsroom/pressannouncements/ucm1193237.htm*, **2011**.

[51] Hans, R.; Andtbacka, I.; Collichio, F.A.; Amatruda, T.; Senzer, N.N.; Delman, K.A.; Spitler, L.E.; Puzanov, I.; Doleman, S.; Ye, Y.; Ari, M. OPTiM: A Randomized Phase III Trial of Talimogene Laherparepvec (T-VEC) versus Subcutaneous (SC) Granulocyte-Macrophage Colony-Stimulating Factor (GM-CSF) for the Treatment (tx) of Unresected Stage IIIB/C and IV Melanoma - Interim Analysis. *J Clin Oncol*, **2013**, *31*, suppl; abstr LBA9008.

[52] Mulcahy, N. Novel Treatment Strategy in Melanoma Misses End Point. *Medscape Medical News © 2014 WebMD, LLC*, **2014**.

[53] Yardley, D. a. Nab-Paclitaxel Mechanisms of Action and Delivery. *J. Control. Release*, **2013**, *170*, 365–372.

[54] Hersh, E.; Vecchio, M. Del; Brown, M.P.; Kefford, R.; Loquai, C.; Testori, A.; Robert, C.; Li, M.; Elias, I.; Renschler, M.F.; Hauschild, A. A Phase III Trial of Nab-Paclitaxel versus Dacarbazine in Chemotherapy-Naive Patients with Metastatic Melanoma: A Subanalysis Based on BRAF Status. In *2013 ASCO Annual Meeting*; **2013**.

[55] Lapidot, T.; Sirard, C.; Vormoor, J.; Murdoch, B.; Hoang, T.; Caceres-Cortes, J.; Minden, M.; Paterson, B.; Caligiuri, M.A.; Dick, J.E. A Cell Initiating Human Acute Myeloid Leukaemia after Transplantation into SCID Mice. *Nature*, **1994**, *367*, 645–648.

[56] Quintana, E.; Shackleton, M.; Sabel, M.S.; Fullen, D.R.; Johnson, T.M.; Morrison, S.J. Efficient Tumour Formation by Single Human Melanoma Cells. *Nature*, **2008**, *456*, 593–598.

[57] Hope, K.J.; Jin, L.; Dick, J.E. Acute Myeloid Leukemia Originates from a Hierarchy of Leukemic Stem Cell Classes That Differ in Self-Renewal Capacity. *Nat. Immunol.*, **2004**, *5*, 738–743.

[58] Dick, J.E. ASH 50th Anniversary Review Stem Cell Concepts Renew Cancer Research. *Stem Cells*, **2008**, *112*, 4793–4807.

[59] Li, C.; Lee, C.J.; Simeone, D.M. Methods in Molecular Biology. **2009**, *568*, 161–173.

[60] Shah, A.; Patel, S.; Pathak, J.; Swain, N.; Kumar, S. The Evolving Concepts of Cancer Stem Cells in Head and Neck Squamous Cell Carcinoma. *Hindawi Publ. Corp.*, **2014**, *2014*.

[61] Wu, C.; Wei, Q.; Utomo, V.; Nadesan, P.; Whetstone, H.; Kandel, R.; Wunder, J.; Alman, B. Side Population Cells Isolated from Mesenchymal Neoplasms Have Tumor Initiating Potential. *Cancer Res.*, **2007**, *67*, 8216–8222.

[62] Dalerba, P.; Dylla, S.J.; Park, I.-K.; Liu, R.; Wang, X.; Cho, R.W.; Hoey, T.; Gurney, A.; Huang, E.H.; Simeone, D.M.; Shelton, A. a; Parmiani, G.; Castelli, C.; Clarke, M.F. Phenotypic Characterization of Human Colorectal Cancer Stem Cells. *Proc. Natl. Acad. Sci.*, **2007**, *104*, 10158–10163.

[63] Monzani, E.; Facchetti, F.; Galmozzi, E.; Corsini, E.; Benetti, A.; Cavazzin, C.; Gritti, A.; Piccinini, A.; Porro, D.; Santinami, M.; Invernici, G.; Parati, E.; Alessandri, G.; La Porta, C. a M. Melanoma Contains CD133 and ABCG2 Positive Cells with Enhanced Tumourigenic Potential. *Eur. J. Cancer*, **2007**, *43*, 935–946.

[64] Sheila K. Singh; Hawkins, C.; Clarke, I.D.; Squire, J.A.; Bayani, J.; Hide, T.; Henkelman, R.M.; Cusimano, M.D.; Dirks, P.B. Identification of Human Brain Tumour Initiating Cells. *Lett. to Nat.*, **2004**, *18*, 396–401.

[65] Schatton, T.; Murphy, G.F.; Frank, N.Y.; Yamaura, K.; Waaga-Gasser, A.M.; Gasser, M.; Zhan, Q.; Jordan, S.; Duncan, L.M.; Weishaupt, C.; Fuhlbrigge, R.C.; Kupper, T.S.; Sayegh, M.H.; Frank, M.H. Identification of Cells Initiating Human Melanomas. *Nature*, **2008**, *451*, 345–349.

[66] Civenni, G.; Walter, A.; Kobert, N.; Mihic-Probst, D.; Zipser, M.; Belloni, B.; Seifert, B.; Moch, H.; Dummer, R.; van den Broek, M.; Sommer, L. Human CD271-Positive Melanoma Stem Cells Associated with Metastasis Establish Tumor Heterogeneity and Long-Term Growth. *Cancer Res.*, **2011**, *71*, 3098–3109.

[67] Morrison, S.J.; White, P.M.; Zock, C.; Anderson, D.J. Prospective Identification, Isolation by Flow Cytometry, and in Vivo Self-Renewal of Multipotent Mammalian Neural Crest Stem Cells. *Cell*, **1999**, *96*, 737–749.

[68] Chesa, P.G.; Rettig, W.J.; Thomson, T.M.; Old, L.J.; Melamed, M.R. Immunohistochemical Analysis of Nerve Growth Factor Receptor Expression in Normal and Malignant Human Tissues. *J. Histochem. Cytochem.*, **1988**, *36*, 383–389.

[69] Quintana, E.; Shackleton, M.; Foster, H.R.; Fullen, D.R.; Sabel, M.S.; Johnson, T.M.; Morrison, S.J. Phenotypic Heterogeneity among Tumorigenic Melanoma Cells from Patients That Is Reversible and Not Hierarchically Organized. *Cancer Cell*, **2010**, *18*, 510–523.

[70] Boiko, A.D.; Razorenova, O. V; Rijn, M. Van De; Swetter, S.M.; Johnson, D.L.; Ly, D.P.; Butler, P.D.; Yang, G.P.; Kaplan, M.J.; Longaker, M.T.; Weissman, I.L. Human Melanoma Initiating Cells Express Neural Crest Nerve Growth Factor Receptor CD271. *Nature*, **2011**, *466*, 133–137.

[71] Boonyaratanakornkit, J.B.; Yue, L.; Strachan, L.R.; Scalapino, K.J.; LeBoit, P.E.; Lu, Y.; Leong, S.P.; Smith, J.E.; Ghadially, R. Selection of Tumorigenic Melanoma Cells Using ALDH. *J. Invest. Dermatol.*, **2010**, *130*, 2799–2808.

[72] Kupas, V.; Weishaupt, C.; Siepmann, D.; Kaserer, M.-L.; Eickelmann, M.; Metze, D.; Luger, T. a; Beissert, S.; Loser, K. RANK Is Expressed in Metastatic Melanoma and Highly Upregulated on Melanoma-Initiating Cells. *J. Invest. Dermatol.*, **2011**, *131*, 944–955.

[73] Roesch, A.; Fukunaga-Kalabis, M.; Schmidt, E.C.; Susan, E.; Brafford, P.A.; Vultur, A.; Basu, D.; Gimotty, P.; Zabierowski, S.E.; Vogt, T.; Herlyn, M. A Temporarily Distinct Subpopulation of

Slow-Cycling Melanoma Cells Is Required for Continuous Tumor Growth. *Cell*, **2010**, *141*, 583–594.

[74] Quintana, E.; Shackleton, M.; Sabel, M.S.; Fullen, D.R.; Timothy, M.; Morrison, S.J. Efficient Tumor Formation by Single Human Melanoma Cells. *Nature*, **2008**, *456*, 593–598.

[75] Bailey, C.M.; Morrison, J.A.; Kulesa, P.M. Melanoma Revives an Embryonic Migration Program to Promote Plasticity and Invasion. *Pigment Cell Melanoma Res.*, **2012**, *25*, 573–583.

[76] Gupta, P.B.; Kuperwasser, C.; Brunet, J.; Kuo, W.; Gray, J.W.; Naber, S.P.; Weinberg, R.A. The Melanocyte Differentiation Program Predisposes to Metastasis Following Neoplastic Transformation. *Nat. Genet.*, **2005**, *37*, 1047–1054.

[77] Caramel, J.; Papadogeorgakis, E.; Hill, L.; Browne, G.J.; Richard, G.; Wierinckx, A.; Saldanha, G.; Osborne, J.; Hutchinson, P.; Tse, G.; Lachuer, J.; Puisieux, A.; Pringle, J.H.; Ansieau, S.; Tulchinsky, E. A Switch in the Expression of Embryonic EMT-Inducers Drives the Development of Malignant Melanoma. *Cancer Cell*, **2013**, *24*, 466–480.

[78] Ramgolam, K.; Lauriol, J.; Lalou, C.; Lauden, L.; Michel, L.; de la Grange, P.; Khatib, A.-M.; Aoudjit, F.; Charron, D.; Alcaide-Loridan, C.; Al-Daccak, R. Melanoma Spheroids Grown under Neural Crest Cell Conditions Are Highly Plastic Migratory/invasive Tumor Cells Endowed with Immunomodulator Function. *PLoS One*, **2011**, *6*, e18784.

[79] Sáez-Ayala, M.; Montenegro, M.F.; Sánchez-Del-Campo, L.; Fernández-Pérez, M.P.; Chazarra, S.; Freter, R.; Middleton, M.; Piñero-Madrona, A.; Cabezas-Herrera, J.; Goding, C.R.; Rodríguez-López, J.N. Directed Phenotype Switching as an Effective Antimelanoma Strategy. *Cancer Cell*, **2013**, *24*, 105–119.

[80] Hoek, K.S.; Schlegel, N.C.; Brafford, P.; Sucker, A.; Ugurel, S.; Kumar, R.; Weber, B.L.; Nathanson, K.L.; Phillips, D.J.; Herlyn, M.; Schadendorf, D.; Dummer, R. Metastatic Potential of Melanomas Defined by Specific Gene Expression Profiles with No BRAF Signature. *Pigment Cell Res.*, **2006**, *19*, 290–302.

[81] Adachi, Y.; Yamamoto, H.; Itoh, F.; Arimura, Y.; Nishi, M.; Endo, T.; Imai, K. Clinicopathologic and Prognostic Significance of Matrilysin Expression at the Invasive Front in Human Colorectal Cancers. *Int. J. cancer*, **2001**, *95*, 290–294.

[82] Boström, P.; Söderström, M.; Vahlberg, T.; Söderström, K.-O.; Roberts, P.J.; Carpén, O.; Hirsimäki, P. MMP-1 Expression Has an Independent Prognostic Value in Breast Cancer. *BMC Cancer*, **2011**, *11*, 348.

[83] Ruokolainen, H.; Pa, P.; Turpeenniemi-Hujanen, T. Expression of Matrix Metalloproteinase-9 in Head and Neck Squamous Cell Carcinoma : A Potential Marker for Prognosis. *Clin. cancer Res.*, **2004**, *10*, 3110–3116.

[84] Guo, C.-B.; Wang, S.; Deng, C.; Zhang, D.-L.; Wang, F.-L.; Jin, X.-Q. Relationship between Matrix Metalloproteinase 2 and Lung Cancer Progression. *Molecular Diagnosis & Therapy*, **2012**, *11*, 183–192.

[85] Iida, J.; Wilhelmson, K.L.; Price, M.A.; Wilson, C.M.; Pei, D.; Furcht, L.T.; Mccarthy, J.B. Membrane Type-1 Matrix Metalloproteinase Promotes Human Melanoma Invasion and Growth. *J. Invest. Dermatol.*, **2004**, *122*, 167–176.

[86] Sahai, E.; Marshall, C.J. Differing Modes of Tumour Cell Invasion Have Distinct Requirements for Rho/ROCK Signalling and Extracellular Proteolysis. *Nat. Cell Biol.*, **2003**, *5*, 711–719.

[87] Ray, J.M.; Stetler-stevenson, W.G. Gelatinase A Activity Directly Modulates Melanoma Cell Adhesion and Spreading. **1995**, *14*, 908–917.

[88] Hofmann, U.B.; Westphal, J.R.; Waas, E.T.; Zendman, A.J.W.; Cornelissen, I.; Ruiter, D.J.; Muijen, G.N.P. Van. Matrix Metalloproteinases in Human Melanoma Cell Lines and Xenografts : Increased Expression of Activated Matrix Metalloproteinase-2 (MMP-2) Correlates with Melanoma Progression. *Br. J. Cancer*, **1999**, *81*, 774–782.

[89] Macdougall, J.R.; Lin, Y.; Muschel, R.J.; Kerbel, R.S. " Proteolytic Switching ": Opposite Patterns of Regulation of Gelatinase B and Its Inhibitor TIMP-1 during Human Melanoma Progression and Consequences of Gelatinase B Overexpression. *Br. J. Cancer*, **1999**, *80*, 504–512.

[90] Girouard, S.D.; Laga, A.C.; Mihm, M.C.; Scolyer, R. a; Thompson, J.F.; Zhan, Q.; Widlund, H.R.; Lee, C.-W.; Murphy, G.F. SOX2 Contributes to Melanoma Cell Invasion. *Lab. Invest.*, **2011**, *00*, 1–9.

[91] Fackler, O.T.; Grosse, R. Cell Motility through Plasma Membrane Blebbing. *J. Cell Biol.*, **2008**, *181*, 879–884.

[92] Jaffe, A.B.; Hall, A. Rho GTPases: Biochemistry and Biology. *Annu. Rev. Cell Dev. Biol.*, **2005**, *21*, 247–269.

[93] Clark, E.A.; Golub, T.R.; Lander, E.S.; Hynes, R.O. Genomic Analysis of Metastasis Reveals an Essential Role for RhoC. *Nature*, **2000**, *406*, 532–535.

[94] Zucker, S.; Cao, J. Selective Matrix Metalloproteinase (MMP) Inhibitors in Cancer Therapy: Ready for Prime Time? *Cancer Biol. Ther.*, **2009**, *8*, 2371–2373.

[95] Wolf, K.; Mazo, I.; Leung, H.; Engelke, K.; von Andrian, U.H.; Deryugina, E.I.; Strongin, A.Y.; Bröcker, E.-B.; Friedl, P. Compensation Mechanism in Tumor Cell Migration: Mesenchymal-Amoeboid Transition after Blocking of Pericellular Proteolysis. *J. Cell Biol.*, **2003**, *160*, 267–277.

[96] Hoek, K.S.; Eichhoff, O.M.; Schlegel, N.C.; Döbbeling, U.; Kobert, N.; Schaerer, L.; Hemmi, S.; Dummer, R. In Vivo Switching of Human Melanoma Cells between Proliferative and Invasive States. *Cancer Res.*, **2008**, *68*, 650–656.

[97] Widmer, D.S.; Hoek, K.S.; Cheng, P.F.; Eichhoff, O.M.; Biedermann, T.; Raaijmakers, M.I.G.; Hemmi, S.; Dummer, R.; Levesque, M.P. Hypoxia Contributes to Melanoma Heterogeneity by Triggering HIF1α-Dependent Phenotype Switching. *J. Invest. Dermatol.*, **2013**, *133*, 2436–2443.

[98] O'Connell, M.P.; Marchbank, K.; Webster, M.R.; Valiga, A. a; Kaur, A.; Vultur, A.; Li, L.; Herlyn, M.; Villanueva, J.; Liu, Q.; Yin, X.; Widura, S.; Nelson, J.; Ruiz, N.; Camilli, T.C.; Indig, F.E.; Flaherty, K.T.; Wargo, J. a; Frederick, D.T.; Cooper, Z. a; Nair, S.; Amaravadi, R.K.; Schuchter, L.M.; Karakousis, G.C.; Xu, W.; Xu, X.; Weeraratna, A.T. Hypoxia Induces Phenotypic Plasticity and Therapy Resistance in Melanoma via the Tyrosine Kinase Receptors ROR1 and ROR2. *Cancer Discov.*, **2013**, *3*, 1378–1393.

[99] Brien, G.L.; Gambero, G.; O'Connell, D.J.; Jerman, E.; Turner, S. a; Egan, C.M.; Dunne, E.J.; Jurgens, M.C.; Wynne, K.; Piao, L.; Lohan, A.J.; Ferguson, N.; Shi, X.; Sinha, K.M.; Loftus, B.J.; Cagney, G.; Bracken, A.P. Polycomb PHF19 Binds H3K36me3 and Recruits PRC2 and Demethylase NO66 to Embryonic Stem Cell Genes during Differentiation. *Nat. Struct. Mol. Biol.*, **2012**, *19*, 1273–1281.

[100] Ghislin, S.; Deshayes, F.; Middendorp, S.; Boggetto, N.; Alcaide-loridan, C. PHF19 and Akt Control the Switch between Proliferative and Invasive States in Melanoma. *Cell Cycle*, **2012**, *11*, 1634–1645.

[101] Goodall, J.; Carreira, S.; Denat, L.; Kobi, D.; Davidson, I.; Nuciforo, P.; Sturm, R. a; Larue, L.; Goding, C.R. Brn-2 Represses Microphthalmia-Associated Transcription Factor Expression and Marks a Distinct Subpopulation of Microphthalmia-Associated Transcription Factor-Negative Melanoma Cells. *Cancer Res.*, **2008**, *68*, 7788–7794.

[102] Pinner, S.; Jordan, P.; Sharrock, K.; Bazley, L.; Collinson, L.; Marais, R.; Bonvin, E.; Goding, C.; Sahai, E. Intravital Imaging Reveals Transient Changes in Pigment Production and Brn2 Expression during Metastatic Melanoma Dissemination. *Cancer Res.*, **2009**, *69*, 7969–7977.

[103] Gilbert, S. Early Mammalian Development. In *Developmental Biology*; Sinauer Associates; 2000: Sunderland (MA), **2000**.

[104] Silva, J.; Smith, A. Capturing Pluripotency. *Cell*, **2008**, *132*, 532–536.

[105] Bethesda, MD: National Institutes of Health, U.S.D. of H. and H.S. Hematopoietic Stem Cells. In *Stem Cell Information [World Wide Web site]*; **2011**; p. http://stemcells.nih.gov/info/scireport/pages/chap.

[106] Lavker, R.M.; Sun, T.T. Heterogeneity in Epidermal Basal Keratinocytes: Morphological and Functional Correlations. *Science*, **1981**, *215*, 1239–1241.

[107] Martin, G.R. Isolation of a Pluripotent Cell Line from Early Mouse Embryos Cultured in Medium Conditioned by Teratocarcinoma Stem Cells. *PNAS*, **1981**, *78*, 7634–7638.

[108] Bethesda, MD: National Institutes of Health, U.S.D. of H. and H.S. Database of Publications Featuring Mouse Embryonic Stem Cell Lines. In *In Stem Cell Information [World Wide Web site]*; **2006**; p. http://stemcells.nih.gov/mouselit.

[109] Gesetz zum Schutz von Embryonen (Embryonenschutzgesetz - ESchG) http://www.gesetze-im-internet.de/eschg/BJNR027460.

[110] Wilmut, I.; Schnieke, A.E.; McWhir, J.; Kind, A.J.; Campbell, K.H.S. Viable Offspring Derived from Fetal and Adult Mammalian Cells. *Lett. to Nat.*, **1997**, *385*, 810–813.

[111] Tada, M.; Takahama, Y.; Abe, K.; Nakatsuji, N.; Tada, T. Nuclear Reprogramming of Somatic Cells by in Vitro Hybridization with ES Cells. *Curr. Biol.*, **2001**, *11*, 1553–1558.

[112] Cowan, C. a; Atienza, J.; Melton, D. a; Eggan, K. Nuclear Reprogramming of Somatic Cells after Fusion with Human Embryonic Stem Cells. *Science*, **2005**, *309*, 1369–1373.

[113] Takahashi, K.; Yamanaka, S. Induction of Pluripotent Stem Cells from Mouse Embryonic and Adult Fibroblast Cultures by Defined Factors. *Cell*, **2006**, *126*, 663–676.

[114] Zhang, W.Y.; Almeida, P.E. De; Wu, J.C. Teratoma Formation : A Tool for Monitoring Pluripotency in Stem Cell Research. In *StemBook*; The Stem Cell Research Community, Ed.; **2012**.

[115] Eggan, K.; Akutsu, H.; Loring, J.; Jackson-Grusby, L.; Klemm, M.; Rideout, W.M.; Yanagimachi, R.; Jaenisch, R. Hybrid Vigor, Fetal Overgrowth, and Viability of Mice Derived by Nuclear Cloning and Tetraploid Embryo Complementation. *Proc. Natl. Acad. Sci.*, **2001**, *98*, 6209–6214.

[116] Okita, K.; Hong, H.; Takahashi, K.; Yamanaka, S. Generation of Mouse-Induced Pluripotent Stem Cells with Plasmid Vectors. *Nat. Protoc.*, **2010**, *5*, 418–428.

[117] Si-Tayeb, K.; Noto, F.K.; Sepac, A.; Sedlic, F.; Bosnjak, Z.J.; Lough, J.W.; Duncan, S. a. Generation of Human Induced Pluripotent Stem Cells by Simple Transient Transfection of Plasmid DNA Encoding Reprogramming Factors. *BMC Dev. Biol.*, **2010**, *10*, 81.

[118] Zhou, W.; Freed, C.R. Adenoviral Gene Delivery Can Reprogram Human Fibroblasts to Induced Pluripotent Stem Cells. *Stem Cells*, **2009**, *27*, 2667–2674.

[119] Stadtfeld, M.; Nagaya, M.; Utikal, J.; Weir, G.; Hochedlinger, K. Induced Pluripotent Stem Cells Genereted Without Viral Integration. *Science*, **2008**, *322*, 945–949.

[120] Fusaki, N.; Ban, H.; Nishiyama, A.; Saeki, K.; Hasegawa, M. Efficient Induction of Transgene-Free Human Pluripotent Stem Cells Using a Vector Based on Sendai Virus, an RNA Virus That Does Not Integrate into the Host Genome. *Proc. Jpn. Acad.*, **2009**, *85*, 348–362.

[121] Seki, T.; Yuasa, S.; Oda, M.; Egashira, T.; Yae, K.; Kusumoto, D.; Nakata, H.; Tohyama, S.; Hashimoto, H.; Kodaira, M.; Okada, Y.; Seimiya, H.; Fusaki, N.; Hasegawa, M.; Fukuda, K. Generation of Induced Pluripotent Stem Cells from Human Terminally Differentiated Circulating T Cells. *Cell Stem Cell*, **2010**, *7*, 11–14.

[122] Warren, L.; Ni, Y.; Wang, J.; Guo, X. Feeder-Free Derivation of Human Induced Pluripotent Stem Cells with Messenger RNA. *Sci. Rep.*, **2012**, *2*, 1–7.

[123] Kim, D.; Kim, C.; Moon, J.; Chung, Y.; Chang, M.; Han, B.; Ko, S.; Yang, E.; Cha, K.Y.; Lanza, R.; Kim, K. Generation of Human Induced Pluripotent Stem Cells by Direct Delivery of Reprogramming Proteins. *Cell Stem Cell*, **2009**, *4*, 472–476.

[124] Anokye-danso, F.; Trivedi, C.M.; Juhr, D.; Gupta, M.; Cui, Z.; Tian, Y.; Zhang, Y.; Yang, W.; Gruber, P.J.; Epstein, J.A.; Morrisey, E.E. Highly Efficient miRNA-Mediated Reprogramming of Mouse and Human Somatic Cells to Pluripotency. *Cell Stem Cell*, **2011**, *8*, 376–388.

[125] Miyoshi, N.; Ishii, H.; Nagano, H.; Haraguchi, N.; Dewi, D.L.; Kano, Y.; Nishikawa, S.; Tanemura, M.; Mimori, K.; Tanaka, F.; Saito, T.; Nishimura, J.; Takemasa, I.; Mizushima, T.; Ikeda, M.; Yamamoto, H.; Sekimoto, M.; Doki, Y.; Mori, M. Reprogramming of Mouse and Human Cells to Pluripotency Using Mature microRNAs. *Cell Stem Cell*, **2011**, *8*, 633–638.

[126] Subramanyam, D.; Lamouille, S.; Robert, J.L.; Liu, J.Y.; Bucay, N.; Derynck, R.; Blelloch, R. Multiple Targets of miR-302 and miR-372 Promote Reprogramming of Human Fibroblasts to Induced Pluripotent Stem Cells. *Nat. Biotechnol.*, **2011**, *29*, 443–448.

[127] Yoshioka, N.; Gros, E.; Li, H.; Kumar, S.; Deacon, D.C.; Dowdy, S.F. Efficient Generation of Human iPS Cells by a Synthetic Self- Replicative RNA. *Cell Stem Cell*, **2013**, *13*, 1–21.

[128] Li, Y.; Zhang, Q.; Yin, X.; Yang, W.; Du, Y.; Hou, P.; Ge, J.; Liu, C.; Zhang, W.; Zhang, X.; Wu, Y.; Li, H.; Liu, K.; Wu, C.; Song, Z.; Zhao, Y.; Shi, Y.; Deng, H. Generation of iPSCs from Mouse Fibroblasts with a Single Gene, Oct4, and Small Molecules. *Cell Res.*, **2011**, *21*, 196–204.

[129] Hou, P.; Li, Y.; Zhang, X.; Liu, C.; Guan, J.; Li, H.; Zhao, T.; Ye, J.; Yang, W.; Liu, K.; Ge, J.; Xu, J.; Zhang, Q.; Zhao, Y.; Deng, H. Pluripotent Stem Cells Induced from Mouse Somatic Cells by Small-Molecule Compounds. *Science*, **2013**, *341*, 651–654.

[130] Yu, J.; Vodyanik, M. a; Smuga-Otto, K.; Antosiewicz-Bourget, J.; Frane, J.L.; Tian, S.; Nie, J.; Jonsdottir, G. a; Ruotti, V.; Stewart, R.; Slukvin, I.I.; Thomson, J. a. Induced Pluripotent Stem Cell Lines Derived from Human Somatic Cells. *Science*, **2007**, *318*, 1917–1920.

[131] Nichols, J.; Zevnik, B.; Anastassiadis, K.; Niwa, H.; Klewe-Nebenius, D.; Chambers, I.; Schöler, H.; Smith, A. Formation of Pluripotent Stem Cells in the Mammalian Embryo Depends on the POU Transcription Factor Oct4. *Cell*, **1998**, *95*, 379–391.

[132] Hart, A.H.; Hartley, L.; Ibrahim, M.; Robb, L. Identification, Cloning and Expression Analysis of the Pluripotency Promoting Nanog Genes in Mouse and Human. *Dev. Dyn.*, **2004**, *230*, 187–198.

[133] Chambers, I.; Colby, D.; Robertson, M.; Nichols, J.; Lee, S.; Tweedie, S.; Smith, A. Functional Expression Cloning of Nanog, a Pluripotency Sustaining Factor in Embryonic Stem Cells. *Cell*, **2003**, *113*, 643–655.

[134] Lengner, C.J.; Camargo, F.D.; Hochedlinger, K.; Welstead, G.G.; Zaidi, S.; Gokhale, S.; Scholer, H.R.; Tomilin, A.; Jaenisch, R. Oct4 Expression Is Not Required for Mouse Somatic Stem Cell Self-Renewal. *Cell Stem Cell*, **2007**, *1*, 403–415.

[135] Hochedlinger, K.; Yamada, Y.; Beard, C.; Jaenisch, R. Ectopic Expression of Oct-4 Blocks Progenitor-Cell Differentiation and Causes Dysplasia in Epithelial Tissues. *Cell*, **2005**, *121*, 465–477.
[136] Okita, K.; Ichisaka, T.; Yamanaka, S. Generation of Germline-Competent Induced Pluripotent Stem Cells. *Nature*, **2007**, *448*, 313–317.
[137] Maherali, N.; Sridharan, R.; Xie, W.; Utikal, J.; Eminli, S.; Arnold, K.; Stadtfeld, M.; Yachechko, R.; Tchieu, J.; Jaenisch, R.; Plath, K.; Hochedlinger, K. Directly Reprogrammed Fibroblasts Show Global Epigenetic Remodeling and Widespread Tissue Contribution. *Cell Stem Cell*, **2007**, *1*, 55–70.
[138] Wernig, M.; Meissner, A.; Foreman, R.; Brambrink, T.; Ku, M.; Hochedlinger, K.; Bernstein, B.E.; Jaenisch, R. In Vitro Reprogramming of Fibroblasts into a Pluripotent ES-Cell-like State. *Nature*, **2007**, *448*, 318–324.
[139] Avilion, A.A.; Nicolis, S.K.; Pevny, L.H.; Perez, L.; Vivian, N.; Lovell-badge, R. Multipotent Cell Lineages in Early Mouse Development Depend on SOX2 Function. *Genes Dev.*, **2003**, *17*, 126–140.
[140] Keramari, M.; Razavi, J.; Ingman, K. a; Patsch, C.; Edenhofer, F.; Ward, C.M.; Kimber, S.J. Sox2 Is Essential for Formation of Trophectoderm in the Preimplantation Embryo. *PLoS One*, **2010**, *5*, e13952.
[141] Utikal, J.; Maherali, N.; Kulalert, W.; Hochedlinger, K. Sox2 Is Dispensable for the Reprogramming of Melanocytes and Melanoma Cells into Induced Pluripotent Stem Cells. *J. Cell Sci.*, **2009**, *122*, 3502–3510.
[142] Masui, S.; Nakatake, Y.; Toyooka, Y.; Shimosato, D.; Yagi, R.; Takahashi, K.; Okochi, H.; Okuda, A.; Matoba, R.; Sharov, A. a; Ko, M.S.H.; Niwa, H. Pluripotency Governed by Sox2 via Regulation of Oct3/4 Expression in Mouse Embryonic Stem Cells. *Nat. Cell Biol.*, **2007**, *9*, 625–635.
[143] Boyer, L.A.; Lee, T.I.; Cole, M.F.; Johnstone, S.E.; Stuart, S.; Zucker, J.P.; Guenther, M.G.; Kumar, R.M.; Murray, H.L.; Jenner, R.G.; Gifford, D.K.; Melton, D.A.; Jaenisch, R.; Young, R.A. Core Transcriptional Regulatory Circuitry in Human Embryonic Stem Cells. *Cell*, **2005**, *122*, 947–956.
[144] Wang, J.; Rao, S.; Chu, J.; Shen, X.; Levasseur, D.N.; Theunissen, T.W.; Orkin, S.H. A Protein Interaction Network for Pluripotency of Embryonic Stem Cells. *Nature*, **2006**, *444*, 364–368.
[145] Gao, Z.; Cox, J.L.; Gilmore, J.M.; Ormsbee, B.D.; Mallanna, S.K.; Washburn, M.P.; Rizzino, A. Determination of Protein Interactome of Transcription Factor Sox2 in Embryonic Stem Cells Engineered for Inducible Expression of Four Reprogramming Factors. *J. Biol. Chem.*, **2012**, *287*, 11384–11397.
[146] Van den Berg, D.L.C.; Snoek, T.; Mullin, N.P.; Yates, A.; Bezstarosti, K.; Demmers, J.; Chambers, I.; Poot, R. a. An Oct4-Centered Protein Interaction Network in Embryonic Stem Cells. *Cell Stem Cell*, **2010**, *6*, 369–381.
[147] Ding, J.; Xu, H.; Faiola, F.; Ma'ayan, A.; Wang, J. Oct4 Links Multiple Epigenetic Pathways to the Pluripotency Network. *Cell Res.*, **2012**, *22*, 155–167.
[148] Jaenisch, R.; Young, R. Stem Cells, the Molecular Circuitry of Pluripotency and Nuclear Reprogramming. *Cell*, **2008**, *132*, 567–582.
[149] Nakagawa, M.; Koyanagi, M.; Tanabe, K.; Takahashi, K.; Ichisaka, T.; Aoi, T.; Okita, K.; Mochiduki, Y.; Takizawa, N.; Yamanaka, S. Generation of Induced Pluripotent Stem Cells without Myc from Mouse and Human Fibroblasts. *Nat. Biotechnol.*, **2008**, *26*, 101–106.
[150] Stadtfeld, M.; Maherali, N.; Breault, D.T.; Hochedlinger, K. Defining Molecular Cornerstones during Fibroblast to iPS Cell Reprogramming in Mouse. *Cell Stem Cell*, **2008**, *2*, 230–240.
[151] Polo, J.M.; Anderssen, E.; Walsh, R.M.; Schwarz, B. a; Nefzger, C.M.; Lim, S.M.; Borkent, M.; Apostolou, E.; Alaei, S.; Cloutier, J.; Bar-Nur, O.; Cheloufi, S.; Stadtfeld, M.; Figueroa, M.E.; Robinton, D.; Natesan, S.; Melnick, A.; Zhu, J.; Ramaswamy, S.; Hochedlinger, K. A Molecular Roadmap of Reprogramming Somatic Cells into iPS Cells. *Cell*, **2012**, *151*, 1617–1632.
[152] Yamanaka, S. Elite and Stochastic Models for Induced Pluripotent Stem Cell Generation. *Nature*, **2009**, *460*, 49–52.
[153] Smith, Z.D.; Nachman, I.; Regev, A.; Meissner, A. Dynamic Single Cell Imaging of Direct Reprogramming Reveals an Early Specifying Event. *Nat. Biotechnol.*, **2010**, *28*, 521–526.
[154] Buganim, Y.; Faddah, D.A.; Cheng, A.W.; Itskovich, E.; Markoulaki, S.; Ganz, K.; Klemm, S.L.; Oudenaarden, A. Van; Jaenisch, R. Single-Cell Gene Expression Analyses of Cellular Reprogramming Reveal a Stochastic Early and Hierarchic Late Phase. *Cell*, **2012**, *150*, 1209–1222.

[155] O'Malley, J.; Skylaki, S.; Iwabuchi, K. a; Chantzoura, E.; Ruetz, T.; Johnsson, A.; Tomlinson, S.R.; Linnarsson, S.; Kaji, K. High-Resolution Analysis with Novel Cell-Surface Markers Identifies Routes to iPS Cells. *Nature*, **2013**, *499*, 88–91.

[156] Samavarchi-Tehrani, P.; Golipour, A.; David, L.; Sung, H.-K.; Beyer, T. a; Datti, A.; Woltjen, K.; Nagy, A.; Wrana, J.L. Functional Genomics Reveals a BMP-Driven Mesenchymal-to-Epithelial Transition in the Initiation of Somatic Cell Reprogramming. *Cell Stem Cell*, **2010**, *7*, 64–77.

[157] Li, R.; Liang, J.; Ni, S.; Zhou, T.; Qing, X.; Li, H.; He, W.; Chen, J.; Li, F.; Zhuang, Q.; Qin, B.; Xu, J.; Li, W.; Yang, J.; Gan, Y.; Qin, D.; Feng, S.; Song, H.; Yang, D.; Zhang, B.; Zeng, L.; Lai, L.; Esteban, M.A.; Pei, D. A Mesenchymal-to-Epithelial Transition Initiates and Is Required for the Nuclear Reprogramming of Mouse Fibroblasts. *Cell Stem Cell*, **2010**, *7*, 51–63.

[158] Hansson, J.; Rafiee, M.R.; Reiland, S.; Polo, J.M.; Gehring, J.; Okawa, S.; Huber, W.; Hochedlinger, K.; Krijgsveld, J. Highly Coordinated Proteome Dynamics during Reprogramming of Somatic Cells to Pluripotency. *Cell Rep.*, **2012**, *2*, 1579–1592.

[159] Gao, Y.; Chen, J.; Li, K.; Wu, T.; Huang, B.; Liu, W.; Kou, X.; Zhang, Y.; Huang, H.; Jiang, Y.; Yao, C.; Liu, X.; Lu, Z.; Xu, Z.; Kang, L.; Chen, J.; Wang, H.; Cai, T.; Gao, S. Replacement of Oct4 by Tet1 during iPSC Induction Reveals an Important Role of DNA Methylation and Hydroxymethylation in Reprogramming. *Cell Stem Cell*, **2013**, *12*, 453–469.

[160] Hu, X.; Zhang, L.; Mao, S.-Q.; Li, Z.; Chen, J.; Zhang, R.-R.; Wu, H.-P.; Gao, J.; Guo, F.; Liu, W.; Xu, G.-F.; Dai, H.-Q.; Shi, Y.G.; Li, X.; Hu, B.; Tang, F.; Pei, D.; Xu, G.-L. Tet and TDG Mediate DNA Demethylation Essential for Mesenchymal-to-Epithelial Transition in Somatic Cell Reprogramming. *Cell Stem Cell*, **2014**, *14*, 512–522.

[161] Bedzhov, I.; Alotaibi, H.; Basilicata, M.F.; Ahlborn, K.; Liszewska, E.; Brabletz, T.; Stemmler, M.P. Adhesion, but Not a Specific Cadherin Code, Is Indispensable for ES Cell and Induced Pluripotency. *Stem Cell Res.*, **2013**, *11*, 1250–1263.

[162] Sakurai, K.; Talukdar, I.; Patil, V.S.; Dang, J.; Li, Z.; Chang, K.-Y.; Lu, C.-C.; Delorme-Walker, V.; Dermardirossian, C.; Anderson, K.; Hanein, D.; Yang, C.-S.; Wu, D.; Liu, Y.; Rana, T.M. Kinome-Wide Functional Analysis Highlights the Role of Cytoskeletal Remodeling in Somatic Cell Reprogramming. *Cell Stem Cell*, **2014**, *14*, 523–534.

[163] Hong, H.; Takahashi, K.; Ichisaka, T.; Aoi, T.; Kanagawa, O.; Nakagawa, M.; Okita, K.; Yamanaka, S. Suppression of Induced Pluripotent Stem Cell Generation by the p53-p21 Pathway. *Nature*, **2009**, *460*, 1132–1135.

[164] Utikal, J.; Polo, J.M.; Stadtfeld, M.; Maherali, N.; Kulalert, W.; Walsh, R.M.; Khalil, A.; Rheinwald, J.G.; Hochedlinger, K. Immortalization Eliminates a Roadblock during Cellular Reprogramming into iPS Cells. *Nature*, **2009**, *460*, 1145–1148.

[165] Warburg, O. On the Origin of Cancer Cells. *Science (80-.).*, **1956**, *123*, 309–314.

[166] Kim, J.; Dang, C. V. Cancer's Molecular Sweet Tooth and the Warburg Effect. *Cancer Res.*, **2006**, *66*, 8927–8930.

[167] Folmes, C.D.L.; Nelson, T.J.; Martinez-fernandez, A.; Arrell, D.K.; Lindor, J.Z.; Dzeja, P.P.; Ikeda, Y.; Perez-terzic, C. Somatic Oxidative Bioenergetics Transitions into Pluripotency-Dependent Glycolysis to Facilitate Nuclear Reprogramming. *Cell Metabollism*, **2012**, *14*, 264–271.

[168] Tai, M.-H.; Chang, C.-C.; Kiupel, M.; Webster, J.D.; Olson, L.K.; Trosko, J.E. Oct4 Expression in Adult Human Stem Cells: Evidence in Support of the Stem Cell Theory of Carcinogenesis. *Carcinogenesis*, **2005**, *26*, 495–502.

[169] T, J.; DR, B.; X, Z.; S, Q.; B, Y.; Goss, P. Examination of POU Homeobox Gene Expression in Human Breast Cancer Cells. *Int. J. Cancer*, **1999**, *81*, 104–112.

[170] Wang, P.; Branch, D.R.; Bali, M.; Schultz, G.A.; Goss, P.E.; Jin, T. The POU Homeodomain Protein OCT3 as a Potential Transcriptional Activator for Fibroblast Growth Factor-4 (FGF-4) in Human Breast Cancer Cells. *Biochem. J.*, **2003**, *205*, 199–205.

[171] Wang, D.; Lu, P.; Zhang, H.; Luo, M.; Zhang, X.; Wei, X.; Gao, J.; Zhao, Z.; Liu, C. Oct-4 and Nanog Promote the Epithelial-Mesenchymal Transition of Breast Cancer Stem Cells and Are Associated with Poor Prognosis in Breast Cancer Patients. *Oncotarget*, **2014**, *5*, 10803–10815.

[172] Paranjape, A.N.; Balaji, S. a; Mandal, T.; Krushik, E.V.; Nagaraj, P.; Mukherjee, G.; Rangarajan, A. Bmi1 Regulates Self-Renewal and Epithelial to Mesenchymal Transition in Breast Cancer Cells through Nanog. *BMC Cancer*, **2014**, *14*, 785.

[173] Lu, X.; Mazur, S.J.; Lin, T.; Appella, E.; Xu, Y. The Pluripotency Factor Nanog Promotes Breast Cancer Tumorigenesis and Metastasis. *Oncogene*, **2014**, *33*, 2655–2664.

[174] Chiou, S.-H.; Wang, M.-L.; Chou, Y.-T.; Chen, C.-J.; Hong, C.-F.; Hsieh, W.-J.; Chang, H.-T.; Chen, Y.-S.; Lin, T.-W.; Hsu, H.-S.; Wu, C.-W. Coexpression of Oct4 and Nanog Enhances Malignancy in Lung Adenocarcinoma by Inducing Cancer Stem Cell-like Properties and Epithelial-Mesenchymal Transdifferentiation. *Cancer Res.*, **2010**, *70*, 10433–10444.

[175] Zhao, X.; Sun, B.; Sun, D.; Liu, T.; Che, N.; Gu, Q.; Dong, X.; Li, R.; Liu, Y.; Li, J. Slug Promotes Hepatocellular Cancer Cell Progression by Increasing sox2 and Nanog Expression. *Oncol. Rep.*, **2015**, *33*, 149–156.

[176] Schoenhals, M.; Kassambara, A.; De Vos, J.; Hose, D.; Moreaux, J.; Klein, B. Embryonic Stem Cell Markers Expression in Cancers. *Biochem. Biophys. Res. Commun.*, **2009**, *383*, 157–162.

[177] Laga, A.C.; Zhan, Q.; Weishaupt, C.; Ma, J.; Frank, M.H.; Murphy, G.F. SOX2 and Nestin Expression in Human Melanoma: An Immunohistochemical and Experimental Study. *Exp. Dermatol.*, **2011**, *20*, 339–345.

[178] Ben-Porath, I.; Thomson, M.W.; Carey, V.J.; Ge, R.; Bell, G.W.; Regev, A.; Weinberg, R. a. An Embryonic Stem Cell-like Gene Expression Signature in Poorly Differentiated Aggressive Human Tumors. *Nat. Genet.*, **2008**, *40*, 499–507.

[179] Sun, A.-X.; Liu, C.-J.; Sun, Z.-Q.; Wei, Z. NANOG: A Promising Target for Digestive Malignant Tumors. *World J. Gastroenterol.*, **2014**, *20*, 13071–13078.

[180] McKinnell, R.; Deggins, B.; Labat, D. Transplantation of Pluripotential Nuclei from Triploid Frog Tumors. *Science*, **1969**, *165*, 394–396.

[181] Li, L.; Connelly, M.C.; Wetmore, C.; Curran, T.; Morgan, J.I. Mouse Embryos Cloned from Brain Tumors Mouse Embryos Cloned from Brain Tumors. *Cancer Res.*, **2003**, *63*, 2733–2736.

[182] Hochedlinger, K.; Blelloch, R.; Brennan, C.; Yamada, Y.; Kim, M.; Chin, L.; Jaenisch, R. Reprogramming of a Melanoma Genome by Nuclear Transplantation. *Genes Dev.*, **2004**, *18*, 1875–1885.

[183] Allegrucci, C.; Rushton, M.D.; Dixon, J.E.; Sottile, V.; Shah, M.; Kumari, R.; Watson, S.; Alberio, R.; Johnson, A.D. Epigenetic Reprogramming of Breast Cancer Cells with Oocyte Extracts. *Mol. Cancer*, **2011**, *10*, 7.

[184] Mahalingam, D.; Kong, C.M.; Lai, J.; Tay, L.L.; Yang, H.; Wang, X. Reversal of Aberrant Cancer Methylome and Transcriptome upon Direct Reprogramming of Lung Cancer Cells. *Sci. Rep.*, **2012**, *2*, 1–10.

[185] Miyoshi, N.; Ishii, H.; Nagai, K.; Hoshino, H.; Mimori, K.; Tanaka, F.; Nagano, H.; Sekimoto, M.; Doki, Y.; Mori, M. Defined Factors Induce Reprogramming of Gastrointestinal Cancer Cells. *Proc. Natl. Acad. Sci.*, **2010**, *107*, 40–45.

[186] Stricker, S.H.; Feber, A.; Engström, P.G.; Carén, H.; Kurian, K.M.; Takashima, Y.; Watts, C.; Way, M.; Dirks, P.; Bertone, P.; Smith, A.; Beck, S.; Pollard, S.M. Widespread Resetting of DNA Methylation in Glioblastoma-Initiating Cells Suppresses Malignant Cellular Behavior in a Lineage-Dependent Manner. *Genes Dev.*, **2013**, *27*, 654–669.

[187] Zhang, X.; Cruz, F.D.; Terry, M.; Remotti, F.; Matushansky, I. Terminal Differentiation and Loss of Tumorigenicity of Human Cancers via Pluripotency-Based Reprogramming. *Oncogene*, **2013**, *32*, 2249–2260.

[188] Suvà, M.L.; Rheinbay, E.; Gillespie, S.M.; Patel, A.P.; Wakimoto, H.; Rabkin, S.D.; Riggi, N.; Chi, A.S.; Cahill, D.P.; Nahed, B. V; Curry, W.T.; Martuza, R.L.; Rivera, M.N.; Rossetti, N.; Kasif, S.; Beik, S.; Kadri, S.; Tirosh, I.; Wortman, I.; Shalek, A.K.; Rozenblatt-Rosen, O.; Regev, A.; Louis, D.N.; Bernstein, B.E. Reconstructing and Reprogramming the Tumor-Propagating Potential of Glioblastoma Stem-like Cells. *Cell*, **2014**, *157*, 580–594.

[189] Boulay JL, Dennefeld C, A.A. The Drosophila Developmental Gene Snail Encodes a Protein with Nucleic Acid Binding Fingers. *Nature*, **1987**, *2*, 395–398.

[190] Barrallo-Gimeno, A.; Nieto, M.A. The Snail Genes as Inducers of Cell Movement and Survival: Implications in Development and Cancer. *Development*, **2005**, *132*, 3151–3161.

[191] Hemavathy, K.; Ashraf, S.I.; Ip, Y.T. Snail/Slug Family of Repressors: Slowly Going into the Fast Lane of Development and Cancer. *Gene*, **2000**, *257*, 1–12.

[192] Paznekas, W.A.; Okajima, K.; Schertzer, M.; Wood, S.; Jabs, E.W. Genomic Organization , Expression , and Chromosome Location of the Human SNAIL Gene (SNAI1) and a Related Processed Pseudogene (SNAI1P). *Genomics*, **1999**, 42–49.

[193] Cohen, M.E.; Yin, M.; Paznekas, W.A.; Schertzer, M.; Wood, S.; Jabs, E.W. Human SLUG Gene Organization , Expression , and Chromosome Map Location on 8q. *Genomics*, **1998**, 468–471.

[194] Masuko Katoh, M.K. Identification and Characterization of Human SNAIL3 (SNAI3) Gene in Silico. *Int. J. Mol. Med.*, **2003**, *11*, 383–388.

[195] Masuko Katoh, M.K. Comparative Genomics on SNAI1, SNAI2, and SNAI3 Orthologs. *Oncol. Rep.*, **2005**, *14*, 1083–1086.

[196] Kataoka, H.; Murayama, T.; Yokode, M.; Mori, S.; Sano, H.; Ozaki, H.; Yokota, Y.; Nishikawa, S.; Kita, T. A Novel Snail-Related Transcription Factor Smuc Regulates Basic Helix – Loop – Helix Transcription Factor Activities via Specific E-Box Motifs. *Nucleic Acids Res.*, **2000**, *28*, 626–633.

[197] Zhuge, X.; Kataoka, H.; Tanaka, M.; Murayama, T.; Kawamoto, T.; Sano, H.; Togi, K.; Yamauchi, R.; Ueda, Y.; Xu, Y.; Nishikawa, S.-I.; Kita, T.; Yokode, M. Expression of the Novel Snai-Related Zinc-Finger Transcription Factor Gene Smuc during Mouse Development. *Int. J. Mol. Med.*, **2005**, *15*, 945–948.

[198] Pioli, P.D.; Dahlem, T.J.; Weis, J.J.; Weis, J.H. Deletion of Snai2 and Snai3 Results in Impaired Physical Development Compounded by Lymphocyte Deficiency. *PLoS One*, **2013**, *8*, e69216.

[199] Ren, J.; Wen, L.; Gao, X.; Jin, C.; Xue, Y.; Yao, X. DOG 1.0: Illustrator of Protein Domain Structures. *Cell Res.*, **2009**, *19*, 271–273.

[200] Knight, R.D.; Shimeld, S.M. Identification of Conserved C2H2 Zinc-Finger Gene Families in the Bilateria. *Genome Biol.*, **2001**, *2*, 1–8.

[201] Peinado, H.; Ballestar, E.; Esteller, M.; Cano, a. Snail Mediates E-Cadherin Repression by the Recruitment of the Sin3A/Histone Deacetylase 1 (HDAC1)/HDAC2 Complex. *Mol. Cell. Biol.*, **2003**, *24*, 306–319.

[202] Lin, Y.; Wu, Y.; Li, J.; Dong, C.; Ye, X.; Chi, Y.-I.; Evers, B.M.; Zhou, B.P. The SNAG Domain of Snail1 Functions as a Molecular Hook for Recruiting Lysine-Specific Demethylase 1. *EMBO J.*, **2010**, *29*, 1803–1816.

[203] Alberga, A.; Boulay, J.; Kempe, E. The Snail Gene Required for Mesoderm Formation in Drosophila Is Expressed Dynamically in Derivatives of All Three Germ Layers. *Development*, **1991**, *111*, 983–992.

[204] Carver, E.A.; Jiang, R.; Lan, Y.U.; Oram, K.F.; Harbor, B.; Gridley, T. The Mouse Snail Gene Encodes a Key Regulator of the Epithelial-Mesenchymal Transition. *Mol. Cell. Biol.*, **2001**, *21*, 8184–8188.

[205] Nieto, M.A. The Snail Superfamily of Zinc-Finger Transcription Factors. *Nat. Rev. Mol. Cell Biol.*, **2002**, *3*, 155–166.

[206] Martínez-Alvarez C, Blanco MJ, Pérez R, Rabadán MA, Aparicio M, Resel E, Martínez T, N.M. Snail Family Members and Cell Survival in Physiological and Pathological Cleft Palates. *Dev. Biol.*, **2004**, *265*, 207–218.

[207] Vega, S.; Morales, A. V; Ocaña, O.H.; Valdés, F.; Fabregat, I.; Nieto, M.A. Snail Blocks the Cell Cycle and Confers Resistance to Cell Death. *Genes Dev.*, **2004**, *18*, 1131–1143.

[208] Kajita, M.; McClinic, K.N.; Wade, P. a. Aberrant Expression of the Transcription Factors Snail and Slug Alters the Response to Genotoxic Stress. *Mol. Cell. Biol.*, **2004**, *24*, 7559–7566.

[209] Sommer, C.; Stadtfeld, M.; Murphy, G.J.; Hochedlinger, K.; Kotton, D.N.; Mostoslavsky, G. Induced Pluripotent Stem Cell Generation Using a Single Lentiviral Stem Cell Cassette. *Stem Cells*, **2009**, *27*, 543–549.

[210] Das, A.T.; Zhou, X.; Vink, M.; Klaver, B.; Verhoef, K.; Marzio, G.; Berkhout, B. Viral Evolution as a Tool to Improve the Tetracycline-Regulated Gene Expression System. *J. Biol. Chem.*, **2004**, *279*, 18776–18782.

[211] Tormo, D.; Ferrer, A.; Bosch, P.; Gaffal, E.; Basner-Tschakarjan, E.; Wenzel, J.; Tüting, T. Therapeutic Efficacy of Antigen-Specific Vaccination and Toll-like Receptor Stimulation against Established Transplanted and Autochthonous Melanoma in Mice. *Cancer Res.*, **2006**, *66*, 5427–5435.

[212] Landsberg, J.; Gaffal, E.; Cron, M.; Kohlmeyer, J.; Renn, M.; Tüting, T. Autochthonous Primary and Metastatic Melanomas in Hgf-Cdk4 R24C Mice Evade T-Cell-Mediated Immune Surveillance. *Pigment Cell Melanoma Res.*, **2010**, *23*, 649–660.

[213] Kühl, S.J.; Kühl, M. On the Role of Wnt/β-Catenin Signaling in Stem Cells. *Biochim. Biophys. Acta*, **2013**, *1830*, 2297–2306.

[214] Neff, A.W.; King, M.W.; Mescher, A.L. Dedifferentiation and the Role of sall4 in Reprogramming and Patterning during Amphibian Limb Regeneration. *Dev. Dyn.*, **2011**, *240*, 979–989.

[215] Wang, W.; Eddy, R.; Condeelis, J. The Cofilin Pathway in Breast Cancer Invasion and Metastasis. *Nat. Rev. Cancer*, **2007**, *7*, 429–440.

[216] Wang, W.; Wyckoff, J.B.; Goswami, S.; Wang, Y.; Sidani, M.; Segall, J.E.; Condeelis, J.S. Coordinated Regulation of Pathways for Enhanced Cell Motility and Chemotaxis Is Conserved in Rat and Mouse Mammary Tumors. *Cancer Res.*, **2007**, *67*, 3505–3511.

[217] Das, D.; Zalewski, J.K.; Mohan, S.; Plageman, T.F.; VanDemark, A.P.; Hildebrand, J.D. The Interaction between Shroom3 and Rho-Kinase Is Required for Neural Tube Morphogenesis in Mice. *Biol. Open*, **2014**, *3*, 850–860.

[218] Violette, M.I.; Madan, P.; Watson, A.J. Na+/K+ -ATPase Regulates Tight Junction Formation and Function during Mouse Preimplantation Development. *Dev. Biol.*, **2006**, *289*, 406–419.

[219] Feng, S.; Zhu, G.; McConnell, M.; Deng, L.; Zhao, Q.; Wu, M.; Zhou, Q.; Wang, J.; Qi, J.; Li, Y.-P.; Chen, W. Silencing of atp6v1c1 Prevents Breast Cancer Growth and Bone Metastasis. *Int. J. Biol. Sci.*, **2013**, *9*, 853–862.

[220] Baxter, R.M.; Crowell, T.P.; George, J. a; Getman, M.E.; Gardner, H. The Plant Pathogenesis Related Protein GLIPR-2 Is Highly Expressed in Fibrotic Kidney and Promotes Epithelial to Mesenchymal Transition in Vitro. *Matrix biology : journal of the International Society for Matrix Biology*, **2007**, *26*, 20–29.

[221] Sun, X.; Fa, P.; Cui, Z.; Xia, Y.; Sun, L.; Li, Z.; Tang, A.; Gui, Y.; Cai, Z. The EDA-Containing Cellular Bronectin Induces Epithelial – Mesenchymal Transition in Lung Cancer Cells through Integrin A 9 B 1-Mediated Activation of PI3-K/AKT and Erk1/2. *Carcinogenesis*, **2014**, *35*, 184–191.

[222] O'Connell, M.P.; Marchbank, K.; Webster, M.R.; Valiga, A. a; Kaur, A.; Vultur, A.; Li, L.; Herlyn, M.; Villanueva, J.; Liu, Q.; Yin, X.; Widura, S.; Nelson, J.; Ruiz, N.; Camilli, T.C.; Indig, F.E.; Flaherty, K.T.; Wargo, J. a; Frederick, D.T.; Cooper, Z. a; Nair, S.; Amaravadi, R.K.; Schuchter, L.M.; Karakousis, G.C.; Xu, W.; Xu, X.; Weeraratna, A.T. Hypoxia Induces Phenotypic Plasticity and Therapy Resistance in Melanoma via the Tyrosine Kinase Receptors ROR1 and ROR2. *Cancer Discov.*, **2013**.

[223] Kudo-Saito, C.; Fuwa, T.; Murakami, K.; Kawakami, Y. Targeting FSTL1 Prevents Tumor Bone Metastasis and Consequent Immune Dysfunction. *Cancer Res.*, **2013**, *73*, 6185–6193.

[224] The Human Protein Atlas http://www.proteinatlas.org/ENSG00000185669-SNAI3/tissue/skin.

[225] Carette, J.E.; Pruszak, J.; Varadarajan, M.; Blomen, V. a; Gokhale, S.; Camargo, F.D.; Wernig, M.; Jaenisch, R.; Brummelkamp, T.R. Generation of iPSCs from Cultured Human Malignant Cells. *Blood*, **2010**, *115*, 4039–4042.

[226] Gandre-Babbe, S.; Paluru, P.; Aribeana, C.; Chou, S.T.; Bresolin, S.; Lu, L.; Sullivan, S.K.; Tasian, S.K.; Weng, J.; Favre, H.; Choi, J.K.; French, D.L.; Loh, M.L.; Weiss, M.J. Patient-Derived Induced Pluripotent Stem Cells Recapitulate Hematopoietic Abnormalities of Juvenile Myelomonocytic Leukemia. *Blood*, **2013**, *121*, 4925–4929.

[227] Tsai, S.-Y.; Clavel, C.; Kim, S.; Ang, Y.-S.; Grisanti, L.; Lee, D.-F.; Kelley, K.; Rendl, M. Oct4 and klf4 Reprogram Dermal Papilla Cells into Induced Pluripotent Stem Cells. *Stem Cells*, **2010**, *28*, 221–228.

[228] Kim, J.B.; Sebastiano, V.; Wu, G.; Araúzo-Bravo, M.J.; Sasse, P.; Gentile, L.; Ko, K.; Ruau, D.; Ehrich, M.; van den Boom, D.; Meyer, J.; Hübner, K.; Bernemann, C.; Ortmeier, C.; Zenke, M.; Fleischmann, B.K.; Zaehres, H.; Schöler, H.R. Oct4-Induced Pluripotency in Adult Neural Stem Cells. *Cell*, **2009**, *136*, 411–419.

[229] Kumar, S.M.; Liu, S.; Lu, H.; Zhang, H.; Zhang, P.J.; Gimotty, P. a; Guerra, M.; Guo, W.; Xu, X. Acquired Cancer Stem Cell Phenotypes through Oct4-Mediated Dedifferentiation. *Oncogene*, **2012**, 1–14.

[230] Guo, Y.; Mazar, A.P.; Lebrun, J.; Rabbani, S.A. An Antiangiogenic Urokinase-Derived Peptide Combined with Tamoxifen Decreases Tumor Growth and Metastasis in a Syngeneic Model of Breast Cancer. *Cancer Res.*, **2002**, *62*, 4678–4684.

[231] Barbero, A.; Palumberi, V.; Wagner, B.; Sader, R.; Grote, M.J.; Martin, I. Experimental and Mathematical Study of the Influence of Growth Factors on the Growth Kinetics of Adult Human Articular Chondrocytes. *J. Cell. Physiol.*, **2005**, *204*, 830–838.

[232] Choi, J.-W.; Lee, H.-W.; Roh, G.-S.; Kim, H.-H.; Kwack, K. CD137 Induces Adhesion and Cytokine Production in Hum an M Onocytic THP-1 Cells. *Exp. Mol. Med.*, **2005**, *37*, 78–85.

[233] Mutskov, V.; Felsenfeld, G. Silencing of Transgene Transcription Precedes Methylation of Promoter DNA and Histone H3 Lysine 9. *EMBO J.*, **2004**, *23*, 138–149.

[234] Shu, X.; Pei, D. The Function and Regulation of Mesenchymal-to-Epithelial Transition in Somatic Cell Reprogramming. *Curr. Opin. Genet. Dev.*, **2014**, *28C*, 32–37.

[235] Brosh, R.; Assia-Alroy, Y.; Molchadsky, A.; Bornstein, C.; Dekel, E.; Madar, S.; Shetzer, Y.; Rivlin, N.; Goldfinger, N.; Sarig, R.; Rotter, V. P53 Counteracts Reprogramming By Inhibiting Mesenchymal-To-Epithelial Transition. *Cell Death Differ.*, **2013**, *20*, 312–320.

[236] Fenouille, N.; Tichet, M.; Dufies, M.; Pottier, A.; Mogha, A.; Soo, J.K.; Rocchi, S.; Mallavialle, A.; Galibert, M.-D.; Khammari, A.; Lacour, J.-P.; Ballotti, R.; Deckert, M.; Tartare-Deckert, S. The Epithelial-Mesenchymal Transition (EMT) Regulatory Factor SLUG (SNAI2) Is a Downstream Target of SPARC and AKT in Promoting Melanoma Cell Invasion. *PLoS One*, **2012**, *7*, e40378.

[237] Niu, D.-F.; Kondo, T.; Nakazawa, T.; Oishi, N.; Kawasaki, T.; Mochizuki, K.; Yamane, T.; Katoh, R. Transcription Factor Runx2 Is a Regulator of Epithelial-Mesenchymal Transition and Invasion in Thyroid Carcinomas. *Lab. Investig.*, **2012**, *92*, 1181–1190.

[238] Robert, G.; Gaggioli, C.; Bailet, O.; Chavey, C.; Abbe, P.; Aberdam, E.; Sabatié, E.; Cano, A.; Garcia de Herreros, A.; Ballotti, R.; Tartare-Deckert, S. SPARC Represses E-Cadherin and Induces Mesenchymal Transition during Melanoma Development. *Cancer Res.*, **2006**, *66*, 7516–7523.

[239] Danen, E.H.J.; de Vries, T.J.; Morandini, R.; Ghanem, G.G.; Ruiter, D.J.; van Muijen, G.N.P. E-Cadherin Expression in Human Melanoma. *Melanoma Res.*, **1996**, *6*, 127–131.

[240] Hsu, M.; Andl, T.; Li, G.; Meinkoth, J.L.; Herlyn, M. Cadherin Repertoire Determines Partner-Specific Gap Junctional Communication during Melanoma Progression. *J. Cell Sci.*, **2000**, *113*, 1535–1542.

[241] Silye, R.; Karayiannakis, A.; Syrigos, K.; Poole, S.; van Noorden, S.; Batchelor, W.; Regele, H.; Sega, W.; Boesmueller, H.; Krausz, T.; Pignatelli, M. E-Cadherin/catenin Complex in Benign and Malignant Melanocytic Lesions. *J. Pathol.*, **1998**, *186*, 350–355.

[242] Kudo-Saito, C.; Shirako, H.; Takeuchi, T.; Kawakami, Y. Cancer Metastasis Is Accelerated through Immunosuppression during Snail-Induced EMT of Cancer Cells. *Cancer Cell*, **2009**, *15*, 195–206.

[243] Kim, J.E.; Leung, E.; Baguley, B.C.; Finlay, G.J. Heterogeneity of Expression of Epithelial-Mesenchymal Transition Markers in Melanocytes and Melanoma Cell Lines. *Front. Genet.*, **2013**, *4*, 1–8.

[244] Johannessen, C.M.; Johnson, L. a; Piccioni, F.; Townes, A.; Frederick, D.T.; Donahue, M.K.; Narayan, R.; Flaherty, K.T.; Wargo, J. a; Root, D.E.; Garraway, L. a. A Melanocyte Lineage Program Confers Resistance to MAP Kinase Pathway Inhibition. *Nature*, **2013**, *504*, 138–142.

[245] Landsberg, J.; Kohlmeyer, J.; Renn, M.; Bald, T.; Rogava, M.; Cron, M.; Fatho, M.; Lennerz, V.; Wölfel, T.; Hölzel, M.; Tüting, T. Melanomas Resist T-Cell Therapy through Inflammation-Induced Reversible Dedifferentiation. *Nature*, **2012**, *490*, 412–416.

[246] Nagase, H.; Visse, R.; Murphy, G. Structure and Function of Matrix Metalloproteinases and TIMPs. *Cardiovasc. Res.*, **2006**, *69*, 562–573.

[247] Wilhelm, I.; Fazakas, C.; Molnár, J.; Haskó, J.; Végh, A.G.; Cervenak, L.; Nagyőszi, P.; Nyúl-Tóth, A.; Farkas, A.E.; Bauer, H.; Guillemin, G.J.; Bauer, H.-C.; Váró, G.; Krizbai, I. a. Role of Rho/ROCK Signaling in the Interaction of Melanoma Cells with the Blood-Brain Barrier. *Pigment Cell Melanoma Res.*, **2014**, *27*, 113–123.

[248] Yoshioka, K.; Foletta, V.; Bernard, O.; Itoh, K. A Role for LIM Kinase in Cancer Invasion. *Proc. Natl. Acad. Sci. U. S. A.*, **2003**, *100*, 7247–7252.

[249] Mouneimne, G.; Soon, L.; DesMarais, V.; Sidani, M.; Song, X.; Yip, S.-C.; Ghosh, M.; Eddy, R.; Backer, J.M.; Condeelis, J. Phospholipase C and Cofilin Are Required for Carcinoma Cell Directionality in Response to EGF Stimulation. *J. Cell Biol.*, **2004**, *166*, 697–708.

[250] Song, X.; Chen, X.; Yamaguchi, H.; Mouneimne, G.; Condeelis, J.S.; Eddy, R.J. Initiation of Cofilin Activity in Response to EGF Is Uncoupled from Cofilin Phosphorylation and Dephosphorylation in Carcinoma Cells. *J. Cell Sci.*, **2006**, *119*, 2871–2881.

[251] Thies, A.; Moll, I.; Berger, J.; Wagener, C.; Brümmer, J.; Schulze, H.J.; Brunner, G.; Schumacher, U. CEACAM1 Expression in Cutaneous Malignant Melanoma Predicts the Development of Metastatic Disease. *J. Clin. Oncol.*, **2002**, *20*, 2530–2536.

[252] Ortenberg, R.; Galore-Haskel, G.; Greenberg, I.; Zamlin, B.; Sapoznik, S.; Greenberg, E.; Barshack, I.; Avivi, C.; Feiler, Y.; Zan-Bar, I.; Besser, M.J.; Azizi, E.; Eitan, F.; Schachter, J.; Markel, G. CEACAM1 Promotes Melanoma Cell Growth through Sox2. *Neoplasia*, **2014**, *16*, 451–460.

[253] Gogas, H.; Eggermont, a M.M.; Hauschild, a; Hersey, P.; Mohr, P.; Schadendorf, D.; Spatz, a; Dummer, R. Biomarkers in Melanoma. *Ann. Oncol.*, **2009**, *20 Suppl 6*, vi8–vi13.

[254] Utikal, J.; Schadendorf, D.; Ugurel, S. Serologic and Immunohistochemical Prognostic Biomarkers of Cutaneous Malignancies. *Arch. Dermatol. Res.*, **2007**, *298*, 469–477.

[255] Balch, C.M.; Buzaid, A.C.; Soong, S.; Atkins, M.B.; Cascinelli, N.; Coit, D.G.; Fleming, I.D.; Gershenwald, J.E.; Jr, A.H.; Kirkwood, J.M.; Mcmasters, K.M.; Mihm, M.F.; Morton, D.L.; Reintgen, D.S.; Ross, M.I.; Sober, A.; Thompson, J.A.; Thompson, J.F. Final Version of the American Joint Committee on Cancer Staging System for Cutaneous Melanoma. *J. Clin. Oncol.*, **2001**, *19*, 3635–3648.

[256] Chen, Q.M.; Tu, V.C.; Catania, J.; Burton, M.; Toussaint, O.; Dilley, T. Involvement of Rb Family Proteins, Focal Adhesion Proteins and Protein Synthesis in Senescent Morphogenesis Induced by Hydrogen Peroxide. *J. Cell Sci.*, **2000**, *113*, 4087–4097.

[257] Hujanen, E.S.; Terranova, V.P. Migration of Tumor Cells to Organ-Derived Chemoattractants. *Cancer Res.*, **1985**, *45*, 3517–3521.

[258] Thorgeirsson, U.P.; Liotta, L.A.; Kalebic, T.; Margulies, I.M.; Thomas, K.; M.Rios-Candelore; Russo, R.G. Effect of Natural Protease Inhibitors and a Chemoattractant on Tumor Cell Invasion In Vitro. *J. Natl. Cancer Inst.*, **1982**, *69*, 1049–1054.

[259] Ramgolam, K.; Lauriol, J.; Lalou, C.; Lauden, L.; Michel, L.; de la Grange, P.; Khatib, A.-M.; Aoudjit, F.; Charron, D.; Alcaide-Loridan, C.; Al-Daccak, R. Melanoma Spheroids Grown under Neural Crest Cell Conditions Are Highly Plastic Migratory/invasive Tumor Cells Endowed with Immunomodulator Function. *PLoS One*, **2011**, *6*, e18784.

8. Supplemental Material

8.1. Supplemental Figures

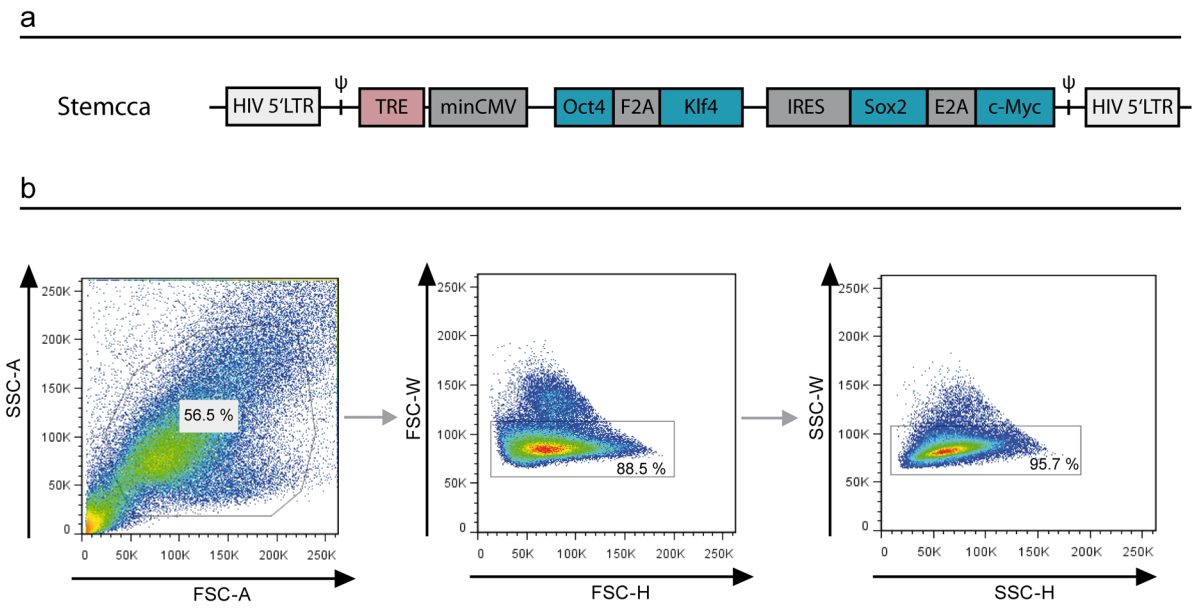

Suppl. Figure 1 | Reprogramming MEFs, HCmel12 and HCmel17

(a) The doxycycline-inducible lentiviral Stemcca vector was used to convert MEFs, HCmel12 and HCmel17 cells into pluripotent cells. Under the control of the TRE and a minimal CMV promoter region, Oct4, Klf4, Sox2 and c-Myc were expressed. The expression cassette is located between two 5'LTRs. Vector was generated by Sommer *et al.* [209]. **(b)** Displayed is the representative gating strategy for FACS in order to exclude dead cells and cell doublets. Shown are stained HCmel17-iPCCs cells that are shown in **Figure 8d**, lower panel. Dead cells were excluded based on scatter profile. Subsequently, doublets were excluded by gating first using FSC-H *vs.* FSC-W, and secondly using SSC-H *vs.* SSC-W blots.

CMV=cytomegalovirus; FACS=fluorescence activated cell sorting; FSC=forward scatter; H=hight; HIV=human immunodeficiency virus; LTR=long terminal repeat; MEF=murine embryonic fibroblast, SSC=side scatter; TRE=tetracycline responsible element; W=width

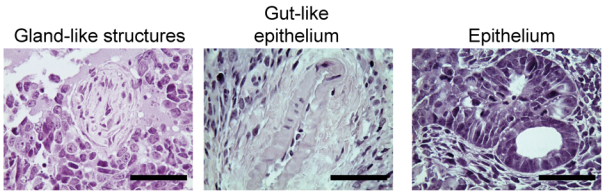

Suppl. Figure 2 | Teratoma formation of HCmel17-iPCCs

(a) H&E staining of tumor sections from HCmel17-derived iPCCs. Cells from one confluent 6-well were injected subcutaneously into NOD/SCID mice. Tumor was excised on day 39 after injection, fixed with paraformaldehyde and subjected to H&E staining, bar=100 µm.

H&E=hematoxylin and eosin

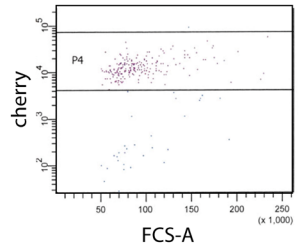

Tube: Reanalyze sorted cells mCherry pos

Population	#Events	%Parent	%Total
All Events	250	####	100.0
P1	238	95.2	95.2
P2	238	100.0	95.2
P4	207	87.0	82.8

Suppl. Figure 3 | Purification of M2-mCherry transduced HCmel17 cells using FACS

HCmel17 cells were transduced with the M2-cherry vector and sorted using FACS. Displayed is the reanalysis of sorted HCmel17-M2 cells. Table shows a purity of more than 85 %.

FSC-A= forward scatter (area); M2=M2-rt-TA (reverse tetracycline-transactivator); P=population

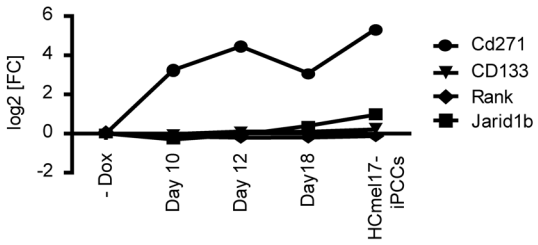

Suppl. Figure 4 | Melanoma stem cell marker expression during reprogramming

Displayed is the log2 [FC] of genes, which were discussed to label melanoma stem cells, at indicated time points during reprogramming.

Dox=doxycycline; FC=fold change; iPCCs=induced pluripotent cancer cells; MEFs=murine embryonic fibroblasts

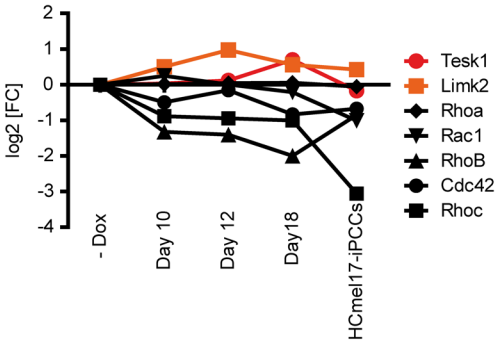

Suppl. Figure 5 | Expression of genes involved in the amoeboid migration mode

Displayed is the log2 [FC] of genes, which have been linked to the amoboeid mode of cellular invasion, independent of their p-value at indicated time points during reprogramming. Tesk1 and Limk2 (red) were shown to impete reprogramming of MEFs.

Dox=doxycycline; FC=fold change; MEFs=murine embryonic fibroblasts

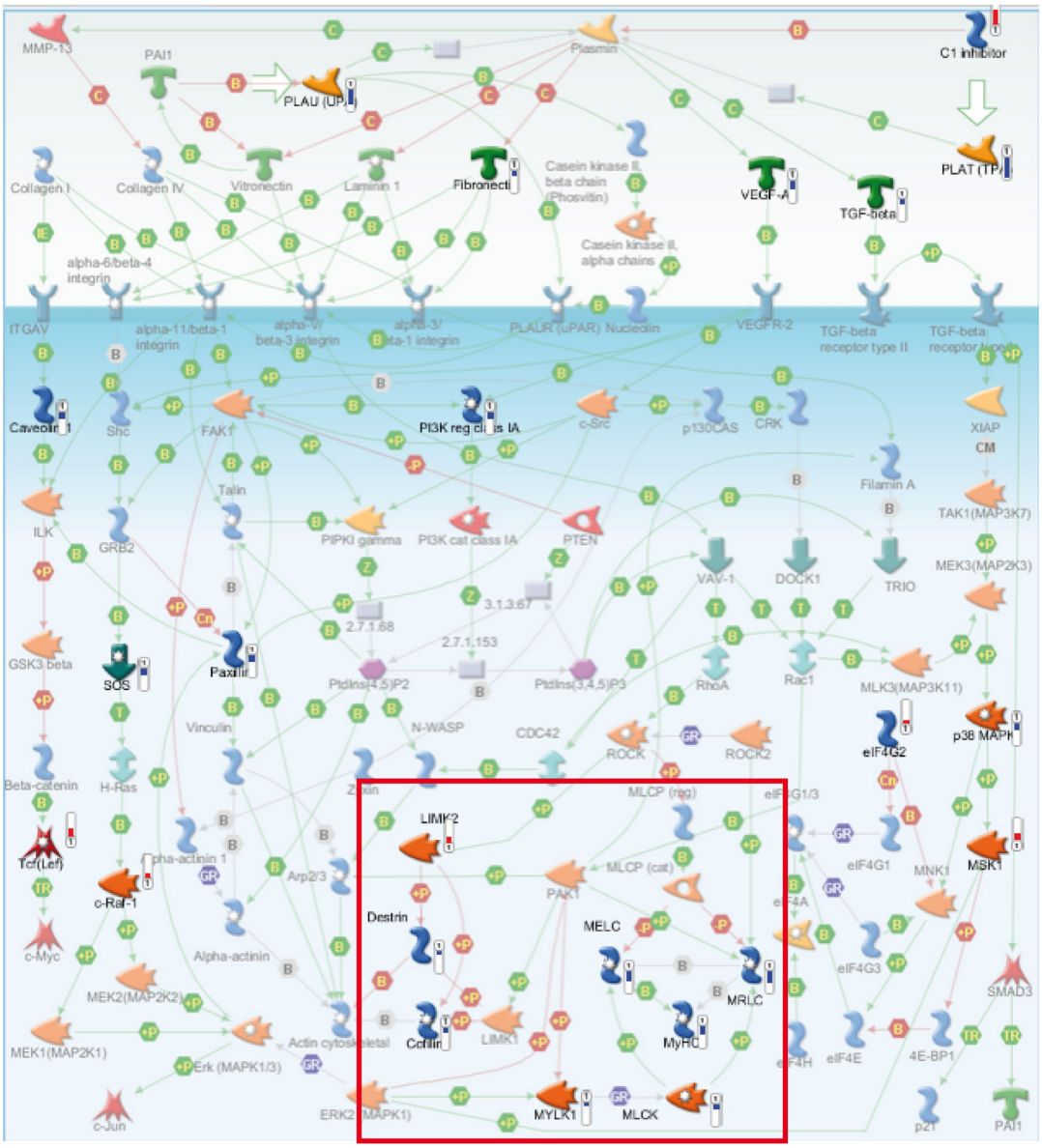

Suppl. Figure 6 | MAPK signaling includes the Cofilin signaling pathway

Gene set enrichment analysis of the process *MAPK signaling* (Table 4) within the pathway *cytoskeleton remodeling* (Table 3). This maps shows genes involved in The MAPK pathway and the thermometer indicates upregulation (red) and downregulation (blue), respectively. Factors involved in Cofilin signaling are indicated by the red box.

Analysis tools: Chipster, Metacore; MAPK=Mitogen-activated protein kinase

8.2. Supplemental Tables

	Process
1	Cytoskeleton remodeling
2	Cell adhesion: ECM remodeling
3	Neurophysiological process
4	Development: Epithelial-to-mesenchymal transition
5	Development: lung epithelial progenitor cell differentiation
6	Upregulation of MITF in melanoma
7	Cell adhesion: chemokines
8	Development: proteases in HSC mobilization
9	Development: ckit ligand signaling
10	Membrane-bound ESR1

Suppl. Table 1 | Processes enriched in downregulated genes comparing HCmel-iPCCs with parental cells

Gene set enrichment analysis of pathway maps involving down-regulated genes after reprogramming HCmel12 and HCmel17 melanoma cells towards full pluripotency. Table shows significant enrichment (p≤0.05) of differentially regulated genes in indicated pathways.

Analysis tools: Chipster, Metacore

ECM=extracellular matrix; ESR1=Estrogen receptor 1; HSC=Hematopoietic stem cells; MITF=Microphthalmia-associated transcription factor

	Networks
1	Cytoskeleton: Intermediate filaments
2	Development: Neurogenesis_Axonal guidance
3	Cell adhesion: Amyloid proteins
4	Cytoskeleton: Regulation of cytoskeleton rearrangement
5	Cell adhesion: Cell-matrix interactions
6	Signal transduction: WNT signaling
7	Development: Neurogenesis in general
8	Development: Regulation of angiogenesis
9	Cell adhesion: Glycoconjugates
10	Cytoskeleton: Actin filaments

Suppl. Table 2 | Gene set enrichment analysis of HCmel17-iPCCs compared to HCmel17 (process networks)

Analysis was performed by applying t-test for significantly up- or downregulated genes using *Chipster software* (p<0.05, p-value adjustment method=BH). Gene list (820 genes) was uploaded into *Metacore* online software and enrichment analysis by process networks was applied. Displayed are the top ten networks.

Analysis tools: Chipster, Metacore

BH= Benjamini-Hochberg; iPCCs=induced pluripotent cancer cells

HCmel-M2			HCmel17-iPCCs			Log2 [FC]
Rep 1	Rep 2	Rep 3	Rep 1	Rep 2	Rep 3	0.00
7.2	7.48	7.95	7.41	7.56	7.66	

Suppl. Table 3 | c-Myc expression

Microarray-derived normalized data for c-Myc expression in HCmel17-iPCCs and in HCmel-M2 cells transduced with Stemcca-blastin (in the absence of doxycycline).

FC=Fold change; iPCCs=induced pluripotent cancer cells

-log [p-value]	Pathways
>10	Positive regulation of ovulation
>10	Regulation of ovulation
>9	**Regulation of cell differentiation**
>8	Regulation of developmental process
>8	Luteinization
>8	Extracellular matrix organization
>8	Extracellular structure organization
>8	Response to endogenous stimulus
>7	Response to lipid
>7	**Positive regulation of cell differentiation**

Suppl. Table 4 | Pathways enriched in genes that are downregulated in partially reprogrammed HCmel17 cells

Displayed are pathways involving downregulated genes after partially reprogramming HCmel17 cells at day 12. Table shows significant enrichment ($p<0.05$) of downregulated genes in indicated pathways. *Analysis tools: Chipster, Metacore*

	- Dox	+ Dox (Day 12)	+ Dox (Day 12)
Snai1	32.1	24.9	26.0
Snai1	23.7	24.5	23.0

Suppl. Table 5 | Ct values of *Snai1* and *Snai2*

After cDNA synthesis, 500 ng of cDNA was used for qPCR and mean Ct values from three technical triplicates are displayed for Snai1 and Snai2 on indicated days during partialy reprorgamming.

Dox=Doxycycline

Probe ID	Gene	p-value	log2[FC]
5050382	Aldh3a1	0.000917	6.68
2600431	Ush1c	2e-06	6.38
1190427	Avil	1e-06	6.19
7040397	NA	1e-06	5.89
5050438	NA	4.2e-05	5.72
2570672	Atp2a3	5.1e-05	5.32
1400402	Pcolce2	5.2e-05	4.92
3140204	NA	1e-06	4.90
6940037	Ltf	4.2e-05	4.85
3060397	NA	1.5e-05	4.81
5310471	Ccdc3	2.9e-05	4.75
6660475	1190003J15	0.002598	4.74
2510280	Gm106	0.000176	4.70
5340762	Mfsd6	1e-05	4.61
50577	Etl4	8e-06	4.52
6650646	NA	8.7e-05	4.50
1690035	Ramp2	2e-06	4.48
4780010	Mal	2e-06	4.48
4050064	Ngfr	1e-06	4.45
2650209	Homer2	7.1e-05	4.42
1440164	Hbb-y	1.4e-05	4.37
3060019	Fbxo15	4e-05	4.35
3170471	Dmrtc2	0.000147	4.30
1400053	NA	0.011744	4.28
1230575	Pcolce2	5.7e-05	4.22
5310379	Scg5	5.2e-05	4.11
4150670	St3gal6	1.4e-05	4.00
6350349	Slc7a3	8e-06	3.99
3360681	Nppb	0.000971	3.99
1300768	1700019D0	1.3e-05	3.97
6200563	Cct6b	2e-06	3.93
2630446	Fbxo15	2e-05	3.88
160377	Scara5	0.002026	3.87
110609	Tmprss5	2e-06	3.84
4610414	Krt13	0.000625	3.72
4050437	Chst3	0.000218	3.65
6620008	Ly6g6c	0.000463	3.65
1740114	Spint1	2.7e-05	3.65
380259	Mal	7e-06	3.63
5700538	Aoah	0.000117	3.62
3400431	Chst4	6e-06	3.62
1190431	Lama1	0.000916	3.53
50292	Cobl	1e-05	3.52
2370563	NA	0.000156	3.47
4120243	Upp1	0.003026	3.46
2190397	Podxl	2e-06	3.43
7150465	Tac2	0.000828	3.41
1050095	Upp1	0.003553	3.37

Probe ID	Gene	p-value	log2[FC]
2340167	Rdm1	0.00252	3.37
940438	Laptm5	0.000389	3.35
4540725	Fetub	0.000102	3.34
3610025	Smagp	2e-06	3.32
3610039	Pcsk1n	1.3e-05	3.31
7330379	Gngt2	0.002946	3.31
2230154	Zcwpw1	4.9e-05	3.29
60288	Atp2a3	0.000328	3.26
7160301	Pga5	1.4e-05	3.25
2810603	Hs3st3b1	0.000598	3.23
4760630	Reep1	0.001185	3.22
3520594	Upp1	0.001919	3.21
1980209	Actg2	0.040916	3.21
1450139	Gfap	3.9e-05	3.20
7160047	AA467197	0.033394	3.20
2810315	Chst3	0.000207	3.19
360348	Gsta4	0.000108	3.18
3360161	Aqp3	1.4e-05	3.16
3390131	Il1rn	0.001534	3.16
3060450	NA	0.039365	3.15
7380241	Fam102a	0.007906	3.14
1570367	NA	1.9e-05	3.13
7610114	Mgst1	0.005399	3.12
1820601	Igfbp3	5.2e-05	3.12
4250437	Fgfbp1	0.00044	3.11
830333	Krtdap	0.000645	3.09
50521	Dmkn	0.01533	3.09
3520142	Zbtb32	0.004645	3.07
160451	Mras	8e-06	3.04
450452	Vat1l	9.2e-05	3.02
4610110	Fst	0.001706	3.00
3940682	Dmkn	0.013007	3.00
1050465	Ceacam1	7e-06	2.98
870445	Lamc2	0.000156	2.96
3420056	Pde1b	0.002928	2.96
3190438	Mgst1	0.002028	2.95
3850326	Itgb4	8e-06	2.94
1770086	Thsd4	0.001694	2.94
2100373	Them5	1.5e-05	2.92
2510598	Otog	0.00238	2.92
7400286	Slc2a6	0.000625	2.90
1340619	Ly6g6d	7e-06	2.88
6100162	Pacs1	1.6e-05	2.87
6840634	Cib2	0.004071	2.87
6860609	Rbp1	0.007153	2.87
2850451	Apcdd1	0.001988	2.85
3360343	Pde1b	0.004067	2.83
3710647	Pdzk1ip1	2.9e-05	2.83
6100209	Wnk4	0.000165	2.81
3360301	Ccdc28b	9.1e-05	2.80

Probe ID	Gene	p-value	log2[FC]	Probe ID	Gene	p-value	log2[FC]
5810414	Cxadr	0.000463	2.78	3520053	Ociad2	0.001215	2.33
6480161	Sigirr	2.8e-05	2.77	630689	Cd109	3.1e-05	2.31
6270192	Ntn5	0.012043	2.76	6380376	Dusp14	0.000382	2.30
5340722	Csrp3	0.003012	2.75	6560193	Chst4	9.2e-05	2.30
4810445	Clock	0.000517	2.74	4920288	NA	0.000947	2.30
5310497	Odz4	0.013135	2.74	2450010	NA	0.000282	2.28
7210270	Miat	0.003712	2.74	1260095	Efhd1	0.00048	2.27
5490187	Srgn	0.00117	2.71	1400152	Efnb1	0.000207	2.27
3940286	Adam23	0.000698	2.70	4200035	Ccdc68	0.001785	2.26
1030438	9930023K05	0.004334	2.70	650711	Dgat2	0.008686	2.26
430278	Pllp	2.3e-05	2.70	4280541	Tcfcp2l1	2.8e-05	2.26
2140022	Cdc42ep5	0.016917	2.69	1440019	Cd59a	0.002707	2.26
2690368	Smagp	1.8e-05	2.68	2060142	Iqgap2	2.9e-05	2.25
2100722	Btn1a1	0.000963	2.68	3060255	Lamc2	0.002479	2.25
6980577	L1td1	0.000173	2.67	60524	Kcnk13	0.000278	2.25
6350324	Gna14	0.002128	2.66	10438	Rb1	0.000402	2.23
2320403	Gch1	0.02668	2.66	2000373	Serping1	0.024545	2.23
540398	E130012A1	0.006816	2.65	7100059	Klhl32	0.000155	2.21
2260398	Zbtb7c	1.5e-05	2.64	3120328	NA	0.001893	2.20
7570215	Kpna7	1.4e-05	2.64	840689	Tmem35	0.009741	2.19
3450170	Ccdc28b	0.000196	2.61	6040142	Pou6f1	0.00618	2.19
3890328	Oas1g	0.033531	2.59	3800168	Tle4	0.00273	2.18
630427	Sox2	1.4e-05	2.58	3850438	Col15a1	0.000545	2.17
1510301	Krt84	0.000207	2.58	6180348	Crabp2	0.004116	2.17
2630370	Arpp21	0.001568	2.58	2340543	NA	0.034289	2.17
6520156	Mras	4.9e-05	2.57	4250487	Tmem45a	0.038015	2.17
830736	NA	0.008171	2.53	150035	Fut8	0.006725	2.15
4900500	Vpreb3	8e-06	2.53	5050093	Prx	0.003274	2.15
4610010	Slc5a9	3e-06	2.52	3710520	Lgals7	0.016233	2.14
2850369	2610034M1	0.001257	2.51	4810328	Nrarp	0.000462	2.14
3180750	Dbp	0.03887	2.51	2810192	Pmm1	0.000467	2.14
4480468	Arhgef3	0.003385	2.49	6270181	Dusp4	0.00229	2.13
2190039	Rnase1	1e-05	2.48	4810324	Serping1	0.023921	2.13
3060382	Odz4	0.006754	2.48	6480326	Ahsg	0.000942	2.11
3710544	Mgst3	0.004465	2.44	3520349	Cxcl14	0.003074	2.11
5570292	Cyp4f39	3.2e-05	2.43	7040142	Cth	0.000634	2.11
4200709	Pipox	0.000569	2.43	7400463	Myoc	0.015341	2.11
2360519	Tek	0.000499	2.42	7000114	Nccrp1	7.5e-05	2.10
3800746	Bcl2l15	1.4e-05	2.42	990364	Ceacam1	2e-04	2.10
4260300	NA	0.000172	2.41	70427	Eef2k	0.000908	2.10
2940301	Ano4	0.001901	2.41	990082	Lamc2	0.002339	2.09
3060487	Pipox	4.2e-05	2.41	2480048	Rb1	0.000602	2.08
6130014	Iqgap2	1.4e-05	2.41	4900296	Prss35	0.001147	2.08
6040524	Tmprss5	7.1e-05	2.41	2350324	Gstt3	0.018927	2.08
380332	Liph	0.000143	2.40	780050	Armcx1	0.000116	2.07
4640711	Edn1	0.000255	2.38	2750209	Ano1	0.000119	2.07
4230367	4931408C2	0.000119	2.38	5130059	Ifitm6	0.042604	2.06
1230703	Nup210	3.2e-05	2.36	4780201	NA	9e-05	2.06
2030367	Sybu	0.006489	2.36	6380333	6330407J23	5.8e-05	2.05
1340390	NA	9e-06	2.35	4230743	NA	0.00044	2.05

Probe ID	Gene	p-value	log2[FC]
2690017	Golph3l	0.000619	2.05
4480221	Sybu	0.003211	2.05
1570102	Gstm5	0.009429	2.03
50519	Porcn	0.015472	2.03
7050674	2610030H0	1.4e-05	2.03
7200739	Sulf2	0.013733	2.02
4290367	Slc29a3	0.002017	2.01
1470619	Krt14	0.008555	2.01
6290133	Endod1	0.001318	2.01
4210619	Mgst3	0.007989	2.00
2650136	Dclk2	0.003432	1.99
6350133	Ociad2	0.000144	1.99
3870095	Stmn2	0.04335	1.98
1090064	Cd55	0.000372	1.98
5080187	Shroom3	0.000225	1.98
6370221	Dock9	0.001147	1.98
1770747	Lrpap1	0.001516	1.98
3290593	NA	0.001706	1.98
7560632	Fkbp14	0.000485	1.97
5420047	Cxadr	0.000105	1.96
1340465	Orai1	0.000566	1.95
4250731	Scube3	2.3e-05	1.95
4070689	NA	5.1e-05	1.95
1440040	Rap1gap2	0.000237	1.94
3140041	2310046K0	0.000203	1.94
510020	Pde2a	0.000878	1.94
5560711	Slc46a3	0.000675	1.92
2370504	Prokr1	0.000947	1.92
5890653	Sostdc1	0.001516	1.92
1450739	Ano4	0.002387	1.92
6380372	Pmm1	0.000698	1.92
5670722	Hspb1	0.000408	1.91
6450687	Abi3	0.007881	1.91
670603	Ces3	0.002632	1.91
1090576	Drp2	0.012214	1.91
3190246	Slc13a4	0.002017	1.91
380465	Prickle2	0.006354	1.91
5550402	Gm867	0.000938	1.90
4880494	Ociad2	0.000272	1.90
70661	Pcyt1b	0.00148	1.89
1430368	St6gal1	8.8e-05	1.88
150373	Tst	0.000185	1.88
4120445	Defb1	0.000536	1.88
150746	Cxcl14	0.008141	1.88
3290239	Plvap	0.026549	1.88
3520328	Glb1l2	0.000727	1.88
7570315	Agpat4	0.000785	1.88
5810470	Aldh1a1	0.001107	1.87
6280240	Crym	0.001926	1.87
840360	AU040829	0.003685	1.87

Probe ID	Gene	p-value	log2[FC]
460731	Adap1	0.000116	1.86
2710709	Bcas3	0.001649	1.86
4120300	Megf10	0.010365	1.86
4610433	Srgn	0.000831	1.83
5910632	Ppm1k	0.009463	1.83
6940753	NA	0.010614	1.82
5080523	NA	8.7e-05	1.81
2480255	Tnfsf11	0.000424	1.81
610491	Fam49a	0.000545	1.80
2470133	Csrp3	0.01237	1.80
4730224	Zfp704	0.002285	1.79
7040598	Slc5a9	1.7e-05	1.79
670397	Krt6b	7.1e-05	1.78
730164	Tgm3	0.000119	1.78
1090730	Krt6b	0.000144	1.77
2100035	Ahsg	0.002459	1.77
1980102	Gsdmd	0.004284	1.76
4900220	B930041F1	0.009764	1.76
2370471	Shroom3	0.000144	1.75
1340050	NA	0.001257	1.75
5900450	Renbp	0.003608	1.75
2340519	Sept6	9.2e-05	1.74
7000746	Darc	0.013718	1.74
4570397	Cyb561	1.9e-05	1.74
6110612	NA	5.7e-05	1.74
2230379	Liph	0.000205	1.74
1450646	Mbp	0.002398	1.74
1230543	Vamp4	0.048086	1.73
3940070	Pkp1	1.9e-05	1.73
4040689	Itpripl1	0.000976	1.73
1580035	Tal1	4.9e-05	1.72
360445	Cd109	0.000176	1.72
460327	Slc2a3	0.008896	1.71
2000433	Fam122b	0.000462	1.70
1980240	L1td1	0.001407	1.70
6760341	NA	0.002678	1.70
4250280	Naprt1	0.010696	1.70
2340047	Dact2	0.000176	1.70
4890112	Tppp3	0.031874	1.69
5310598	Cryab	0.041954	1.67
1090767	Eno2	0.022316	1.67
6290709	Adamts7	0.002404	1.67
1030386	Acp6	0.002715	1.67
3120719	Tmem79	0.00019	1.66
1410279	Wasf1	0.000727	1.66
4040746	Usp50	0.002619	1.65
7550431	NA	0.013173	1.65
4280431	Ccdc92	0.013991	1.65
7610343	Etv5	0.001232	1.64
4040435	Chchd10	0.0044	1.64

4200204	Sh3bp2	0.000625	1.64	**870072**	**Snai3**	**0.00449**	**1.51**
1850307	NA	0.003602	1.64	6510468	NA	0.011032	1.51
2680370	Sept6	0.000525	1.63	3940242	Samd9l	0.018167	1.51
2120707	Plekhf2	0.000504	1.62	5130156	Ccrl2	9.2e-05	1.51
5130487	Rgs12	0.000963	1.62	20095	Shf	0.001147	1.51
5260433	NA	0.017211	1.62	3520093	Avpi1	0.006171	1.51
2490561	NA	0.023573	1.62	1050091	Hus1	0.011032	1.51
1570021	Hs3st3a1	0.004227	1.61	1110326	Fcgr2b	0.000831	1.50
6980048	Olig3	5.6e-05	1.61	6510575	H2afz	0.0189	1.50
4210300	Leng9	0.000319	1.61	4180674	E330009J07	0.001215	1.50
2000280	Gper	1.8e-05	1.61	6350537	Apoa2	0.005466	1.50
2630240	She	0.000596	1.61	380102	Ahnak	0.005999	1.50
7570475	Tmc6	0.000878	1.61				
270050	Scn10a	0.001879	1.60				
4610338	Efs	0.000321	1.60				
6100433	Taf13	0.00048	1.60				
7100300	Tmc6	0.001706	1.60				
730243	Prx	0.014219	1.60				
5870201	Myo1e	0.006657	1.59				
3310564	Scarb2	0.000463	1.59				
6520576	NA	0.000563	1.59				
7040133	Avpi1	0.003426	1.59				
630608	Thsd4	0.004103	1.59				
4200653	Mavs	0.00273	1.58				
360324	Tlx2	0.000487	1.58				
6420349	Hdac6	0.000831	1.58				
70221	Mtap7	0.011605	1.58				
5820626	NA	0.00114	1.58				
1850427	Vamp4	0.003468	1.58				
3990397	Nipsnap1	0.009345	1.58				
4780138	Mfsd7a	0.027556	1.58				
3140397	Gprasp2	0.014775	1.57				
5220600	NA	0.000319	1.57				
5490079	Tmc6	0.000524	1.56				
6330048	8430410A17	0.001237	1.56				
1710239	Itpr1	0.001361	1.56				
6180411	Gltp	0.000282	1.56				
4230368	NA	0.000777	1.55				
6370184	Lefty2	0.002756	1.55				
6620519	Fzd5	0.023577	1.54				
2340300	Ddc	4.9e-05	1.54				
4290114	Cib2	0.008648	1.54				
5550176	Gm129	0.004885	1.53				
4850196	Syngr1	0.000625	1.53				
380500	B3galnt1	0.002017	1.53				
3450102	NA	0.012312	1.53				
6560497	Nnmt	0.02552	1.53				
5900593	Ptpn22	0.042897	1.53				
6900189	NA	0.011284	1.52				
2940600	NA	0.001074	1.51				

Suppl. Table 6 | Genes upregulated in HCmel17 cells at day 12 after reprogramming
Table shows fold change calculations of an emperical Bayes test comparing HCmel17 cells reprogrammed for 12 days to their parental cells (p≤0.05 and log2[FC]≥1.5).
Analysis tools: Chipster; data are normalzied using Illumina quantile normalization

9. Acknowledgement

First, I want to thank **Prof. Jochen Utikal**, who gave me the great opportunity to carry out this thesis at the German Cancer Research Center. Thank you for your advice, for helpful discussions, for supporting side projects and for letting me create my own ideas.
I also thank **Prof. Viktor Umansky**, who enabled this thesis with being my first referee. I am thankful for your support during all TAC meetings, for providing cell lines and for revealing discussions.
I am grateful for the sustained financial support from the **Hanns-Seidel-Stiftung e.V.** throughout all the years. Also, I want to acknowledge **Prof. Ralf Bartenschlager** and **Dr. Karin Müller-Decker** for enrolling as examiners in my disputation. Thank you for taking your precious time to let me defend my work.
I thank **Prof. Ursula Klingmüller** for providing additional cell lines.
In particular, I thank **Dr. Martin Sprick** for supporting me throughout the years with ideas and helpful discussions. Thank you for your understanding and for your positive encouragement.

I also want to thank all lab members for their support and for sharing their knowledge with me. I thank **Jenny** for being the helping hand in cell culture and **Sayran** for her help with histological stainings.
In particular, I thank **Mathias, Kathrin** and **Maike**, who always had a helping hand when I needed one, scientific advice when I was confused and who always found the right words when I needed those. My great gratitude I also owe to **Daniel Roth** who helped me out with all possible lab work and who made the grey days brighter. Special thanks also to **Daniel Novak**, who encouraged me especially during the last year with all its failures and successes. Thank you for providing an endless stock of chocolate and for your motivating and laudatory words.

My great gratitude I owe to **Kasia** who did not only share the desk with me, but my whole life during these three years. Thank you for encouraging me, for your caring advice – scientific and non-scientific – and for making me laugh throughout every hassle.

Thanks to **Janis** and **Jule**, who read this thesis and helped me to get the best out of it. In particular, I thank **Steffy** for always being there, caring for me, for correcting the thesis and for spending the best coffee breaks together. I thank my dear friends **Saskia, Joana** and **Steffi** for supporting me and listening to everything I had to say about being a PhD student.

To my family boys **Ralf** and **Daniel** – thank you for trusting me to finish this from the very beginning. Thank you for making me feel loved and cared about.

To my sister **Kathi** – thank you for being my other half and for always being there when the big, the small, the good and the bad things happen. Thanks for being a big part of my life.

I also thank my beloved **Dad** for teaching me not to take knowledge for granted.

To my **Mom** – I thank you for your endless love and your support. You made this thesis possible by letting me choose my own way.

To the love of my life, my husband **Kevin -** I will not find the right words to describe how grateful I am for you being by my side. Thank you for your support, your care and your encouragement, for believing in me and for making me smile every single day.
With you I feel complete.